Author:
Sosa Moreno, Jeison E

Title:
New developments in flood modelling at continental-scale

Case studies in Europe and the US

University of BRISTOL

New developments in flood modelling at continental-scale: Case studies in Europe and the US

Jeison Ebert Sosa Moreno

A thesis submitted to the University of Bristol in accordance with the requirements for award of the degree of Doctor of Philosophy in the Faculty of Science

School of Geographical Sciences

December 2020

Word count 40,559

This page was intentionally left blank.

Dedicated to my father and mother

This page was intentionally left blank.

Abstract

Floods are the costliest and most deadly class of natural disaster each year, and this situation is not expected to change in the future. Furthermore, the study of floods is relevant for a wide variety of applications ranging from nature conservancy to urban planning and rapid disaster response. Generally, the nature of floods at continental scale has been studied using streamflow data from gauge stations or satellite imagery. Although these approaches can characterise past floods quite well, they do not cover all the locations of interest and do not directly estimate hazards to people and assets. Alternatively, hydrodynamic models specifically designed to capture floodplain hydraulics are an effective option to simulate floods. At continental scale, hydrodynamic models have successfully been able to estimate the risk associated with floods at very high resolutions (i.e. <100 m), however, limited research has been devoted to the understand the evolution of floods over time. This thesis presents new developments in continental sale flood modelling to characterise floods in a multi-decal time window. Firstly, an open-source software package to automatise the input data processing needed for continental scale modelling was developed. Then, a new flood modelling framework that couples streamflow data from a hydrological model with a flood inundation model is presented. The framework was able to predict flood depths over time at continental scale in an efficient way, an approach that to date has not been done before with an inundation model but a routing model. The framework was used to build a European Flood Hindcast where floods hydraulics for 298 basins were mapped over 26 years (1990-2016). The data generated in Europe showed that among the largest basins the Danube, Rhine, Rhone and Elbe were the ones hit the most by floods. Conversely, the least impacted basins in the same period were the Douro, Ebro, Guadiana and Tagus. Building the modelling framework from scratch helped to uncover potential source of errors in the modelling chain, one of which was poor geolocation of rivers. To substantially improve river geolocation, a new data set of river streamlines was generated for the contiguous US based on national high-quality data.

This page was intentionally left blank.

Acknowledgments

I would like to thank my supervisors who positively supported me during this process. I really appreciate your guidance, Paul and Jeff, your help was exceptional.

This thesis would not be possible without the unconditional support of my family who has been there for me, digitally, but present. Mom, dad, Vivi and Andrea, thanks.

My friends who have been an important part of my life, from here and there, new and old ones. Alejandro, Andy C., Andy B., Danico, Gabysh, Dieguish, Dani Z., Milton, Alf, Paddy, Anna, Nico', Angelo, Luca, Rob, Julia (Iuliia), Ann, Pedro, Helena, Sarah, thanks.

My colleagues. Without you, Browns would not have been so fun. Laurence, Tom, Giada, Tian, Xue, Simbi, Isaac, Pete, Seerat, Markus, Ali, thanks.

I would like to thank the European Commission that through a Marie Curie Scholarship and the System-Risk project funded this PhD research. Special thanks to all the people within the System-risk project.

This page was intentionally left blank.

Author’s declaration

I declare that the work in this dissertation was carried out in accordance with the requirements of the University's Regulations and Code of Practice for Research Degree Programmes and that it has not been submitted for any other academic award. Except where indicated by specific reference in the text, the work is the candidate's own work. Work done in collaboration with, or with the assistance of, others, is indicated as such. Any views expressed in the dissertation are those of the author.

SIGNED: ..... DATE: .....

This page was intentionally left bank.

Table of contents

This page was intentionally left blank.

List of figures

List of tables

CHAPTER 1

Introduction

1.1. Background

Floods are the costliest and most deadly class of natural disaster each year and studies predict that the situation is not going to change in the future (Winsemius et al., 2016; Alfieri et al., 2017). Hirabasyashi et al., 2013 reports that between 1970 and 2000 the total number of people exposed to flooding globally was up to ~5 million. This number is expected to rise in the future where by 2070-2100 ~15 million people will be exposed to floods under a RCP2.6 scenario or ~70 million under a RCP8.5 scenario. This negative outcome is also reported by other studies (Winsemius et al., 2016; Dottori et al., 2018; Koks et al., 2019; Bloschl et al., 2019). The study of floods is relevant for a wide variety of sectors ranging from insurers, multi-national corporations, NGOs and national governments to tackle problems such as rapid flood disaster response, urban planning and climate change adaptation.

Generally, the nature of floods is investigated in three different ways. First, using data collected from river gauge stations where time series of discharge or stage provides information of high flows or water levels, respectively (e.g. Bloschl et al., 2019). Secondly, using remote sensing techniques over satellite imagery to depict inundated areas (e.g. Brakenridge et al., 2018). And third, using computational simulations of river hydrodynamics (i.e. flood modelling) (e.g. Smith et al., 2018). Whilst river gauge stations and satellite imagery can characterise floods, providing information on flood occurrence and inundated area respectively, they lack the ability to reveal information on inundation depth during a flood event. Additionally, these approaches are localised in the sense that they cannot always be applied to cover all areas of interest, for example an entire continent. In lieu of these approaches, flood modelling is an alternative method that can be employed to tackle this issue, in particular 2D flood modelling which is the main topic of this thesis.

The past 15 years have seen the emergence of two-dimensional flood models capable of simulating flood wave dynamics at reach scale with decimetres of accuracy for water level prediction under certain conditions (Hunter et al., 2008). The models solve variants of the Shallow Water Equations using efficient numerical schemes (e.g. Bates et al., 2010; Moulinec et al., 2011; Sanders et al., 2019). This computational and numerical efficiency has led to the expansion of flood modelling studies from reach to continental scale. At continental scale, flood models are generally driven by terrain elevations data sets derived from space-borne satellites (e.g. Farr et al., 2007; Tadono et al., 2015; Yamazaki et al., 2017; Rizzoli et al., 2017, Wessel et al., 2018). Yet, better predictions are achievable by representing river channel geometries at sub-grid level (Neat et al., 2012). The sub-grid approach uses geolocated river centrelines, widths and depths to calculate in-channel hydrodynamics. Therefore, the more accurate these variables are the better the prediction is. From space-borne satellites, river geolocation data sets (e.g. Lehner et al., 2008; Yamazaki et al., 2019) and river width data sets (e.g. Andreadis et al., 2013; Yamazaki et al., 2014; Allen and Pavelsky, 2018) have been derived. Nonetheless, space-borne satellites cannot penetrate water surfaces, and this means river depths have to be approximated, for example using a simple power law formulation (e.g. Leopold and Maddock, 1953; Neal et al., 2012) or the Manning's equation (e.g. Sampson et al., 2015).

Flood modelling is still a field in active development where flood footprint (i.e. inundated area, flood extent) accuracy is a key factor in disaster risk management, urban planning, insurance market pricing and climate change adaptation (e.g. Schuman et al., 2018). As a result, producing accurate flood maps has become an important element in flood modelling (Schumann and Bates, 2018).

The primary research aim of this thesis is to improve our understanding of methods for continental-scale flood modelling. To this end, this thesis has identified three specific problems which are the principal subjects of the work. The problems identified are as follows:

First, deploying a flood model can be time-consuming since input data needs to be processed from a variety of different sources. Commonly, pre-processing input data for flood models is carried out in software packages such as ArcGIS or QGIS (e.g. Seenath et al., 2016; Hutanu et al., 2020; Shen, 2020). However, pre-processing tasks are constrained to local-scale problems (i.e. a few tributaries in a river basin) due to lack of computational memory. At continental scales, there is still a need for a general-purpose set of tools to deploy in flood studies to be able to process large amounts of

data without running into memory problems. The set of tools must include common operations such as DEM resampling, bank height estimation, riverbed estimation, in-channel bed elevation smoothing in a single software package. This will facilitate the deployment of studies for different flood study applications. The fundamental difficulty of processing the data is that it is not uniform: the grid resolution, data format, data geographical projection differs from each data set. A user therefore usually spends a considerable amount of time in pre-processing steps, so the software should be able to deal with these constraints as well.

Second, most of the continental scale flood modelling efforts to date have been oriented toward hazard prediction, or the estimation of flood depths for a particular return period (or recurrence interval) in Europe (Alfieri et al., 2014; Paprotny et al., 2017), the US (Wing et al., 2017), Africa (Trigg et al., 2016) and globally (Winsemius et al., 2013; Dottori et al., 2016; Sampson et al., 2015). However, the limited literature and formal methodology have delayed the progress towards flood depth time series at continental-scale. Schumann et al., (2016) produced the first continental level flood hindcast for the Australian continent. The study used a small number of gauge stations coupled to a 2D flood model to create a multi-decal set of flood depth times series in the most important river basins. The study had some limitations, for example, gauged tributaries were not considered, and flood defences were not taken into account. The problem of ungauged tributaries can be treated by adopting a hydrological model to generate simulated streamflows, however, coupling several hundreds to thousands of inflows to a hydrodynamic model in a multi-decal simulation has been a limited to basin-scale problems only (e.g. Grimaldi et al., 2019).

Third, a better representation of in-channel hydrodynamics results in better floodplain hydrodynamic predictions (Neal et al., 2012). In this context, accurately geolocated river centrelines are a key component for flood models. Most continental studies use space-borne derived hydrography to obtain this variable (e.g. HydroSHEDS Lehner et al., 2008; MERIT Hydro Yamazaki et al., 2019) and whilst current hydrography data sets have helped to build flood modelling studies at continental scales, data-rich countries are not advantaged as better quality terrain elevations are available along with curated river centrelines data sets. A framework to produce a hydrography from local sources of data in particular a high resolution DEM and a database of river centrelines is the main subject of the last results chapter of this thesis.

This thesis presents three main objectives along with research questions to address these gaps.

1.2. Research objectives

Objective 1

Develop an open-source software package to automatically pre-process input data for hydraulic models in a computationally efficient manner.

- Is there any way to facilitate and automatise the deployment of flood inundation studies at local, continental and global scales?

Objective 2

Develop a framework to build a European Flood Hindcast by means of simulated streamflows from a hydrological model.

- Is there any parametrization or methodology that can improve the representation of rivers depths and flood defences in continental scale flood inundation studies?
- Is there any effective way to facilitate the coupling between hydrologic and a hydrodynamic model in continental scale studies?
- What is the best approach to handle continental scale hydrodynamic simulations at high resolutions (100 m)?
- What is the feasibility to create a European wide flood inundation hindcast by means of a hydrological model output and taking into account flood defences interaction?

Objective 3

Develop a framework to generate a new hydrography from a high-quality national DEM (the National Elevation Dataset) and a high-quality survey-based hydrography (National Hydrography Dataset)

- Can hydrographic estimates be improved by using high quality and high-resolution national data sets instead of global ones?
- Is it possible to generate raster-based hydrographic estimates based on vector-based river network maps accurately?

The objectives and research questions detailed above will be explored within three results chapters. Details of these chapters are given below:

Results for Objective 1, Chapter 3

A toolbox to quickly prepare flood inundation models for LISFLOOD-FP simulations

This chapter presents the development of LFPtools http://github.com/jsosa/lfptools, an open-source Python package which encompasses the most commonly used methods to prepare input data for large scale flood inundation studies. The tool has been developed for use with the LISFLOOD-FP hydrodynamic model, but the functions are generic and could be used for any grid-based hydrodynamic code and even for non-hydrodynamics applications.

Results for Objective 2, Chapter 4

A flood inundation hindcast for Europe based on 26-year simulated river discharge

This chapter introduces a semi-automated modelling framework to produce a multi-decal flood depth time series (or flood hindcast) for Europe at ~90 m resolution. The framework uses free globally available sources of river width, flood protection standards, terrain information and hydrography to represent river geometries explicitly. The framework uses daily river discharge simulated by a large-scale hydrology model coupled to a 2D flood model to map flood patterns over 26 years (1990-2016) in 298 European river basins.

Results for Objective 3, Chapter 5

On the extraction of a precise river hydrography in the contiguous US

This chapter presents a new hydrography for the contiguous US. The new hydrography was built on the National Elevation Dataset (NED) and the National Hydroraphy Dataset Plus (NHDPlus). The data set extends the coverage of NHDPlus providing estimates of flow accumulation and flow direction with better accuracy than global hydrography data sets (e.g. HydroSHEDS Lehner et al., 2008; MERIT Hydro Yamazaki et al., 2019) and extents the current coverage of NHDPlus. Unlike NHDPlus, the new hydrography provides a raster-based river network suitable for models based on computational grid to carry out computations.

1.3. Chapter summary

There is still the need to develop novel methods and tools to continue improving flood inundation maps, especially at continental scale. Three important problems that still need attention are i) how to quickly build accurate flood inundation models to boost continental-scale floods studies? ii) which insights can we get from a complete long catalogue of historical flood events at continental scale? and iii) can hydrographic estimates be improved by using high quality and high-resolution national data sets instead of global ones? These are important questions in flood modelling and are the main subject of thesis.

This thesis will detail new developments in flood modelling at continental-scale. In particular, an open-source project and Python package that was developed to easily assist the fast-growing non-experienced and experienced flood modellers to build flood inundation models globally at any scale. Additionally, this study will explore concepts such as large-scale hydrodynamic modelling, hydrologic-hydrodynamic coupling, long time period simulations and flood defences interactions by analysing these components in a European flood hindcast. Lastly, this thesis will present the development of a new hydrography for the contiguous US, the new hydrography is based on the National Elevation Dataset (NED) and the National Hydrography Dataset Plus (NHDPlus).

1.4. Overview of the thesis

Chapter 2 summarises main concepts in continental-scale flood modelling. Chapter 3 details the development of an open-source project and Python package to quickly build flood inundation models everywhere at any scale. Chapter 4 describes the development of a European flood hindcast based on a continues simulation of river hydrodynamics. Chapter 5 presents the development of a new hydrography for the contiguous US. Chapter 6 ends this thesis summarising conclusions and future research lines of this work.

1.5. Peer-Reviewed Work

Material in this thesis has been presented in peer-reviewed journals and at academic conferences. All of which are my own work and are detailed below

1.5.1. Peer-reviewed publications

Sosa, J., Hawker, L., Sampson, C., Smith, A., Neal, J., Bates, P. (2020). On the extraction of a precise river hydrography in the contiguous US. In preparation

Sosa, J., Salamon, P., Yamazaki, D., Neal, J., Bates, P. (2020). A flood inundation hindcast for Europe based on 26-year simulated river discharge. *Water Resource Research*. Submitted

Sosa, J., Sampson, C., Smith, A., Neal, J., & Bates, P. (2020). A toolbox to quickly prepare flood inundation models for LISFLOOD-FP simulations. *Environmental Modelling & Software*, 104561. doi.org/10.1016/j.envsoft.2019.104561

Yamazaki, D., Ikeshima, D., **Sosa, J.**, Bates, P. D., Allen, G., & Pavelsky, T. (2019). MERIT Hydro: A high-resolution global hydrography map based on latest topography datasets. *Water Resources Research*. doi.org/10.1029/2019WR024873

1.5.2. Conference presentations

Sosa, J., Salamon, P., Neal, J., Bates, P. (2019). A flood inundation hindcast for Europe based on 26-year simulated streamflow. *Global Flood Partnership*. https://bit.ly/jsosagfp19

Sosa, J., Sampson, C., Smith, A., Neal, J., & Bates, P. (2019). LFPtools, a package to quickly prepare flood inundation models for LISFLOOD-FP. *CSDMS*. https://bit.ly/jsosacsdms19

Sosa, J., Salamon, P., Neal, J., Bates, P. (2018). A flood inundation hindcast for the UK based on 24-year simulated streamflow. *AGU*. https://bit.ly/jsosaagu18

Sosa, J., Salamon, P., Neal, J., Bates, P. (2018). A flood inundation hindcast for the UK based on 24-year simulated streamflow. *Global Flood Partnership*. https://bit.ly/jsosagfp18

Sosa, J., Salamon, P., Neal, J., Bates, P. (2018). A flood inundation reanalysis of Europe. *EGU*. https://bit.ly/jsosagfp18

CHAPTER 2

Flood modelling at continental-scale

This chapter begins with an introduction to hydrodynamic modelling. Model governing equations, and the advantages and disadvantages of 1D and 2D hydrodynamic models are discussed later. The chapter presents the 2D hydrodynamic model LISFLOOD-FP, a model that is capable of predicting floodplain inundation at local to continental scales. The chapter continues by detailing data requirements for hydrodynamic models at continental scale and concludes by outlining recent developments in the field.

2.1. Introduction

A flood is defined as a body of water under movement characterised by a large and low amplitude wave. The phenomenon is a consequence of unusual high stage or flow which exceeds the channel's capacity and as a result inundates low-lying floodplains adjacent to the river channel. The phenomenon has been modelled using a number of different approaches. First, using hydrologic and geomorphic relationships, flooding can be predicted with methods such as the Rapid Flood Spreading Method (RFSM) (L'homme et al., 2008) which discretise floodplains in small areas representing terrain depressions. Later, flood volumes are spread over those areas using filling and spilling mechanisms. Another popular method based on hydrogeomorphic relationship is the Height Above the Nearest Drainage (HAND) (Renno et al., 2008) that normalizes the topography according to the local relative heights found along the drainage network and determines nearby flood inundation extent by selecting the surrounding cells whose HAND values are less than the known water depth in the stream. Other methods that use a similar approach are (Manfreda et al., 2011; Degiorgis et al., 2012; Samela et al., 2017). At continental scales, the use of hydrogeomorphic relationships

provide sensible results for a rapid flood damage assessment, however, these are not a preferable method for flood risk management or water resources planning as they lack any linkage with basin hydraulics since the physical process of inundation is not simulated, but rather based on simplified hydraulic concepts (Teng et al., 2017).

As opposed to the hydrogeomorphic approach, hydrodynamic modelling is an alternative method that has been widely used to model floods (Bates and De Roo, 2000). The fundamental idea is to solve variants of the Shallow Water Equations (SWE). The SWE describe the motion of fluids under two main assumptions i) the horizontal length scale is greater than the vertical length scale and ii) vertical pressure gradients are hydrostatic. The Saint-Venant Equations (SVE) are a variant of the shallow water equations that describe transient open-channel flow. Computational techniques exist to solve the SVE, in particular formulations based on finite difference, finite volume and finite element with the time discretised either in an explicit or implicit way. For example, TELEMAC 2D (Moulinec et al., 2011) is a code that implements both finite element and volume formulations, with time discretised in an implicit or explicit way. TRENT (Villanueva and Wright, 2006) solves the SVE using an explicit finite volume approach and LISFLOOD-FP (Bates et al., 2010) uses an explicit finite difference approach. Unlike hydrogeomorphic approaches, hydrodynamic modelling provides physically-based outputs aligned with real fluid motion behaviour.

At continental scales, hydrodynamic models are driven with data sets derived primarily from space-borne satellites with spatial resolutions varying from ~30 m to ~90 m. Continental-scale flood modelling became more available after the release of near-global digital elevation data through the Shuttle Radar Topography Mission (Farr et al., 2007). Most recently, the Landsat imagery inventory has provided a new era for flood modelling. For example, by using remote sensing techniques, it has been possible to measure river widths (Allen and Pavelsky, 2018) and map long-term changes in flood areas (Pekel et al., 2016) for rivers wider than ~30 m globally.

In summary, the three components that boost the generation of flood inundation maps at high spatial resolutions (from 1 km to 30 m) are i) the development of efficient numerical schemes to solve the SVE ii) the emergence of satellite data sets for public access and iii) the progress in hardware. These components have driven flood inundation maps in places where it was not able before.

In the next sections, 1D and 2D hydrodynamic models are described in detail, a description of data requirements for continental-scale flood modelling is presented next and recent developments in the field are explained at the end of the chapter. 3D hydrodynamic models are not considered in this section as this type of model are computationally expensive as this type of model requires more input data. Additionally, 3D models present problems representing the water free surface, high-order turbulence and transient flood shoreline (Hunter et al., 2007). These constraints in 3D models are main reason why large scale flood modelling have been treated predominantly with 1D or 2D approaches.

2.2. Hydrodynamic models

This section describes two types of flood models 1D and 2D, and the governing set of equations in each case in addition to its advantages and disadvantages.

2.2.1. 1D models

One way to predict hydrodynamics variables in floodplains is the use of a 1D hydrodynamic model. This type of model calculates hydraulics along the centre line of the river discretised by segments Δx using the Saint-Venant Equations Equations 2.1 and 2.2 which describe transient open-channel flow:

Conservation of mass $$\frac{\delta Q}{\delta x} + \frac{\delta A}{\delta t} = 0 \qquad (2.1)$$

Conservation of momentum $$\frac{1}{A}\frac{\delta Q}{\delta t} + \frac{1}{A}\frac{\delta\left(\frac{Q^2}{A}\right)}{\delta x} - g\left(S_0 - S_f\right) = 0 \qquad (2.2)$$

where Q is the flow discharge, t is the time, h is the water depth, g is gravity, S_f is the friction slope, S_o is the channel bed slope and A is the cross-section area.

1D models are computationally more efficient than 2D models, however they are unable to capture the lateral diffusion effect of the flood wave and underrepresent floodplain terrain as they have to discretise it as cross-sections. 2D models, on the other

hand, discretise a flood inundation problem in a 2D grid rather than cross-sections allowing wave spreading according to topographic and hydraulic gradients across shallow gradient floodplains to be more correctly represented. Some hydrodynamic models in this category are MASCARET (Goutal et al., 2012), HEC-RAS (USACE,2016), SOBEK (Deltares, 2019) or MIKE 11 (DHI, 2017).

2.2.2. 2D models

2D models have also been used to predict floodplain hydrodynamics in the two dimensional spatial domain (e.g. x and y). By assuming that the third dimension (i.e. water depth) is shallow compared to the other two the depth-averaged Navier-Stokes equations result in Equations 2.3, 2.4 and 2.5:

Conservation of mass:

$$\frac{\partial h}{\partial t} + \frac{\partial (hu)}{\partial x} + \frac{\partial (hv)}{\partial y} = 0 \qquad (2.3)$$

Conservation of momentum:

$$\underbrace{\frac{\partial (hu)}{\partial t}}_{\text{local acceleration}} + \underbrace{\frac{\partial (hu^2)}{\partial x}}_{\text{convective acceleration}} + \underbrace{\frac{\partial (huv)}{\partial y}}_{\text{water slope}} + \underbrace{g \frac{1}{2} \frac{\partial (h^2)}{\partial x}}_{\text{friction slope}} = 0 \qquad (2.4)$$

$$\frac{\partial (hv)}{\partial t} + \frac{\partial (hv^2)}{\partial y} + \frac{\partial (huv)}{\partial x} + g \frac{1}{2} \frac{\partial (h^2)}{\partial y} = 0 \qquad (2.5)$$

here the horizonal velocity is given by the vector (u, v) which is averaged over the vertical column. The spatial representation in this type of models can be on a rectangular grid (structured mesh), triangular grid (unstructured mesh) or flexible mesh.

Simplifications to the shallow water equations can reduce the complexity and run time of the computation. Thus, by neglecting terms in the Saint-Venant Equations different approximations can be achieved. For example, the diffusive wave approximation neglects the inertial terms (i.e. the local and convective accelerations) and is used where

the flow is in a subcritical condition, with low Froude values (Hunter et al., 2005). The kinematic wave approximation assumes a uniform flow where the friction slope approximates the slope of the channel (Hunter et al., 2007). These approximations lead to computationally efficient models and paved the way to the first large area floodplain inundation predictions for a section of the central Amazon floodplain in Brazil (Wilson et al., 2007), and Ob river in Western Siberia (Biancamaria et al., 2009).

Both the kinematic and diffusive approximations are suitable approximations for larger length scales (i.e. long reaches using grid resolutions of the order of >100) as bed friction dominates over convective acceleration leading to relative small errors for not including the acceleration term. The inertial wave approximation neglects only the advection term (also known as the convective acceleration) (Bates et al., 2010). Including the advection term is relevant for small scale studies with supercritical flow as these types of forces generate significant velocity derivatives. Additionally, the inertial approximation is faster than the diffusive approximation. Bates et al., (2010) found that the computational speed can increase from 1-3 times, nonetheless it is highly dependent on the grid resolution. This local inertial approximation has been used to simulate continental scale studies in sensible amount of time. For example, the local Inertial approximation has been successfully solved to: (a) estimate global hazard at ~90 m resolution for catchments larger than 50 km^2 (Sampson et al., 2015); (b) produce a continental scale flood hindcast for Australia for rivers larger than 10,000 km^2 and ~90 m resolution (Schumann et al., 2016); and most recently (c) to estimate flood hazard under changing climate conditions in the Ganges–Brahmaputra–Meghna basin in south Asia (Uhe et al., 2019).

2D models are computationally more expensive than 1D models, however, are the preferable choice for flood hydraulics. The main reason is 2D models are capable of representing hydraulic processes induced by the floodplain topography. Additionally, advances in remote sensing techniques along with increasing publicly availability of satellite data have been important to consider 2D models as the way for floodplain inundation prediction. Satellite data can be used to validate 2D floodplain models (Schumann et al., 2018), but also helped to estimate Digital Elevation Models (DEM) at global scale (e.g. SRTM Farr et al., 2007). Some codes within this category are TUFLOW (Syme, 1991), JFLOW (Bradbrook et al., 2004), TRENT (Villanueva and Wright, 2006), LISFLOOD-FP (Bates et al., 2010) or PRIMO (Sanders et al., 2019).

For a more detailed comparison between hydrodynamic models the reader is advised to consult Teng et al., (2017)

2.3. Hydrodynamic model selection

In order to fulfil the objectives of this thesis, a 2D hydrodynamic model able to solve for flood hydraulics at continental scales and high resolutions (<100 m) is needed. As mentioned before, solving the full version of Saint Venant Equations (SVE) is an ineffective option as at large scales (i.e. hundreds of kilometres of river reaches) flood hydraulics are mostly driven by bed friction rather than inertial processes. In this context, using the kinematic or the diffusive wave approximation to solve for the hydraulics is an effective way as these approximations reduce the computational time compared to the full version of SVE. The inertial formulation where only the advection term is neglected from the full SVE provides flood inundation predictions very similar to the diffusive wave model (Hunter et al., 2008), but at a significantly reduced computational cost (1-3 orders of magnitude faster). This is due to the minimum stable time step scales with Δx, rather than with $(1/\Delta x)^2$ as would be the case for a purely diffusive scheme.

In order to build a flood hindcast at continental scales, it is important to select the fastest approximation (in terms of computational) able to simulate water dynamics. In this view, the inertial formulation was selected as the best option. One of the codes that implements this approximation is LISFLOOD-FP, an open-source model for research purposes that has a novel structure suitable for continental scale applications and has been largely validated. More details about the LISFLOOD-FP model are given in the following subsection.

2.3.1. LISFLOOD-FP

LISFLOOD-FP (Bates et al., 2010; Bates et al., 2013) is a 2D hydrodynamic model that solves the Saint-Venant Equations (SVE) using the inertial wave approximation (i.e. neglecting the advection term from the SVE). This approximation provides accurate results for flows in the lower range of subcritical flow ($0 > Fr > 0.5$) when compared

to solutions of the full SVE. Most floodplains and lowland rivers behave within this subcritical flow range. In the upper range of the subcritical flow regime ($0.5 < Fr < 1$) the local inertial approximation provides accurate results only under mild depth gradients. The approximation presents less accuracy for Fr values close to 1 with large depth gradients (e.g. mountain rivers), to accurately obtain water depths in these type of rivers the full set of SVE must be used instead (de Almeida and Bates, 2013).

LISFLOOD-FP simulates water depths in each grid cell and at each time step thereby simulating the dynamic propagation of flood waves over fluvial, coastal and estuarine floodplains. The model calculates the hydrodynamics in the floodplain using a staggered grid so that whilst the solution is first order in time it has some of the properties of a second order solution in space (Shaw et al., 2020). The model is decoupled in x and y (i.e. it treats 2D flow by computing the 1D flows through each of the four cell faces).

For each cell the continuity equation over time step Δt is:

$$h_{i,j}^{t+\Delta t} = h_{i,j}^{t} + \Delta t \frac{Q_{x,i-1/2,j}^{t+\Delta t} - Q_{x,i+1/2,j}^{t+\Delta t} + Q_{y,i,j-1/2}^{t+\Delta t} - Q_{y,i,j+1/2}^{t+\Delta t}}{A_{i,j}} \qquad (2.6)$$

where Q is the flow between cell, h is the water depth at the centre of each cell, A is the water surface/cell area, and subscripts i and j are cell spatial indices in x and y directions, respectively. The momentum equation to calculate flow Q between two cells in the x direction is described by:

$$Q_{i+1/2}^{t+\Delta t} = \frac{q_{i+1/2}^{t} - g h_{\text{flow}}^{t} \Delta t S_{i+1/2}^{t}}{\left[1 + g\Delta t n^2 \left|q_{i+1/2}^{t}\right| / \left(h_{\text{flow}}^{t}\right)^{7/3}\right]} \Delta x \qquad (2.7)$$

where Δx is the cell width, g is the acceleration due to gravity, q^t is the low from the previous time step Q^t divided by cell width Δx, S is the water surface slope between cells, n is the Manning's roughness coefficient, and h_{flow} is the depth between cells through which water can flow, defined from the water depths and cell elevations z as:

$$h_{\text{flow}}^{t} = \max(h_i^t + z_i, h_{i+1}^t + z_{i+1}) - \max(z_i, z_{i+1}) \qquad (2.8)$$

and the water surface slope S as:

$$S_{i+1/2}^{t} = \frac{(h_i^t + z_i) - (h_{i+1}^t + z_{i+1})}{\Delta x} \qquad (2.9)$$

To maintain stability the model, time step must be limited to:

$$\Delta t = \alpha \frac{x}{\sqrt{\max(h^t) g}} \qquad (2.10)$$

where α is a stability coefficient typically set around 0.7 for most floodplains and $max(h^t)$ is the maximum water depth in the model domain. This time-stepping equation is based on the Courant-Friedrichs-Lewy condition (Courant et al., 1928).

LISFLOOD-FP Sub-grid (Neal et al., 2012) extends the basic structure of LISFLOOD-FP to make it easier to simulate large area applications. It uses the formulation of Bates et al., 2010 to calculate flow in floodplain and the equations of Neal et al., 2012 to estimate flow in channels. Thus, water surface slope in the channel follows:

$$S_{i+1/2}^{t} = \frac{(h_i^t + z_{c,i}) - (h_{i+1}^t + z_{c,i+1})}{0.5(x_c + x_{c,i+1})} \qquad (2.11)$$

where z_c is the channel bed elevation and x_c is the length of the flow (Δx). Depth of flow $h_{c,flow}^t$ is calculated similarly to Equation 2.8, but using channel bed elevations instead:

$$h_{c,flow}^{t} = \max\left(h_i^t + z_{c,i}, h_{i+1}^t + z_{c,i+1}\right) - \max\left(z_{c,i}, z_{c,i+1}\right) \qquad (2.12)$$

Channel flow is calculated using the momentum equation employing the same approach as Bates et al., 2010:

$$Q_c^{t+\Delta t} = \frac{Q_c^t - g A_{c,\,\text{flow}}^t \Delta t S_c^t}{\left\{1 + g \Delta t n_c^2 |Q_c^t| / \left[\left(R_{c,\,\text{flow}}^t \right)^{4/3} A_{c,\,\text{flow}}^t \right] \right\}} \qquad (2.13)$$

where the hydraulic radius R_c^t is derived for a more general case as the flow in channels is usually narrow and deep:

$$R_c^t = \frac{A_{c,\,\text{flow}}^t}{w_c + 2h_{c,\,\text{flow}}^t} \qquad (2.14)$$

with channel flow area obtained from the channel width $(w_{c,flow})$ and channel water depth $(h_{c,flow}^t)$ according to:

$$A_{c,\,\text{flow}}^t = w_{c,\,\text{flow}}\, h_{c,\,\text{flow}}^t \qquad (2.15)$$

The model has been widely used for different applications at small and large scales (e.g. Wilson et al., 2007; Biancamaria et al., 2009; Neal et al., 2012; Schumann et al., 2013, 2016; Alfieri et al., 2014; Sampson et al., 2015; Wing et al., 2018) due its computational efficiency, which is mainly given by neglecting the flow advection in the shallow water equation but also by employing a highly efficient finite difference numerical solution scheme (de Almeida et al., 2012; de Almeida and Bates, 2013). The source code of the model has been parallelized to take advantage of HPC clusters, bringing additional speed ups in computation time under both CPU (Neal et al., 2018) and GPU architectures (Shaw et al., 2020).

2.4. Data requirements

Data requirements for 2D hydrodynamic models is reviewed in this section. Hydrodynamic models are driven by different variables in order to produce water depth, velocity and consequently flood extent. The quality of the input data largely dictates the quality of the prediction, and thus extensive research has been done in this area. A number of these data sets have been derived using remote sensing techniques applied to satellites orbiting the Earth (e.g. SRTM, GRWL), but also numerical modelling of rainfall-runoff processes (e.g. EFAS, GloFAS). Figure 2.1 shows a diagram of the data requirements for 2D hydrodynamic models applied at a continental-scale.

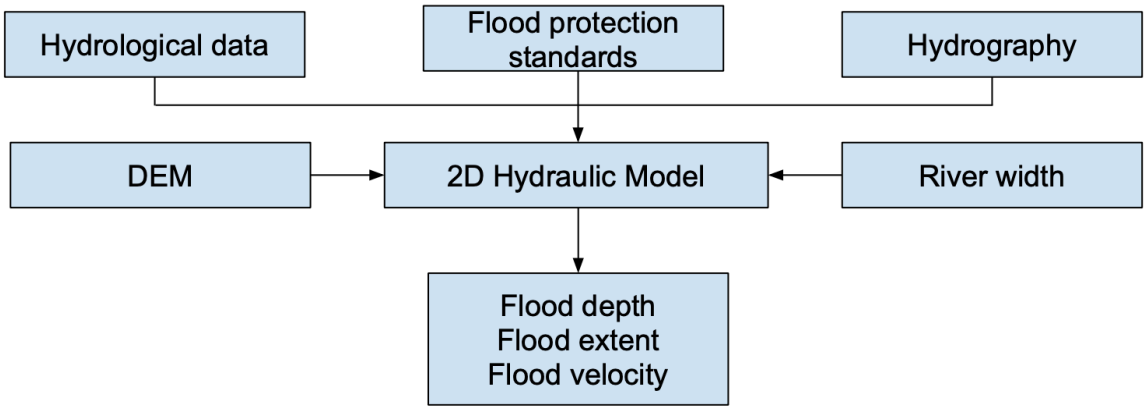

Figure 2.1 Diagram of data requirements in flood modelling at continental-scale

In this section, the most commonly used data sets for continental-scale flood modelling are discussed in detail.

2.4.1. Digital elevation models

Several fields in geosciences need a precise representation of global terrain to carry out their studies, for example earthquake motion assessment (Hough et al., 2010), flood inundation modelling (Sampson et al., 2015; Yamazaki et al., 2014b), global wetland carbon dynamics (Laudon et al., 2011), soil erosion and sediment yield prediction (de Vente et al., 2013), and water mapping by remote sensing (Pekel et al., 2016). However, only developed countries are able to undertake projects whose main goal is to obtain high-accuracy digital elevation models (DEM) (e.g. Austria, Australia, Denmark, Norway, Spain, Japan, The UK, The US, The Netherlands). Developing countries still rely on spaceborne DEMs to undertake geosciences studies. Examples of spaceborne DEMs which have facilitated geoscience research are: the Shuttle Radar Topography Mission (SRTM) which measured land elevations using radar interferometry and provides a near-global DEM at 1″ and 3″ resolution (i.e. ~30 and ~90 m at the equator) (Farr et al., 2007), ASTER GDEM (Advanced Spaceborne Thermal Emission and Reflection Radiometer-Global DEM) (Tachikawa et al., 2011), AW3DDEM (ALOS: Advanced Land Observing Satellite, World 3D-DEM) (Tadono et al., 2015) and the TanDEM-X DEM (Rizzoli et al., 2017). Note that DEMs derived from spaceborne satellites contain height errors which may be significantly problematic in flood modelling studies. These errors are classified as speckle noise, stripe noise, absolute bias and positive bias due to tree canopies in forested areas (Farr et al., 2007; O'Loughlin

et al., 2016). The speckle noise is caused by the variability of surface reflectance over flat areas resulting in a random height error in addition to instrument noise (Rodriguez et al., 2006; Takaku et al., 2015). The stripe noise is characterised by a regular height undulation, which in the case of SRTM it has a wavelength of 500 m to 100 km (Gallant and Read, 2009; Crippen et al., 2016). The absolute error is evident when there is shift in the average elevation over a large domain (~20 km) (Takaku et al., 2015; Crippen et al., 2016). Finally, the positive bias due to vegetation canopies is caused as both radar interferometry and stereo viewing are not able to measure elevations beneath forests (O'Loughlin et al., 2016; Carabajal and Harding, 2006). Yamazaki et al., 2017 developed the Multi-Error-Removed Improved-Terrain (MERIT) data set, a very accurate mapping of global terrain elevations achieved by correcting errors mentioned before in a fused DEM data set.

2.4.2. Water bodies

Mapping global surface water is key for many geoscience studies. Delineating the spatial and temporal distribution of rivers and lakes is important for understanding the water, energy and carbon cycles, both at local and global scales (Downing et al., 2012, 2014; Allen and Pavelsky, 2018). In flood modelling, hydrodynamic models use this information to identify permanent water bodies and map them directly in the flood inundation output. Water bodies are also useful in hydrographic studies such as HydroSHEDS (Lehner et al., 2008) or MERIT Hydro (Yamazaki et al., 2019) which use water body data to identify the largest river locations. Several data sets which map water bodies have been produced to date, for example the SRTM Water Body Data (SWBD) (NASA/NGA, 2003) was one of the first databases to document surface water bodies at high spatial resolution (~30 m). It is a very accurate high-resolution data set derived from the SRTM mission; however, it does not cover the entire globe (coverage is between N60°–S54°). Subsequent studies improved the coverage, but lack the ability to distinguish between temporary and permanent waters or water occurrence (e.g. GLCF MODIS Carroll et al., 2009; GLCF GIW Feng et al., 2016; GLOWABO Verpooter et al., 2014). Thanks to public release of Landsat imagery in particular, water occurrence was able to be depicted (e.g. GLWD Lehner and Döll 2004; GIEMS Papa et al., 2010; GIEMS-D15 Fluet-Chouinard et al. 2015; G3WBM Yamazaki et al., 2015). Most recently, the Global Surface Water Occurrence (GSWO) (Pekel et al., 2016) has been produced and is considered the most complete database of water bodies to account

for occurrence. It used ~three million images from the Landsat inventory to map 32 years of water surface change globally.

2.4.3. Hydrography

In addition to DEMs which determine the terrain elevation of floodplains, the location of rivers is also needed when simulating river hydrodynamics at continental-scales. To date, three global hydrography data sets exist which have helped to identify very accurately and with enough resolution ($10^2 - 10^3$ m) main rivers and channels at global scale: HYDRO1K (USGS, 2001), HydroSHEDS (Lehner et al., 2008) and more recently MERIT Hydro (Yamazaki et al., 2019). These hydrography data sets were developed using DEMs as a proxy. The procedure is as follows; the DEM is used to derive a flow direction map or a map consisting of drainage directions (e.g. north, northeast, northwest, south, etc.) in every cell of the DEM. Then, the direction map is used to calculate the number of upstream cells within the drainage basin. However, as seen in Section 4.2.1 DEMs can contain errors which could lead to inconsistent river flow patterns. One way to tackle this problem is overlaying additional sources of river location data, for example the water-related features of OpenStreetMaps (www.openstreetmap.org) or water body datasets (e.g. GSWO Pekel et al., 2016). Alternatively, if local data sources of river centrelines along with high quality terrain elevations are available then the hydrography can see substantial improvement. Chapter 5 presents a computational framework to calculate hydrography data sets using as case study the contiguous US.

2.4.4. River width

Accurate simulations of river hydrodynamics require river width to be known beforehand. Models typically need to know the width of rivers when these flow is at mean or bankfull discharge. Andreadis et al., (2013) developed one of the first such data sets with global coverage of river width at ~500 m spatial resolution. Andreadis et al., used hydraulic geometry relationships (Leopold and Maddock, 1953) to estimate river width in rivers and channels from the HydroSHEDS data set. The hydraulic relationships employed bankfull flow estimated from streamflow information in the Global Runoff Data Center archive (GRDC) (www.bafg.de/GRDC). Yamazaki et al., 2014a

continued this line of development and instead of employing hydraulic relationships used observed water bodies from the SRTM Water Body Data (SWBD) to derive river width estimates thereby generating the Global Width Database for Large Rivers (GW-DLR), a river width database at ~90 m spatial resolution. The observed water bodies mask used in GW-DLR considerably improved river width estimates and unlike previous studies is based on empirical data. To date, the best estimate of river width is obtained through the Global River Width from Landsat (GRWL) product (Allen and Pavelsky, 2018), a database of river widths derived from the Landsat inventory. Similar to GW-DLR, this new database estimates river widths based on water masks at ~30 m spatial resolution from 7,376 Landsat images.

2.4.5. Hydrological data

Inflow boundary conditions in the form of discharge (e.g. m^3/s) or water level (e.g. meters) are needed to calculate hydrodynamics for every time step within the computational grid. At global scale, discharge data are available for long periods of time (>50 years). For example, with more than 9,500 gauge stations all over the world the Global Runoff Data Base (GRDC) (GRDC, 2007) keeps record of observed discharge data since 1980. This data set has contributed extensively to improved flood inundation modelling. It helped to build one of the first river width database at global scale (Andreadis et al., 2013), it was used to estimate river flow magnitude for a given probability using regional flood frequency analysis (RFFA) (Smith et al., 2015), or as a useful validation database for hydrological models. It is worth noting that river discharge data can be subject to uncertainty, primarily caused by changes in channel shape due to weed growth, sedimentation, erosion, measurement collection and the presence of a bypassing flow. Several different methods exist to deal with this issue, including traditional statistical methods (Petersen-Øverleir and Reitan, 2005) where uncertainty is estimated from the residual variance of a regression function, and Bayesian methods (Juston et al., 2014) where hydraulic knowledge is incorporated prior to the rating-curve and non-parametric regression methods. For the Bayesian methods, temporal changes in the rating curves are used to pool groups of stage-discharge measurements and rating curves are fitted using a multi-sectional approach (Coxon et al., 2015).

Discharge data can be also simulated via hydrological models from local to global scales (e.g. Doll et al., 2003; Lane et al., 2019). At continental scales, there are two

popular public services that have contributed to monitor and predict floods i) the European Flood Awareness System (EFAS) (Thielen et al., 2009) and ii) the Global Flood Awareness System (GLOFAS) (Alfieri et al., 2013). Both are part of the European Commission Copernicus Emergency Management Service and have provide useful information on flood monitoring and forecasting using simulated discharge data. Other continental to global scale simulated discharge data sets include Cama-Flood (Yamazaki et al., 2011, 2012), PCR-GLOBWB (PCRaster Global Water Balance van Beek et al., 2011; Sutanudjaja et al., 2018) and more not mentioned here. Simulated discharge data have been largely used in flood modelling. Indeed, cascading from rainfall to floodplain dynamics is a pivotal component of any flood forecast and flood risk analysis (e.g. Bonnifait et al., 2009; Grimaldi et al., 2019; Komi et al., 2017; Pappenberger et al., 2005).

2.4.6. Flood protection standards

At continental scale, it is still very difficult to obtain detailed information about flood protection infrastructure in main rivers and channels. This information is critical to produce accurate flood hazard maps at any scale. The reason is because typically countries have flood protections in place for the most frequent return periods (i.e. 1 in 5 yrs., 1 in 10 yrs.) preventing flood inundation of events of such magnitudes. If flood defences are not taken into account, the modelling framework will overestimate the hazard. Most countries do not release flood defence data publicly, with some exceptions (e.g. The UK and US). Thus, most studies have made estimates of flood protection standards using other types of data as a proxy. Sampson et al., (2015) detailed a methodology to develop estimates of flood protection standards based on GDP per capita or population density. Jongman et al., (2014) used instead catchment level descriptors based on potential losses from an insurance database. At global scale, Scussolini et al., (2016) presented FLOPROS, which is a global database that contains empirical information about the 'actual' standard of existing protection already in place, the standard protection based on policy regulations and for countries where this information is not available the data set includes a modelled standard of protection. The modelled standard of protections was calculated using a combination of GDP per capita along with simulated flood risk from the GLOFRIS framework (Ward

et al., 2013; Winsemius et al., 2013). Most recently, flood defences have been extracted from high resolution DEMs such the case of National Elevation Dataset (NED) where resolution can go up to 3 m in some places. Wing et al., 2019 developed an automatic algorithm to extract flood defences using a machine learning based approach. In this approach, defences from known places are used to train a machine learning model that can be used to help detect location of flood defences elsewhere.

2.5. Recent developments

Most of the continental to global scale flood modelling studies can fit within two broad categories. First, flood modelling to map the hazard associated with a given probability (or return period, recurrence interval). Second, flood modelling to map the evolution of inundated areas over long periods of time (i.e. hindcasts of flood inundtion). In the first type of modelling boundary conditions are given typically in the form of flows for a given probability. For this, a regional flood frequency analysis approach can be carried out (Smith et al., 2015). Alternatively, an approach that involves cascading a climate reanalysis dataset cascaded through atmospheric and land surface models is possible (e.g. Pappenberger et al., 2012; Winsemius et al., 2013; Yamazaki et al., 2011). For the second problem, flood modelling simulation over long periods of time uses as boundary conditions a continuous time series of flow estimates, usually provided by in-situ gauge stations (e.g. Global Runoff Database GRDC) or a rainfall-runoff models (e.g. Global Flood Awareness System GloFAS www.globalfloods.eu, European Flood Awareness System EFAS www.efas.eu)

Flood hazard modelling has received significant attention during the last decade. Several contributions have marked pivotal achievements for continental-scale flood modelling at high resolution (grid cell <1 km). For example, Winsemius et al., (2013) presented a global river flood risk framework that maps flood hazard by combining a hydrological model for boundary conditions, a flood-routing model to simulate channel hydrodynamics and an inundation downscaling routine to predict flood depths at ~1 km spatial resolution. Alfieri et al., (2014) introduced a higher resolution flood

hazard model (~100 m) limited to Europe only, which similarly used a hydrological model to obtain boundary conditions. However, in this study inundated area was calculated using a 2D hydrodynamic model although river channels were not explicitly represented. Sampson et al., (2015) used a 2D hydrodynamic model which directly represented river channels as sub-grid scale features that substantially improved channel hydrodynamics to produce estimates of global flood hazard for a variety of return periods at ~90 m resolution. Dottori et al., (2016) presented another global model using a 2D hydrodynamic model that solves the Saint-Venant Equations using the formulation implemented in LISFLOOD-FP, but following a cellular-automaton finite volume approach. Despite the emergence of a large number of continental models, Trigg et al., 2016 showed that their output flood extent only agreed by between 30% - 40% when several models were compared in Africa. The disagreement can be attributed to differences in the structure of modelling framework (e.g. resolution, treatment of vegetation, process to treat river channels) and the methodology applied. For example, some frameworks used a series of discharge gauging stations within a regional flood frequency approach to obtain boundary conditions, others instead used climate model reanalysis followed by a hydrological model to obtain boundary conditions.

Data availability has been central to the creation of high resolutions models. As the resolution increases, additional data can be ingested in modelling frameworks to improve the representation of modelled inundated areas. Such is the case in the US where a vast amount of data is available, including a consistent source of DEM, a great collection of gauges stations and a levees database. Wing et al., (2017) created a flood hazard model for the contiguous US at 30 m by including in the framework additional water control structures such as levees. The resolution of the model was high enough to depict the population exposed to flooding (Wing et al., 2018).

Flood modelling simulation over time has received less attention. Progress here has been delayed by the lack of boundary condition data in the form of consistent, long term discharge time series and formal modelling frameworks. Schumann et al., (2016) introduced a framework that maps daily flood inundation in Australia at 90 m resolution. The study used 40 stream gauges coupled to a hydrodynamic model to create 40 years of flood depth times series in 13 river basins. The study had some limitations, for example, ungauged tributaries were not considered, and flood defences were not taken into account.

This is only a brief summary of recent developments in the field, more progress is introduced in Chapter 3, 4 and 5.

2.6. Chapter Summary

This chapter presents an overall view of continental-scale flood modelling. Section 2.1 presents an introduction of the subject. Section 2.2 discusses two types of hydrodynamic models used in these studies and their governing equations. Sections 2.3 details the 2D hydrodynamic model LISFLOOD-FP and its numerical scheme. Section 2.4 briefly describes data sets used in continental-scale flood modelling and Section 2.5 reviews recent developments in continental-scale flood studies. The next three chapters present results chapters to address the objectives and research questions from Section 1.2.

CHAPTER 3

A toolbox to quickly prepare flood inundation models for LISFLOOD-FP simulations

As noted in the Chapter 1, there is still a need to streamline the deployment of continental-scale flood studies in a fast, simple and methodology-consistent way. This chapter introduces a new software package that helps to accomplish this. The main problem arises as the data input for flood models comes in a variety of forms (i.e. grid resolution, data format, geographical projection). Despite the fact that data can be shaped to the user's problem using GUI interfaces such QGIS or ArcGIS, this is only achievable after several hours of manual editing, an even harder task if the problem is at continental scales. In this chapter the development of LFPtools is presented, an open-source Python package which encompasses most commonly used methods to prepare input data for continental scale flood studies and automatise data preparation for the LISFLOOD-FP hydrodynamic model.

This chapter consists of a paper published in Environmental Modelling & Software. All the source code development and original idea was carried out by the lead author. Christopher Sampson and Andrew Smith contributed suggestions for some methods. All co-authors provided text suggestions to improve the final manuscript.

Peer-reviewed article associated with this chapter:
Sosa, J., Sampson, C., Smith, A., Neal, J., Bates, P. (2019). A toolbox to quickly prepare flood inundation models for LISFLOOD-FP simulations. *Environmental Modelling & Software*, 104561. doi.org/10.1016/j.envsoft.2019.104561. Source code: http://github.com/jsosa/lfptools

3.1 Introduction

Hydrodynamic models designed to simulate floodplain inundation have been popular for many years and are widely used in engineering applications. These models, such as TUFLOW (Syme, 1991), JFLOW (Bradbrook et al., 2004), TRENT (Villanueva and Wright, 2006), LISFLOOD-FP (Bates et al., 2010), TELEMAC-2D (Moulinec et al., 2011) or PRIMO (Sanders and Schubert, 2019) route water through channels and floodplains following shallow water flow theory.

Global to continental scale flood studies are being used for insurers, multi-national corporations, NGOs and national governments. They have been made possible as a result of the appearance of global coverage datasets of terrain elevation (Farr et al., 2007; Tadono et al., 2015; Yamazaki et al., 2017; Rizzoli et al., 2017, Wessel et al., 2018), hydrography (Lehner et al., 2008; Yamazaki et al., 2019) and river width based on simple hydraulic geometry equations (Andreadis et al., 2013) or based on the analysis of the Landsat repository (Yamazaki et al., 2014; Allen and Pavelsky, 2018). These data sets, coupled with the parallel development of efficient two-dimensional flood models such as LISFLOOD-FP or TELEMAC-2D and advances in computational power (Neal et al., 2018; Lamb et al., 2009), have led to the implementation of flood inundation studies in data-sparse areas around the world at very high resolutions (10^2-10^3 m). As consequence, a variety of applications involving flood hydrodynamic variables (e.g., flood extent, water depth, flow velocity, flow discharge) have been explored. These applications range from flood risk assessment (see e.g. Wing et al., 2018; Winsemius et al., 2013), early warning systems (see e.g. Dottori et al., 2017), climate change scenarios (see e.g. Alfieri et al., 2018), hind-cast simulations (see e.g. Schumann et al., 2016) to biogeochemistry (see e.g. Lu et al., 2016).

Building a flood model can be time-consuming since input data need to be processed from a variety different sources and adapted to a particular user's problem. The increasing quantity, complexity and resolution of useful datasets imparts an ever-growing burden of knowledge on model developers. Furthermore, the frequent update cycles of some datasets can cause module builds to go out of date quickly. Therefore, developing a flood inundation model requires a high level of skill in handling geographical information using Graphical User Interface (GUI) driven software packages

such as ArcGIS and QGIS. These present a workable solution for the treatment of data, but typically only at small-scales due to their high demands for computing resource and user intervention. Instead, at continental-scale command line interface (CLI) software packages are the best candidates for the preparation of flood inundation models since they provide robustness and computational efficiency. CLI packages can also be simpler and more streamlined than general GIS software, providing only the functionality that users need and thus making sophisticated flood inundation modelling more accessible to specialist users.

In this chapter we present *LFPtools*, a Python CLI package which attempts to encompass the most commonly used methods to prepare input data for flood inundation studies using LISFLOOD-FP and are described in detail here (Sampson et al., 2015; Schumann et al., 2013; Hawker et al., 2018). Among the capabilities LFPtools can provide are: DEM upscaling, bank elevation estimation, bed elevation estimation, river width subtraction and interpolation, elevation smoothing algorithms, continent basin splitting, and more. Whilst the software has been built specifically for the LISFLOOD-FP model, many of the operations it encodes are useful for a wide range of other flood inundation models, especially those operating on regular grids. LFPtools can act as an intermediate platform to streamline the preparation of local, continental or global flood inundation studies in different fields by bringing ease of use to non-expert users and efficiency to expert ones. For example, new experimental studies on hydrological-hydrodynamic modelling, sensitivity analysis (SAFE Toolbox Pianosi et al., 2015; SALib Herman et al, 2017) will be achievable more straightforwardly. LFPtools is open-source and presents a series of tools to estimate the variables required for flood inundation modelling in rapid and automated manner. As open-source, users can revise the code, modify or add new methods easily and transparently. The tools were verified over the Severn basin where a 1 km flood inundation model was built in under 2 minutes on a standard laptop (1.6 GHz Intel Core i5; 8 GB 1600 MHz DDR3).

3.2 Methods

The LFPtools package is written in Python and built on top of well-known open-source libraries: GDAL (gdal.org), Cython (cython.org), Pandas (pandas.pydata.org), Numpy (numpy.org) and xarray (xarray.pydata.org). The TauDEM toolbox (Tarboton, 2005) is also required for some functionalities. The library handles I/O

operations via well-known file formats such as ESRI Shapefiles and GeoTIFF. The code is publicly available is available at http://github.com/jsosa/lfptools

3.2.1 Floodplain elevations

Floodplain elevations define the grid output resolution. Those elevations can be obtained directly using a Digital Elevation Model (DEM) as-is (i.e., at native resolution). Alternatively, if the native DEM contains noise, usually derived from instrument error, upscaling the native data will reduce that noise in a coarser floodplain elevation grid, but may also smooth or loose important small scale elevation features (Neal et al., 2012; Hawker et al., 2018).

lfp-rasterresample is the program included in the library to upscale DEMs. The program can handle arrays of any size since it never loads entire arrays on memory but instead it loads a small portion of the array corresponding to the aggregation kernel to be upscaled. The program receives three inputs: a high-resolution DEM, a target resolution mask and a searching window threshold. Only cells with `mask=1` will be considered for calculation. The upscaling method is described as follows:

1. A user-defined threshold is applied to a centre cell of the target mask to lump together high-resolution values.
2. A modified z-score (Iglewicz and Hoaglin, 1993; based on the median absolute deviation) is calculated for every DEM cell in the kernel. *z-score* values larger than 3.5 are identified as outliers and subsequently removed from the aggregation kernel.
3. In the aggregation kernel, different reduction algorithms can be applied (e.g., `mean`, `min`, `meanmin`). `meanmin` is an interesting reduction method which averages the minimum and mean values from the kernel and emphasises topographic valleys in the calculation. Important to mention that more reduction algorithms can be easily added in the source code by users should they be required.

Step 2 is important to consider since native DEMs might present irregularities in some places. For example, in development testing a disagreement was found in the aggregation kernel for a target cell in the Seine River using the native ~90 m resolution MERIT DEM. In particular, some strong negative values (~-10 m) were found in an

area where the typical topographic elevation was ~30 m (See Figure 3.1). The automatic detection algorithm in Step 2 prevents inclusion of these values before step 3.

Different aggregation methods from Step 3 are compared for a small part of the River Thames using the toolbox in Figure 3.2

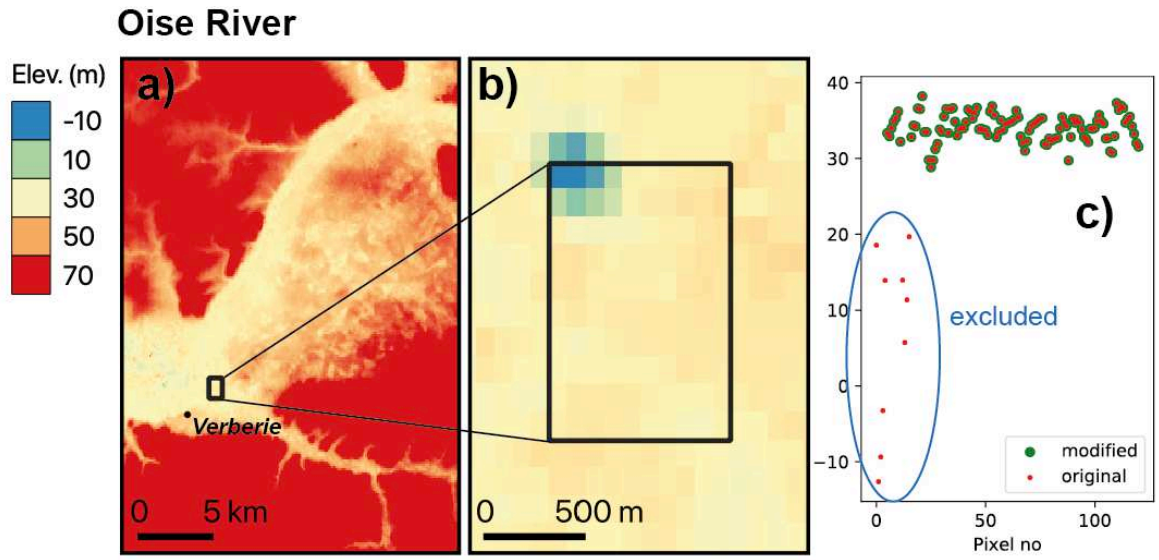

Figure 3.1. Outlier detection procedure: **a)** original 90 m resolution DEM and aggregation kernel (in black), **b)** zoom-in at aggregation kernel (area ~1 km^2) and **c)** automatic detection of outliers in kernel (in green) points retained for upscaling and (in red) all points.

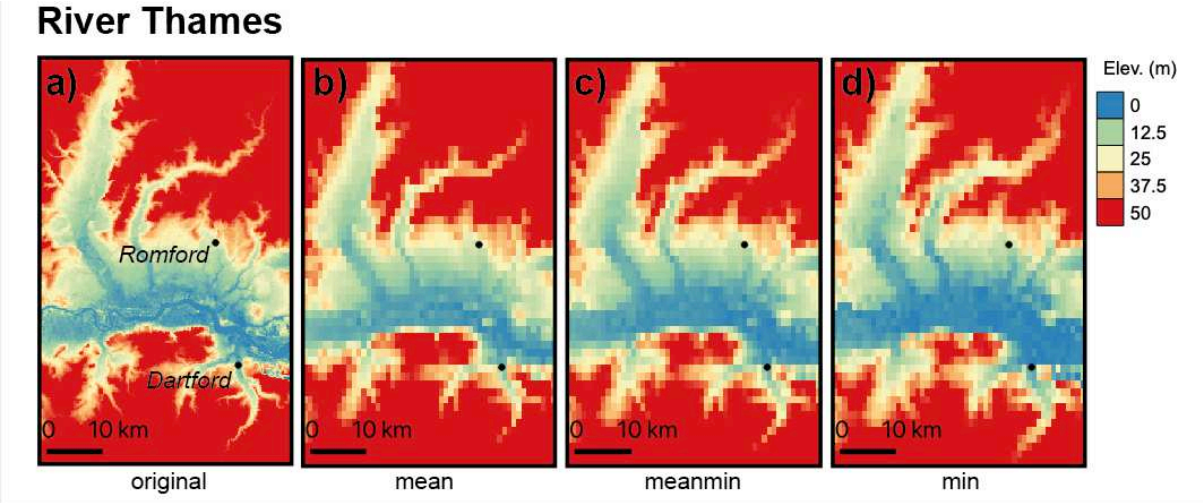

Figure 3.2. Upscaling methods comparison at 1 km resolution: **a)** original 90 m resolution DEM, **b)** `mean` aggregation, **c)** `meanmin` aggregation and **d)** `min` aggregation

3.2.2 Channel widths

LISFLOOD-FP Sub-Grid needs several input variables to run a flood simulation, one of which is river width estimates at every cell in the river network. With the appearance of global river width data sets based on remote sensing techniques (GWD-LR Yamazaki et al., 2014; GRWL Allen and Pavelsky 2018) and empirical formulations (Andreadis et al., 2013) it is now feasible to use these data sets as width sources in flood studies for data-sparse regions.

Global river width databases may have some degree of geolocation shift in relation to the corresponding rivers extracted from hydrography databases making them difficult to use in their native format. This problem may appear if these databases are derived from different sources or due to resolution dissimilarity; for example, DEM derived river networks and remotely sensed open water locations. Commonly, a nearest neighbour function in a searching window is used to assign the nearest value from a river width database to a river cell in a flood study. However, there might be cases where the searching window is too small and no width values are found, in this case increasing the window size is not an appealing option since it might result in an incorrect river width assignment from a tributary. Instead, it is advisable to use an interpolation with values already assigned. It is important to note that leaving a river cell with no width assigned is a critical issue since LISFLOOD-FP Sub-Grid cannot perform calculations on river cells with zero width.

LFPtools includes a routine (*lfp-getwidths*) to automatically assign width values to river cells, it works in the following way:

1. River cell widths are assigned based on the nearest neighbour within a searching window.
2. If no width value is assigned from the source database, the missing value is automatically interpolated with values already assigned.

Figure 3.3 shows an example of three river cells with widths unassigned due to the searching window size problem. Figure 3.3-a shows a river reach (blue) at ~1 km, red dots are centroids of river cells and the black solid line is river vector from the GRWL database (~30 m). From the figure only three points (*A*, *B*, *C*) were not able to find an

appropriate width value in their neighbourhood (red dash line), those values were automatically calculated by interpolation in *lfp-getwidths* see Figure 3.3-b

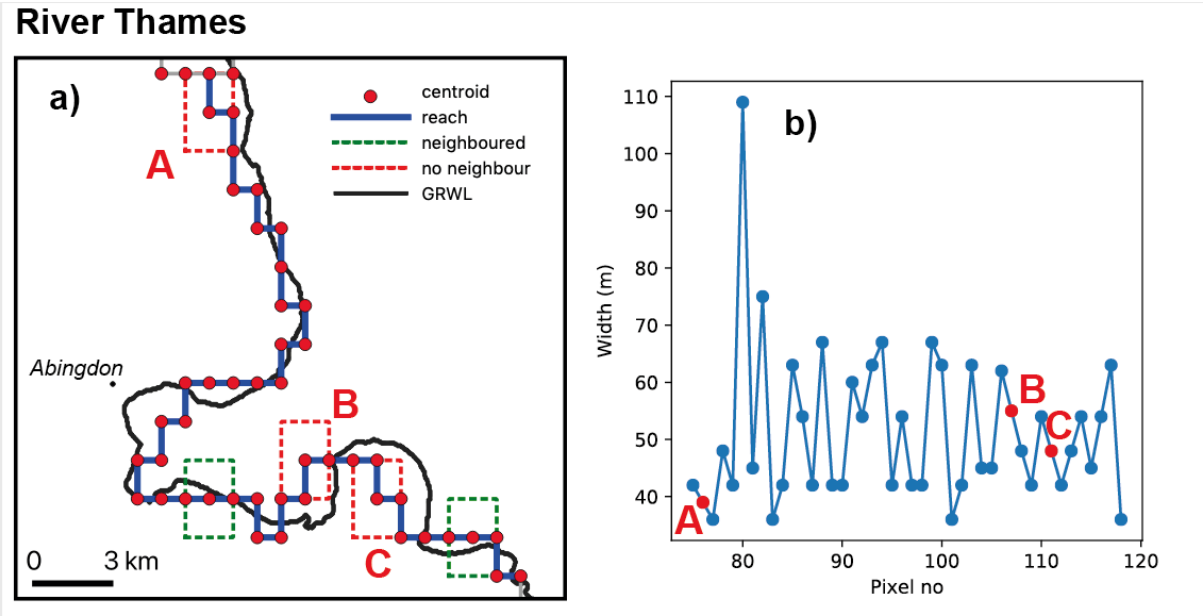

Figure 3.3. River widths assignment: **a)** Example showing three river cells unassigned due to small size in searching window at locations A, B and C and **b)** (in blue) width values that yield in the searching window (in red) width values interpolated.

3.2.3 Bank elevations

The LISFLOOD-FP Sub-Grid uses the DEM elevation as the bank height elevations, which when combined with the channel bed elevation defines the channel bankfull depth. It is therefore recommended to recalculate the bank height elevations to get better estimates because of the critical role this value plays in flooding simulations.

If a native resolution DEM is used, bank height elevations are self-defined. However, if a coarser resolution model is created, high-resolution cell aggregation is required. *lfp-getbankelevs* reads a target river network mask (`mask=1` will be considered for calculation), a high-resolution DEM, and a searching window threshold to aggregate cells and apply a reduction algorithm (`nearest`, `mean`, `min`, `meanmin`). Resulting elevations might contain irregularities that may result in model instabilities caused by local supercritical flows and flow blocking effects if the channel bed follows the banks. Those irregularities can be solved by applying a smoothing algorithm along the river.

LFPtools includes a routine (*lfp-fixelevs*) which includes two approaches to deal with this problem:

1. Adjust bank heights by minimising the amount of modifications following the method developed by Yamazaki et al., (2012). This algorithm removes all the pits in the spaceborne DEM caused by vegetation canopies, sub-pixel sized structures, and random radar speckles while minimizing the amount of modification required for removing the pits.
2. Apply a weighted local regression (LOWLESS) (Cleveland, 1979) in the downstream direction as in Schumann et al., (2013).

Both methods are compared for the main channel of the River Thames, UK in Figure 3.4-b

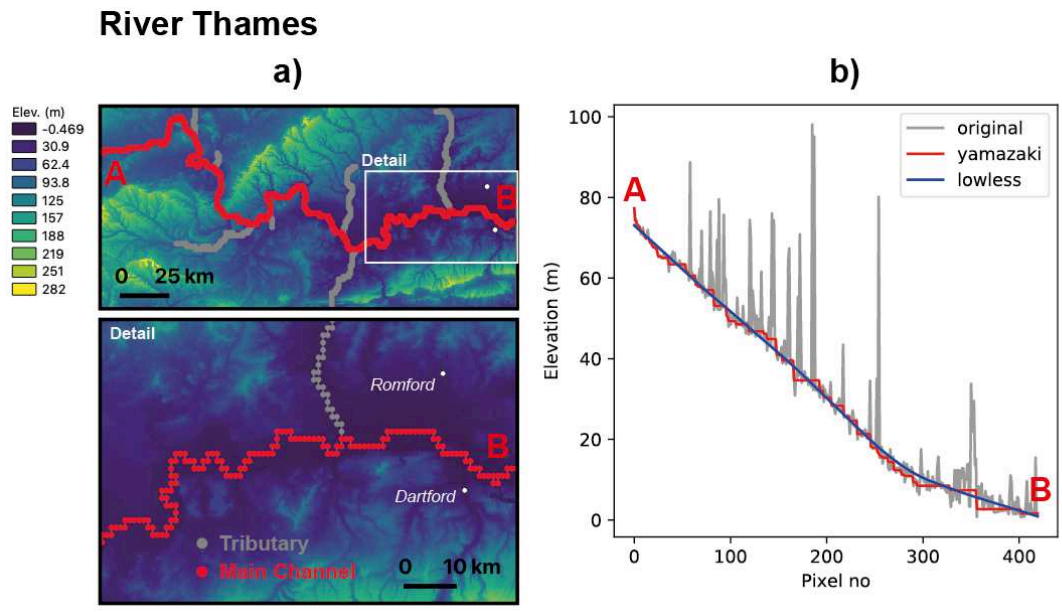

Figure 3.4. Smoothing method available in LFPtools. These methods were applied to the main channel of the River Thames: **a)** (in red) main channel of the River Thames and (in grey) tributaries, **b)** (in grey) original elevation extracted by the nearest-neighbour (in red) Yamazaki's method (in blue) Locally weighted smoothing.

3.2.4 River depths

Standard LISFLOOD-FP Sub-Grid treats river cross-sections as rectangular. Due to this fact channel depths may differ from in-situ river depth surveys. With some calibration this approximation works very well at large scales producing reasonable results in most places as long as accurate estimations of bank heights and widths are used. Unlike bank heights and river widths that can be determined from satellite data,

river depths need to be approximated. Two approaches have been proposed to achieve this goal and are included *lfp-getdepths* i) a simple empirical power law formulation (Neal et al., 2012) ii) the Manning's equation (Sampson et al., 2015). A user-defined raster (e.g., survey data on river bathymetry) can also be used to assign depths to cells if none of the previous methods are used.

3.2.4.1 Power law relationship

Leopold and Maddock (1953) derived a series of power law relationships given by Equation 3.1-3.3 where W is water-surface width, Q is discharge, D is mean depth and V is mean velocity.

$$W = aQ^b \qquad (3.1)$$

$$D = cQ^f \qquad (3.2)$$

$$V = kQ^m \qquad (3.3)$$

It is straightforward to equate Equation 3.1-3.2 to obtain Equation 3.4

$$D = \left(\frac{c}{a^{f/b}}\right) W^{f/b} \qquad (3.4)$$

where (a, b, c, f) are empirical values depending on the geomorphology of the bed.

Sometimes it is preferred to use only one pair of constants (r,p) as in Equation 3.5. See Hey and Thorne (1986) for empirical values for gravel-bed rivers in the UK.

$$D = rW^p \qquad (3.5)$$

3.2.4.2 Manning's equation

The Manning's equation for a rectangular channel is described by Equation 3.6 where A is the cross-section area expressed as $A = WD$ with W width and D depth, R is the hydraulic radius $R = A/(W + 2D)$, S is the channel cell slope (i.e., it can be calculated via *lfp-slopes* or directly extracted from an external data set (Cohen et al., 2018) n is the Manning's coefficient and Q_{bf} is the bankfull flow.

$$Q_{bf} = \frac{AR^{2/3}S^{1/2}}{n} \qquad (3.6)$$

The Manning's equation considers bankfull flow Q_{bf} as a known variable, however it is not always the case. If not measured in the field, bankfull flow is usually estimated by fitting a statistical distribution on the annual flow peaks of a streamflow time series where bankfull conditions occur at return periods of 1.5-2 years (Scheneider et al., 2011). Figure 3.5 shows the aforementioned procedure for the Kingston gauging station from the National River Flow Archive (NRFA) on the River Thames, UK.

A comparison between the Power law relationship and Manning's equation is presented for the River Thames in Figure 3.6. Bankfull flow (yellow dots) was obtained by subtracting the 2-year return period in a Pearson Type III distribution fitted on the annual maxima time series derived by means of a 24-year streamflow reanalysis from the European Forecasting Awareness System (EFAS) (Thielen et al., 2009). River width estimates used in Equation 3.5 were obtained from the GRWL database using *lfp-getwidths*. At locations where no-bankfull width is available, the nearest bankfull value was assigned. Figure 3.6-c shows (in grey) bank elevations after smoothing in the main channel, (in blue) bed elevations (i.e., bank elevation *minus* depth) using the Manning's Equation 3.6 and (in red) using the power law relationship Equation 3.5. A zoom for the downstream section is shown in Figure 3.6-c and reveals considerable differences in the delta area.

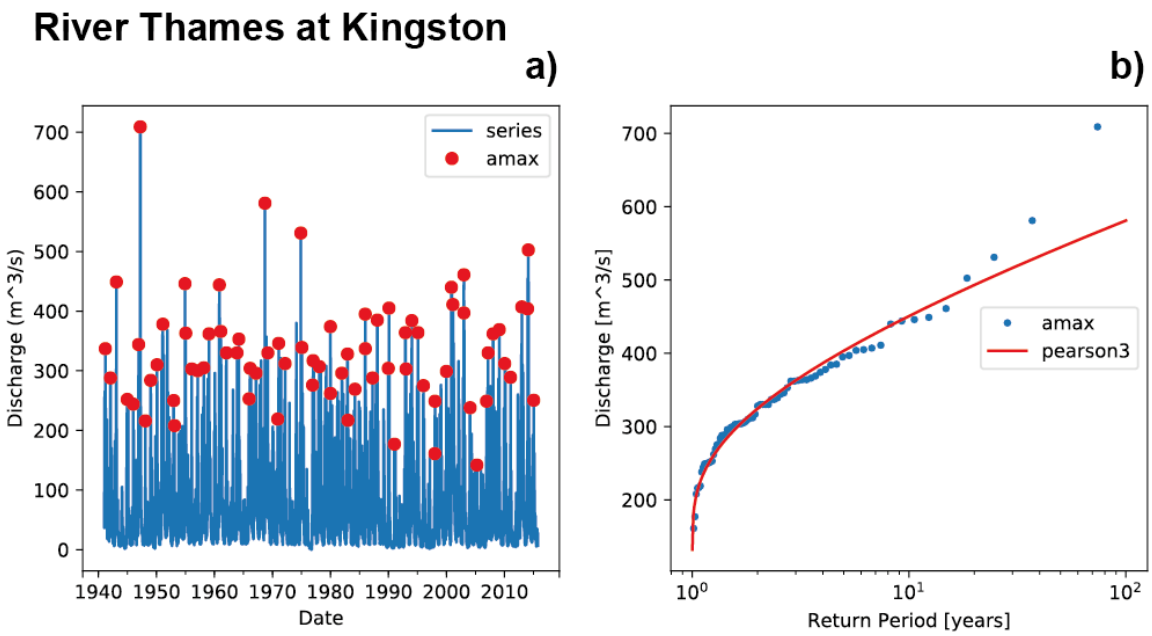

Figure 3.5. Observed river discharge in the River Thames at Kingston Station. Bankfull was estimated by fitting a statistical distribution on the annual maxima and retrieving the discharge value for the 2-yr return period: **a)** annual maxima between 1940-2015 (red dots). **b)** Pearson Type III distribution fitted on the annual maxima (red line), here the distribution parameters were estimated via L-moments. This figure was generated by using the *hydroutils* library (code available at http://github.com/jsosa/hydroutils).

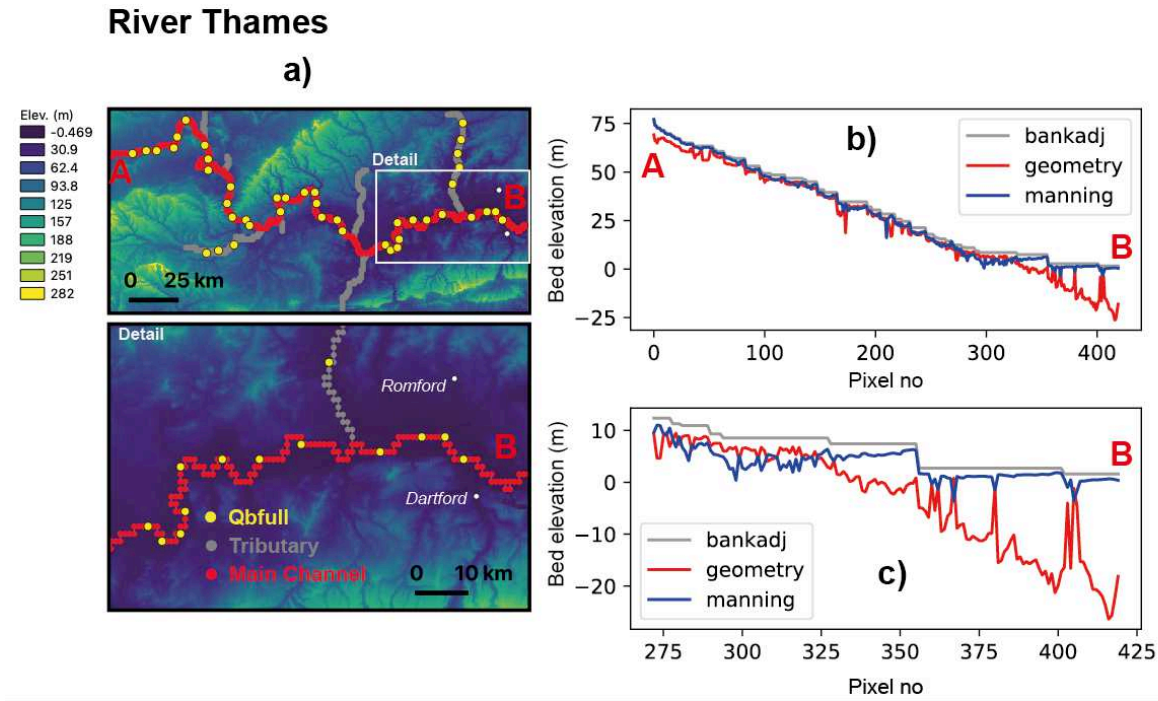

Figure 3.6. River depth estimation using hydraulic geometry equations and Manning's equation: **a)** River Thames (in red) tributaries (in grey), **b)** depth estimation via hydraulic geometry (in red) and

Manning's equation (in blue) for the lower part of the River Thames and **c)** zoom-in delta area of the River Thames.

3.2.5 Continental tools

The library includes two programs designed to automate delineation of basins within large regions *lfp-prepdata* and *lfp-split*.

lfp-prepdata incorporates a subroutine to clip global data sets of DEM, hydrography and river width based on a user-defined extent. Thereafter, a user-defined threshold is applied to the flow accumulation area (or upslope drainage area) to define a river network. The TauDEM toolbox (Tarboton, 2005) is used to generate a network topological connectivity for the whole area and to delineate basins within the region (`NNN_Tree.csv`, `NNN_Coord.csv` and `NNN_Rec.csv` in Figure 3.7). The routine also includes a function to convert D8 connected river networks to D4 connectivity based on the flow directions map given by the hydrography. *lfp-split* breaks up the region into individual basins with a basin-number associated. Folders are created with a basin-number and each of them contains clipped data associated with that basin. After basin required data is split in this way the tools described in Sections 3.2.1-3.2.4 can be applied. Figure 3.7 shows a flowchart describing how the tools can connect to each other to automatically build models at continental-scale.

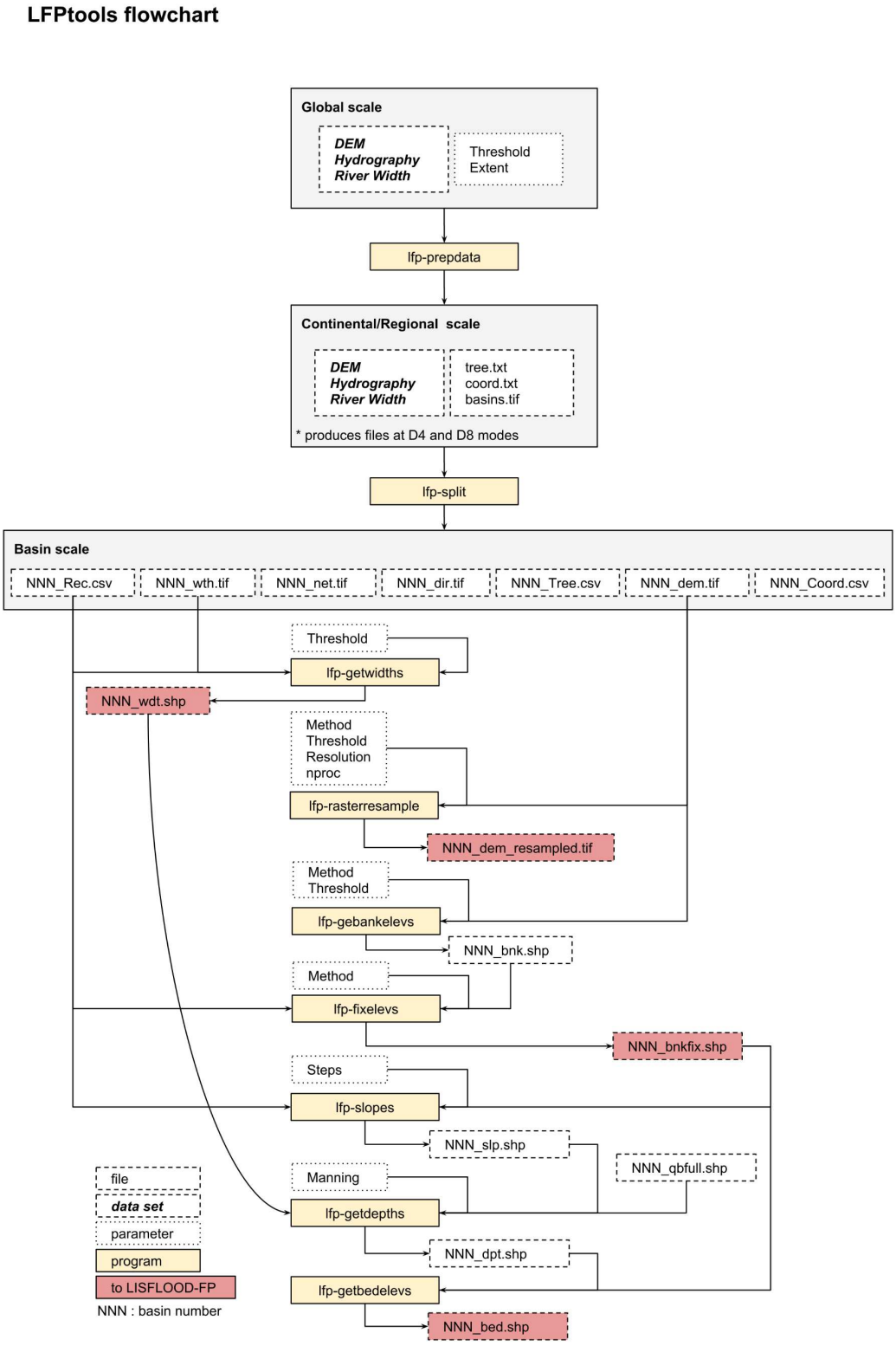

Figure 3.7. Flowchart using LFPtools for continental-scale studies. Command-line tools are presented in yellow boxes, white dashed boxes represent input data sets and white dotted boxes free parameters. Outputs to LISFLOOD-FP are coloured in red.

3.2.6 Usage

In order to facilitate the use of the tools LFPtools can be called via command-line, however if preferred it can also be imported as a Python module. All tools can be invoked via the command line by typing the name of the tool followed by the `-i` keyword and the name of the configuration file:

```
$ lfp-getwidths -i config.txt
```

where the configuration file `config.txt` is a text file containing a `[tool-name]` header followed by `variable=argument` entries. Input variable descriptions are specified when typing the name of the tool in the command-line followed by the `–h` keyword:

```
$ lfp-getwidths -h
```

LFPtools can be imported as a Python module as follows:

```
import lfptools as lfp
```

An overview of tools with a brief description is given in Table 3.1.

Program	**Description**
lfp-depths	Get estimates of depth
lfp-fixelevs	Smooth elevations
lfp-getbankelevs	Retrieve bank elevations
lfp-slopes	Estimate slopes in a river network
lfp-getwidths	Retrieve river widths
lfp-rasterresample	Upscale a high-resolution DEM into a user-defined resolution
lfp-split	Breaks up a study area in individual basins with a basin number associated
lfp-prepdata	Clip global data sets given a user-defined extent and threshold. The threshold is used to define a river network based on the upslope area

Table 3.1. Summary of programs in LFPtools

3.3 Results

3.3.1 A flood inundation model for the Severn River in England, UK

LFPTools was used to build a flood inundation model for the Severn river basin in the UK. A one-month simulation (April 1998) was undertaken in order to capture an observed flood event that happened during this period. An additional one-month *warm-up* period was included to bring the model into a hydraulic steady state condition prior to the commencement of the April 1998 period. The model was built from LIDAR-based terrain data (at 90 m resolution) where the floodplain terrain was upscaled to 1 km resolution using the `mean` aggregation method and removing outliers. Bank heights were defined using the *nearest neighbour* method. River channels were explicitly represented using HydroSHEDS (Lehner et al., 2008) as input hydrography at 1 km resolution. Channel widths were retrieved from the GRWL database while river depths were estimated through the hydraulic geometry method (Equation 3.5) with $r = 0.12$ and $p = 0.78$. The model was forced using daily gauged flows from the UK National River Flow Archive (NRFA) for the simulation period mentioned before. Data sources used in this study are briefly described in Table 3.2.

Data set	Description	Source
LIDAR DTM	Composite at 1 m resolution	Data available at `data.gov.uk`
HydroSHEDS (Lehner et al., 2018)	Hydrography at 1 km resolution	Data available at `hydrosheds.org`
GRWL (Allen and Pavelsky, 2018)	Landsat-based global river width database at 30 m resolution	Data available at `https://zenodo.org/record/1297434`
NRFA	Streamflow data from gauge stations	Data available at `nrfa.ceh.ac.uk`
Recorded Flood Outlines for UK	Records of historic flooding from rivers, the sea, groundwater and surface water	Data available at `data.gov.uk`

Table 3.2. Data sets used to build the flood inundation model in the Severn river basin

Resulting water depths from LISFLOOD-FP at 1 km resolution were subsequently downscaled onto 90 m resolution using an algorithm similar to Schumann et al., 2014.

In particular, the algorithm takes water surface elevation (WSE) at 1 km resolution and subtracts its corresponding 90 m DEM values. From this arithmetic operation, a grid at 90 m resolution is created with positive values representing the water depth (wet cells) whilst negative values (dry cells) are replaced with `nodata` values.

The performance of flood model in the Severn river basin in terms of flood extent was quantified using three scores: Hit rate (H), Falsa alarm ratio (F) and Critical success index (C). *H* tests the tendency of the model towards underprediction and can range from 0 (none of the wet benchmark data is wet model data) to 1 (all of the wet benchmark data are wet model data). *F* examines the tendency of the model towards overprediction and can range from 0 (no false alarms) to 1 (all false alarms). *C* accounts for both overprediction and underprediction and can range from 0 (no match between modelled and benchmark data) to 1 (perfect match between modelled and benchmark data). A detailed explanation of these scores is available in Wing et al., 2017.

Simulated water depth results for the 15th April 1998 are shown in Figure 3.8. From the figure is clear that in most places water remains in the channel and where water elevations exceed bankfull heights water spreads onto the floodplains. Simulated water depth on the 15th April 1998 were compared with the official event footprint from the English Environment Agency (EA) and the "Agreement" between both flood extents are presented in the Figure 3.8 right-hand panel. The "Agreement" in Figure 3.8 refers to areas in the map where the EA flood extent and the simulated flood extent overlap each other. In terms of flood extent, the model obtained satisfactory comparison scores against observations: $H = 0.79$, $F = 0.24$ and $C = 0.63$.

Example files are available at the LFPtools web repository
`http://github.com/jsosa/lfptools`

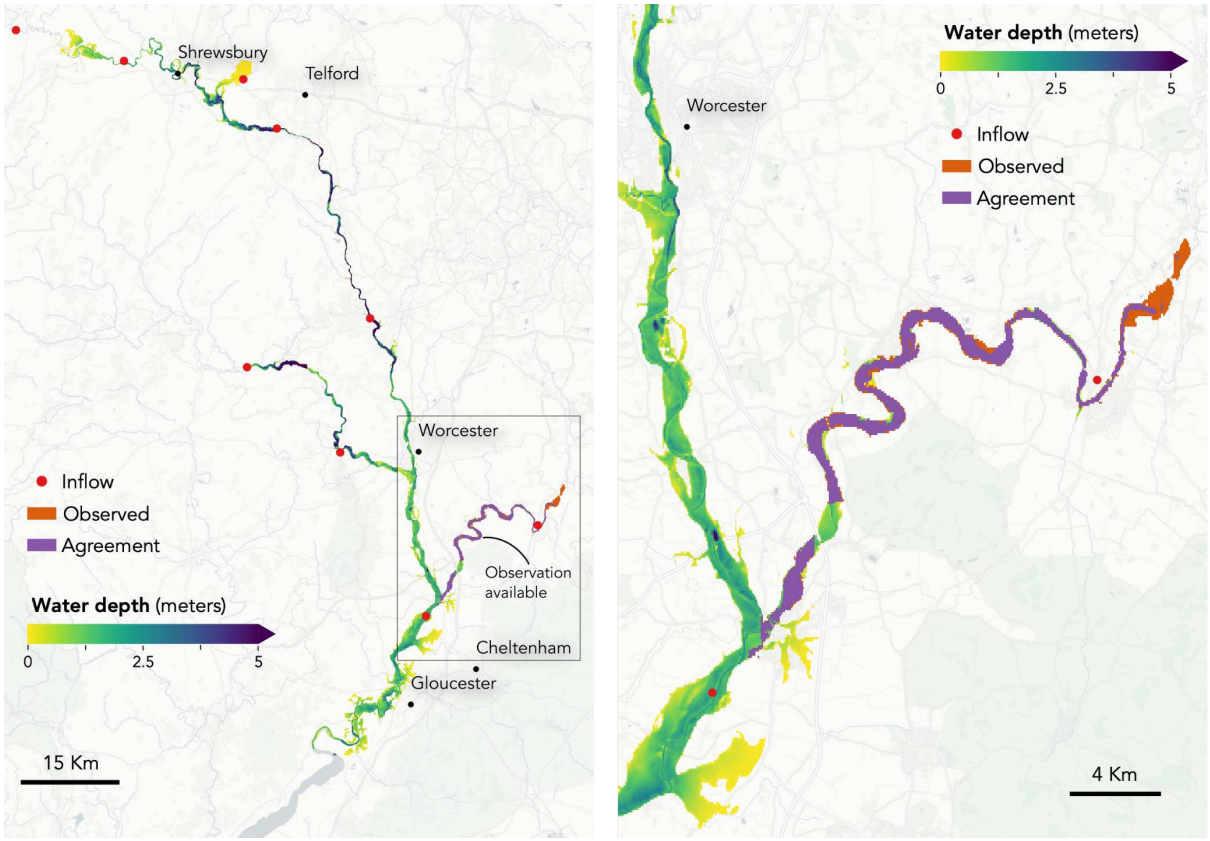

Figure 3.8. Flood inundation model prepared for the Severn basin in England, UK during the flood event of April 1998. The event was compared with official footprint of the event (orange). The agreement between the model and the output is also shown (purple). Note that the observed data only cover limited portions of the model domain which are not contiguous. In areas with no observed data we simply plot the modelled water depth. Also, the moderately low *Hit Rates* occur since the observed flood extent area is upstream of the inflow point (East of the domain in the right-hand panel), hence, no forcing data is available to predict water depths in that area.

3.4 Conclusion

A Python CLI package has been developed to help prepare input data for flood studies carried out using LISFLOOD-FP. The package encompasses the most frequently used methods for flood inundation modelling data preparation, and also facilitates the addition of new ones if desired. LFPtools can be thought of as a platform to streamline the preparation of flood inundation studies in different fields by bringing ease of use to non-expert users and efficiency to expert ones. It is built on top of the state-of-the-art Python libraries to handle large sets of data and it is in active development. It is important to mention that these tasks could be done in a GIS package, but only with quite extreme difficulty and for small data arrays. The tasks performed by LFPtools

are generic for structured grids and can be used to prepare input data sets for any hydraulic model.

LFPtools programs were verified in the UK's Severn basin on a model built at 1 km resolution using publicly available data sets only. The test basin was used to simulate the event of April 1998 and results are presented in Figure 3.8. From the figure it is clear that most of the water is kept in channels with some places inundated suggesting a normal hydrodynamic behaviour. After comparison, the model obtained satisfactory scores against the official event footprint: $H = 0.79$, $F = 0.24$ and $C = 0.63$. It is important to mention that the Severn scenario was used only to broadly test the tools and not to simulate the real event to an engineering standard.

The Severn river basin used in this study is only a small example on how the tools can be employed and the tools have been designed so they can be integrated within a framework to build continental to global scale studies. For example, LFPtools can be used within a modelling framework to build a continental-scale flood hindcast or reanalysis, a modelling framework of continental-scale flood extent for an early warning system or even within a framework to predict flood inundation variables (flood extent, water depth, etc) in a climate change context.

Global to continental scale models are being used by insurers, multi-national corporations, NGOs and national governments to tackle problems such as rapid flood disaster response, urban planning and climate change adaptation. Thus, flood models at such scales are important decision-making tools and building them demands great effort to research scientists. We envisage that this innovative set of tools will help to significantly reduce these costs.

3.5 Postscript

This chapter presented the development of the software package LFPtools. The package facilitates the deployment of continental-scale flood studies in a seamless way. This suite of tools will enable novel science questions in the field, for example it can be integrated in a modelling chain to produce a flood inundation hindcast which is the subject of the Chapter 4. The tools were useful to identify potential source of errors in flood modelling, thus it became clear from the flood hindcast application that

current hydrography data sets need to be further developed for continental-scale applications, this forms the subject of the Chapter 5

CHAPTER 4

A flood inundation hindcast for Europe based on 26-year simulated river discharge

The previous chapter introduced, LFPtools, a software package to streamline the deployment of flood studies at continental scales. In this chapter, LFPtools is used to build a European Flood Hindcast. Such application would not be possible without this toolbox, it forms the basis of the computational framework facilitating quality control along the process in a consistent and efficient way. In particular, the development of an automated framework to produce a multi-decal flood time series for Europe at ~90 m resolution is introduced. Producing flood hindcasts at such resolution is a challenging problem which to date only Schumann et al., 2016 have tackled it. Here an alternative methodology is presented. The framework used best estimates of river geometry, flood protection standards and terrain information and it was forced by simulated river discharge. This chapter will explore concepts such as continental scale hydrodynamic modelling, hydrologic-hydrodynamic coupling, long time period simulations and flood standards integration in flood models.

This chapter consist of a paper submitted to *Water Resources Research*. All simulations, analysis, writing and figures were completed by the lead author with advice from Jeffrey Neal and Paul Bates. Peter Salamon and Dai Yamazaki contributed facilitating data accessibility to the EFAS streamflow and MERIT DEM data sets, respectively. All co-authors helped to shape the final manuscript.

Peer-reviewed article associated:

Sosa, J., Salamon, P., Yamazaki, D., Neal, J., Bates, P. (2020). A flood inundation hindcast for Europe based on 26-year simulated river discharge. *Water Resources Research*. Submitted

4.1 Introduction

Over recent decades Europe has suffered significant economic losses due to floods. Between 1990-2016, European countries reported around 140 billion EUR in financial losses (normalised to 2011 values) resulting from events which affected ~3.5 million people (Barredo, 2009; Paprotny et al. 2018b). Many of these events occurred during the flood-rich decade of the 1990s, but significant floods also occurred during the 2000s (Kundzewicz et al., 2013). The most severe floods have occurred in central Europe, with important events in 2002 and 2013 (Ulbrich et al., 2003; Blöschl et al., 2013), although the UK was also severely hit in 2000, 2005, 2007, 2012 and 2015/16 (Miller et al., 2013; Barker et al., 2016). The current changing climate, expressed in terms of increased precipitation in the region, has had a significant effect on flood occurrence in northwestern Europe (Bloschl et al., 2019), in addition there have been increases in exposure due to population growth and rapid urbanisation in floodplain zones.

A better understanding of areas exposed to floods at continental scales is still lacking, and is especially needed in Europe. Despite the ability of small scale studies to identify zones where population and assets are at risk (Castellarin et al., 2011; Vorogushyn et al., 2012; Ballesteros-Canovas et al., 2013), continental scale studies are needed for many classes of flood risk management decision, such as insurance, re-insurance and guiding governmental budget allocations for strategic investment in flood defences. Wide area models can place flooding hotspots in a broader context such that relevant institutions can allocate resources efficiently. This is paramount for the Europe Union, where the European Civil Protection Mechanism, a centralised mechanism for coordinating the response to disasters in Europe and beyond, is charged with planning and deploying state aid for flood relief (Pappenberger et al., 2015). Small scale studies also lack the ability to explain flood characteristics in transnational river basins. For instance, if a flood event occurs at the lower part of the Elbe basin (in Germany), its origins could lie in a flood event that took place a few days before in the upper part of the basin (in the Czech Republic). Thus, understanding flood timing and development at large scales can play an essential role in disaster preparedness. Because of this, the most effective way to treat flood management in transnational river basins is by adopting continental level strategies. This change in emphasis from local to large scale

assessment of flood risk has been said to require an 'evolutionary leap' in the approaches that are used (Vorogushyn et al., 2018).

Previous research that has focused on understanding the nature of European floods over time has typically been based on two different approaches. First, river discharge time series have been used to characterise floods, for example, in a climate change context (Hall and Bloschl, 2018; Bloschl et al., 2019; Bertola et al., 2020). Second, satellite imagery has been used to capture inundated areas over time (Kundzewicz et al., 2013). Both approaches can characterise floods, providing information on flood occurrence and inundated area respectively, however, their sampling in time and space can be sparse and they lack the ability to reveal information on inundation depth during a flood event. Flood depth information can be critical for disaster management, to plan insurance and re-insurance effectively, to improve urban planning and to inform floodplain ecological preservation. As a result, there is still a research need to explore changing patterns of inundation depths in time during floods at large scales.

One way to infer inundation depths is using hydrodynamic simulations where estimates of water depths are calculated using variants of the Shallow Water Equations (Bates et al., 2010; Moulinec et al., 2011; Sanders and Schubert, 2019). Efficient numerical models can allow estimation of flood inundation depths at continental and global levels at resolutions that can produce actionable information for flood risk management. For example, previous research has focused on the evaluation of flood inundation depths for different return periods in Europe (Alfieri et al., 2014; Paprotny et al., 2017), the US (Wing et al., 2017), Africa (Trigg et al., 2016) and globally (Winsemius et al., 2013; Sampson et al., 2015). Nonetheless, the limited literature and lack of a formal methodology for hindcasting studies have delayed the progress towards the production of flood depth time series over large areas and for multi-year or even multi-decadal periods. Schumann et al. (2016) produced the first continental level flood hindcast at 1 km resolution for Australia. This study used 40 gauge stations coupled to a hydrodynamic model to create 40 years of flood depth times series in 13 river basins. Despite its ground-breaking nature, this study had a number of limitations: only a very limited number of river gauge sites were used, ungauged tributaries were not considered, flood defences were not taken into account, and the 1km simulation was not downscaled to the finer scales need for risk management. All of these steps are critical in flood depth estimation, particularly for highly managed European rivers,

and prevent such an approach from being used to gain insights into changing inundations patterns.

This chapter presents a new method for the development flood inundation hindcasts which addresses the limitations of previous work. Like Schumann et al (2016), we use a ~1 km spatial resolution 1D/2D hydrodynamic model to simulate inundation for the whole of Europe, but instead of forcing this with sparse and intermittent gauge data we use output from a continental scale hydrological model at 5km resolution to provide multi-decadal time series of flow across the whole European river network. This allows ungauged tributaries and small streams to be represented in the model and provides a more consistent set of input information that does not suffer from coverage gaps. In addition, flood defences are represented based on a recent global database with good coverage over Europe and we implement a downscaling approach to recover high resolution (~90m) inundation patterns from the ~1km native resolution simulation. Using this approach, we are able to produce for the first time a European Flood Hindcast, a ~90 m resolution flood depth catalogue for the period 1990-2016 for 298 river basins in Europe. This provides users with a homogenous data catalogue of flood events in terms of their extent and depth at a continental scale. The data set was validated in different basins across the UK and mainland Europe using observed flood extent from previous events. Finally, an automatic flood detection algorithm was developed to extract discrete flood events for the 16 largest basins in Europe in order to look at changes in flood inundation events over time.

4.2 Methods

This section describes in detail the development of the European Flood Hindcast.

4.2.1 Input data sources

The European Flood Hindcast used the LISFLOOD-FP hydrodynamic model (Bates et al., 2010; Neal et al., 2012) to simulate river and floodplain hydrodynamics on a 1 km resolution grid. The model was forced with river discharge from the European Forecasting Awareness System (EFAS) (Thielen et al., 2009; Smith et al., 2016; Salamon et al., 2019) which is part of the Copernicus Emergency Management Service. EFAS uses LISFLOOD (Bartholmes et al., 2008; van der Knijff et al., 2010) a spatially distributed

hydrological rainfall-runoff model, to calculate river discharge and related variables such as snow depth water equivalent, soil depth and volumetric soil moisture at pan-European scale. Note that LISFLOOD and LISFLOOD-FP are separate models but were initially developed together and share the same design concept. This explains the somewhat confusing naming convention: 'LISFLOOD' is the name of the model suite, whilst '-FP' stands for 'floodplain' and denotes the hydrodynamic module. The EFAS system produces two sets of river discharge i) 'Forecasted" and ii) "Historical", this study used the later set only. The "Historical" set is driven by observed hydrometeorological data acquired via the EFAS Hydrological data collection centre and the EFAS meteorological data collection centre. The EFAS system also uses static input maps from a large variety of sources CORINE (Batista et al., 2013), SRTM (Farr et al., 2007), EU-DEM (Dufourmont et al., 2014), HydroSHEDS (Lehner et al., 2008), HYPRES (Wösten et al., 1999), GRanD (Lehner et al., 2011), and more. A complete list of sources is available in (Smith et al., 2016; Salamon et al., 2019). The spatial and temporal resolution of the EFAS system is 5 km and one day, respectively. The "Historical" river discharge data set was calibrated and validated with 717 stations using the Kling-Gupta efficiency (KGE) where it scored a KGE higher than 0.5 in 75% of all stations during calibration and 57% during validation (Salamon et al., 2019).

The European Flood Hindcast explicitly represented main channels and tributaries using the HydroSHEDS hydrography at 1 km resolution (Lehner et al., 2008). This data set is validated and ensures downstream connectivity in the vast majority of rivers and tributaries. The European hydrography EU-Hydro (Gallaun et al, 2019) is another hydrography available for this study area, however it is not suitable for flood modelling as it does not consider all rivers and tributaries and it has not yet been validated. River width estimates were retrieved from the GRWL database, a 30 m resolution global river width database derived from Landsat imagery (Allen and Pavelsky, 2018). Flood protection standards were considered using the FLOPROS database, a global scale database for protection measures in the form of a return period for each river reach (Scussolini et al., 2016).

The European Flood Hindcast used terrain elevations mainly from the MERIT DEM (Yamazaki et al., 2017), a 90 m resolution multisource and bias-corrected global DEM derived (over Europe) from Shuttle Radar Topography Mission data. We opted for this DEM rather than the alternative European DEM EU-DEM (Dufourmont et al., 2014) as the latter is not suitable for flood modelling studies since it contains vertical

elevation bias from different sources (e.g. speckle noise, stripe noise, absolute bias, and tree height bias). Whilst MERIT DEM is a reliable source of terrain elevations, freely available airborne LIDAR terrain elevations were used instead of the default MERIT DEM in England as better quality terrain data produces better skill in flood modelling (Schumann and Bates, 2018). Although some countries, such as the Netherlands, Luxembourg and Spain, do have free-access LIDAR DEM data, this information was not used in this study as it might lead to inconsistencies in terrain elevation estimates for cross-boundary basins and an advanced data fusion procedure might be required.

Over England the Environment Agency's 2 m resolution Composite LIDAR DTM was resampled to 5 m, then 10 m, 20 m and 50 m resolution using bilinear interpolation to obtain an upscaled DTM. The LiDAR DTM covers more than 75% of floodplains leaving voids in upload areas that need to be filled to avoid problems during flood simulations. Hence, voids found in the resampled 50 m LIDAR Composite were filled with the UK Ordnance Survey Terrain 50 DTM (Ordnance Survey, 2019) using the Delta Surface Fill Method (Grohman et al., 2006). Finally, the resulting void-filled DTM was resampled to 90 m for consistency with terrain estimates in Continental Europe.

A brief description of the data sources is presented in Table 4.1 and how they interact in the computational framework is shown in Figure 4.1.

Data source	Description	Note
EFAS streamflow (Thielen et al., 2009; Smith et al., 2016 Salomon et al., 2019)	Gridded streamflow estimates with a spatial and temporal resolution of 5 km and 1 day, respectively	Available at https://cds.climate.copernicus.eu
MERIT DEM (Yamazaki et al., 2017)	SRTM bias corrected global DEM at 90 m resolution	Available at http://hydro.iis.u-tokyo.ac.jp/~yamadai/MERIT_Hydro/
LIDAR Composite DTM	A raster elevation model covering ~75% of England at 2 m spatial resolution	Available at http://data.gov.uk
OS Terrain 50 (Ordnance Survey, 2019)	50 m resolution DTM used to fill missing data in the LIDAR Composite DTM in England	Available at https://www.ordnancesurvey.co.uk/
HydroSHEDS (Lehner et al., 2008)	Hydrography at 1 km resolution	Available at https://www.hydrosheds.org/

GRWL (Allen and Pavelsky, 2018)	Landsat-based global river width database at 30 m resolution	Available at https://doi.org/10.5281/zenodo.1297434
FLOPROS (Scussolini et al., 2016)	A global protection measures in the form of return period at different spatial scales	Available at http://dx.doi.org/10.5194/nhess-16-1049-2016-supplement

Table 4.1. Data sources used in the European Flood Hindcast

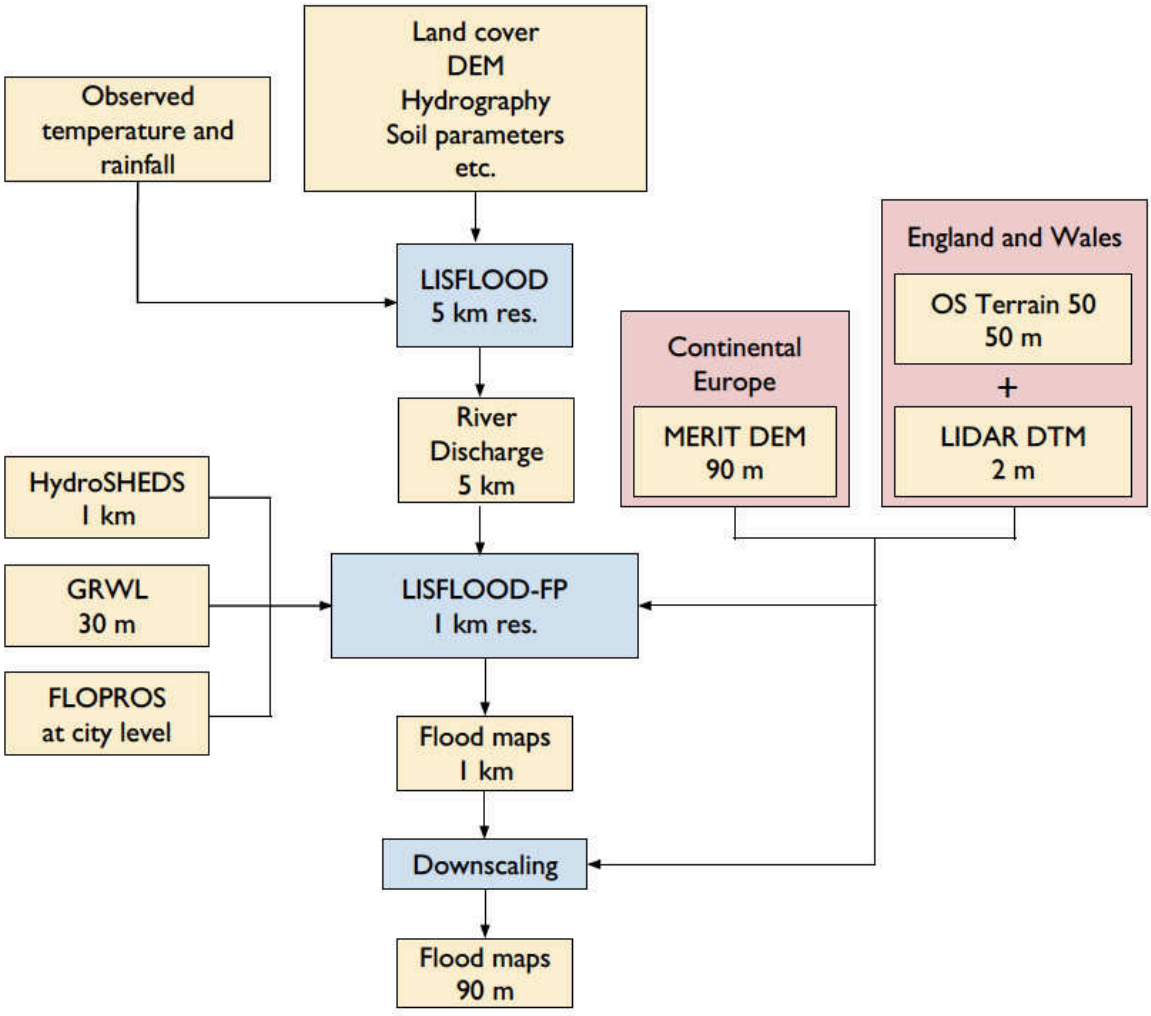

Figure 4.1. Computational framework diagram for the European Flood Hindcast

4.2.2 Preparing the flood inundation model

The European Flood Hindcast runs at 30 arcseconds (~1 km) native resolution, which is a computationally tractable grid size at which to produce multi-decadal simulations of continental scale river hydrodynamics. This resolution was selected after

comparing different computational times for the same simulation period over the Elbe basin (~148,268 km2 or 449,328 cells at 1 km resolution given a rectangular domain). For example, it was estimated that producing 26 years of water depth data for a basin as large as the Elbe river at ~90 m resolution would require 125 days of computational time, a considerable amount of time compared to 30 hours at ~1 km. The previous scenarios are based on one node of the University of Bristol's High Performance Computing BlueCrystal Phase3 (BC3) System. Each of these nodes has 2 x 2.6 GHz 8-core Intel E5-2670 processors and 4 GB of RAM.

The EFAS system does not attempt to resolve local scale hydrological conditions for catchments below 2,000 km2, urban flooding or flash flood and debris flows (Smith et al., 2016). For this reason, the European Flood Hindcast considered only catchments larger than 2,500 km2 (see Figure 4.2). Despite EFAS outputs covering the Scandinavian area, our study did not include this area as the river network from HydroSHEDS has coverage only up to °60N

Evaporation rate was parametrized in LISFLOOD-FP with constant value of 5 mm/day as the availability of time/space variable evaporation data in European countries is limited. The evaporation rate has small effect to the inundation peaks but rather helps to dry areas of the floodplain after events that may not have connectivity back to channel. Finally, note that all basin simulations in LISFLOOD-FP used the same standard values for floodplain and channel friction Manning's coefficients of 0.06 and 0.035, respectively. Thus, no individual calibration was carried out to adjust these parameters to a particular scenario.

LISFLOOD-FP is the hydrodynamic model used in this study to simulate river and floodplain hydrodynamics. It has been successfully used over large domains to produce satisfactory simulations of hydrodynamic variables such as flow velocity, water depth, water surface elevation and river discharge in an efficient way. For example, Wilson et al., (2007) implemented the model for 300 km of the central Amazon River, Biancamaria et al., (2009) built a hydrologic-hydraulic model for ~1,000 km of the Ob River, Neal et al., (2012) used it to simulate the Niger Inland Delta, Schumann et al., (2013) modelled the Lower Zambezi River for forecasting purposes, Alfieri et al., (2014) produced a pan-European flood hazard map, Sampson et al., (2015) built a global high resolution flood hazard map, Wing et al., (2018) produced estimates of present and future flood risk assessment in the US, Hawker et al., (2018), and Archer (2018) investigate in detail the effect of DEM choice in the Mekong Delta and the Ba

catchment in Fiji respectively. The reader is advised to consult the user manual (Bates et al., 2013) for more information on technical aspects, or Bates et al., (2018) for a recent history of the LISFLOOD-FP development.

To facilitate data management in the simulations at continental scale and to perform quality control operations in a simple way it was decided to run the European Flood Hindcast basin-wise; thus, the entire period (26 years) for each basin was simulated independently and we assume that inter-basin transfers are not significant to the flood response over the duration of extreme events. Figure 4.2 shows the 298 river basins and tributaries considered in this study. This provides a logical and efficient way to decompose the modelling domain into spatial units that could then easily fit into memory on a single compute node. This then allows multiple basins to be simulated simultaneously if more than one compute node is available. Simulations were carried out on the University of Bristol's High-Performance Computing BlueCrystal Phase3 (BC3) System which has 223 base nodes available. Not all nodes were used at once as this system is shared with other users following a queue system; instead, the simulation was carried out using only 30 nodes simultaneously.

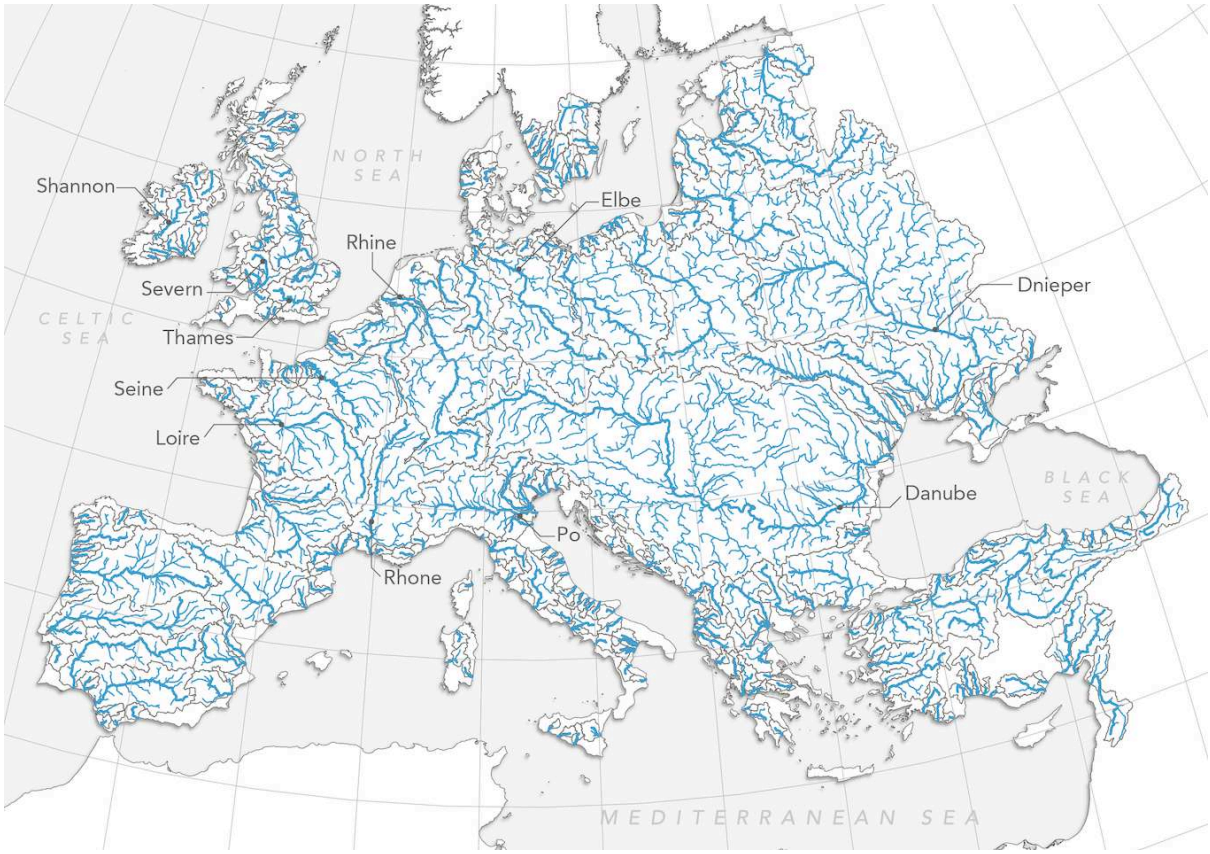

Figure 4.2. River basins and tributaries considered in this study. In total 298 basins were considered in this study, each with a catchment area larger than 2,500 km^2.

4.2.3 Preparing input data using LFPtools

The European Flood Hindcast used the "Sub-grid" version of LISFLOOD-FP (Neal et al., 2012) to estimate river and floodplain hydrodynamics. Input data for the Sub-grid version consists of five components: floodplain elevation, river width, river bed elevation, river bank elevation and inflow boundary conditions.

Floodplain elevations were obtained by resampling the ~90 m base MERIT DEM to 1 km using a kernel window of 10 x 10 cells (or a square of 0.08 degrees per side). The DEM was resampled using a weighted average ensuring that outliers values were not taken into account in the calculation, this calculation is wrapped in a single operation in the automatic toolbox LFPtools (Sosa et al., 2020). River width estimates were retrieved from the GRWL data set using the nearest neighbour method on a 10 x 10 searching window. For those river cells with no width associated, a linear interpolation of upstream and downstream values was carried out to obtain an estimate of river width. Both floodplain elevation and river width were estimated using LFPtools.

Estimation of inflow boundary conditions, river bed and river bank elevations are explained in Sections 4.2.4-4.2.6

4.2.4 Coupling the hydrological model to the flood inundation model

Coupling a hydrological to a flood model is not an easy task. Both the hydrological and the floodplain inundation model run at different resolutions and use different river network maps. River networks map is a layer providing information about the location of river centre lines. Hereafter, "flood model pixels" are defined as those cells in the river network used by the flood inundation model, and "river discharge cells" are those cells in the river network used by the hydrological model. Among all pixels in the flood model, only a few of them should be considered as inflows. Those inflow pixels will carry the river discharge data from the hydrological model over into the floodplain inundation model. Identifying inflow pixels in the flood model based on river discharge cell location in the hydrological model can be achieved as follows:

1. The river network map from the hydrological model should be determined first. Generally, this is available, however it could be derived as follows. First, calculate the weighted average of the gridded daily river discharge, then apply a threshold to the resulting map to discard cells outside of the river network map. In this study, a threshold of 5 m3/s was used to determine the river network (see Figure 4.3).
2. The centroid of an inflow pixel for the flood model must lie within a particular narrow threshold/buffer of the centroid of river discharge cells from the hydrological model (see Figure 4.4, step 2).
3. As the flood model has a higher resolution than the hydrological model, several inflow pixels might carry the same information to the flood model generating water mass double-counting. To solve this problem, we use the LFPtools program *lfp-split* (Sosa et al., 2020) to obtain the topological information for the river network in every pixel in the flood model. Then, only those cells with discharge larger than its upstream cell in the downstream direction were considered (see Figure 4.4, step 3).
4. River discharge values extracted in the previous step provide cumulative values of discharge. The flood model receives instead the contribution of each pixel to avoid mass-double counting. To fix this, differences between pixels in the downstream direction are calculated to estimate their contribution (in terms of discharge) to each cell in the network in the flood model (see Figure 4.5).

These concepts were applied to every river basin and reach from Figure 4.2 and the approach is generic, in that it could be implemented for any combination of hydrologic and hydraulic models and not just LISFLOOD and LISFLOOD-FP.

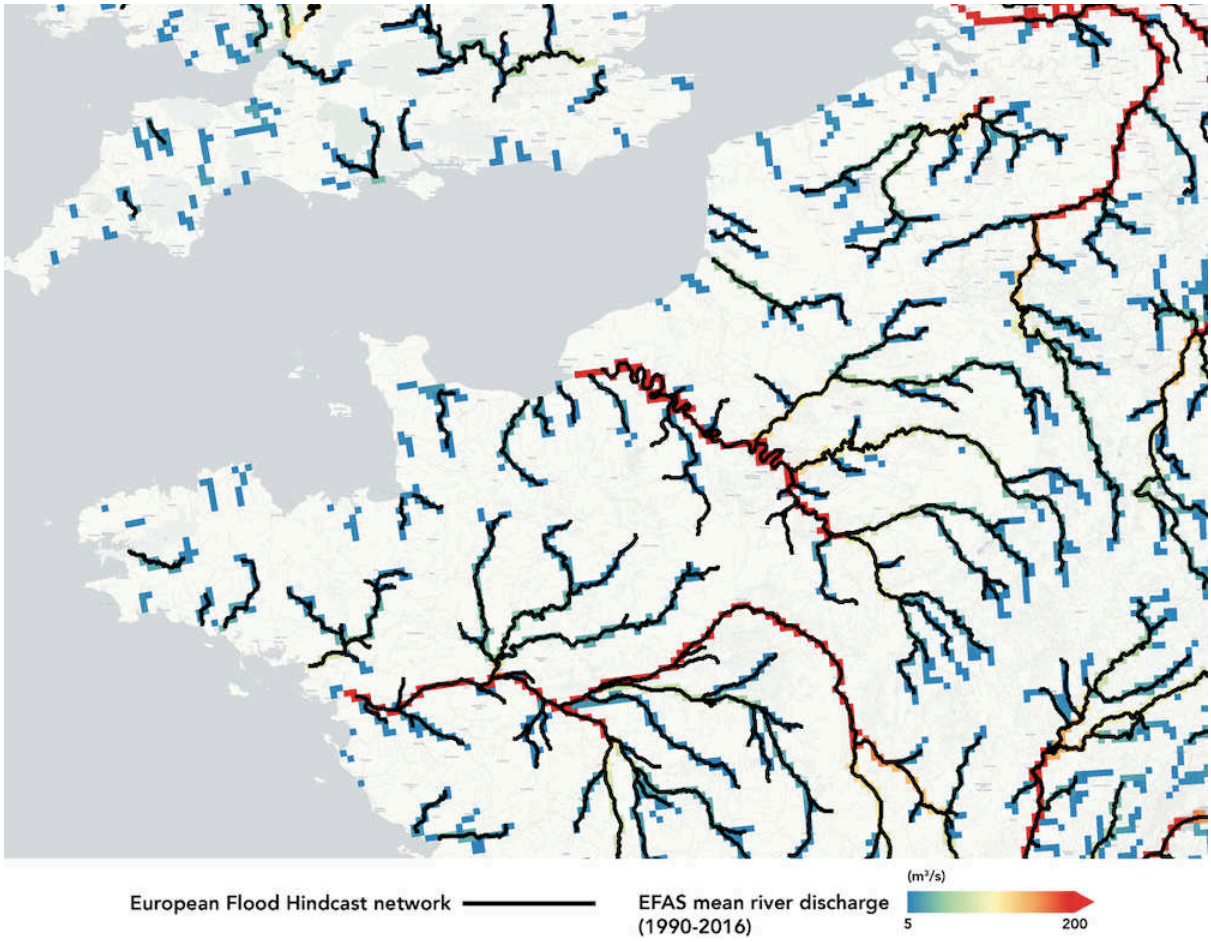

Figure 4.3. EFAS mean river discharge with European Flood Hindcast river network superimposed in the Western Coast of Europe

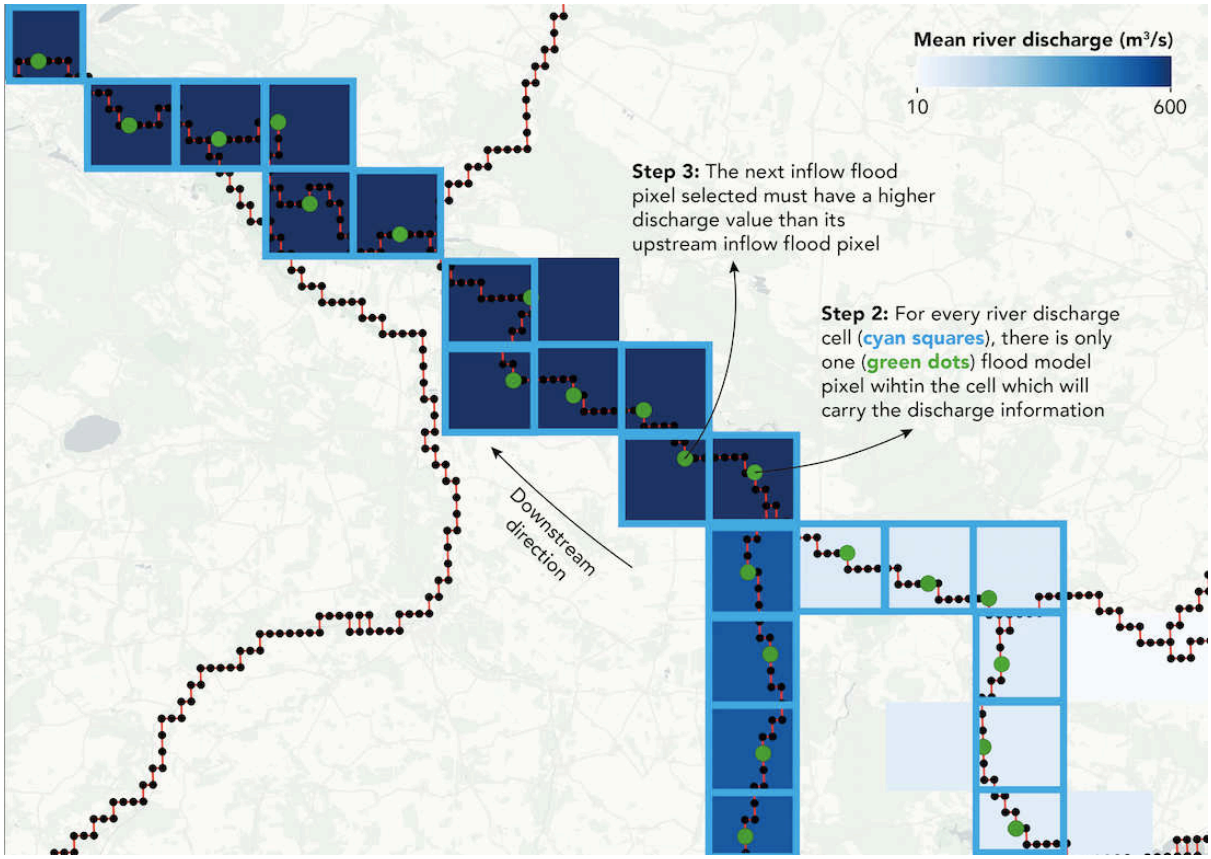

Figure 4.4. Visual explanation on the procedure used to couple a hydrological model to a flood inundation model.

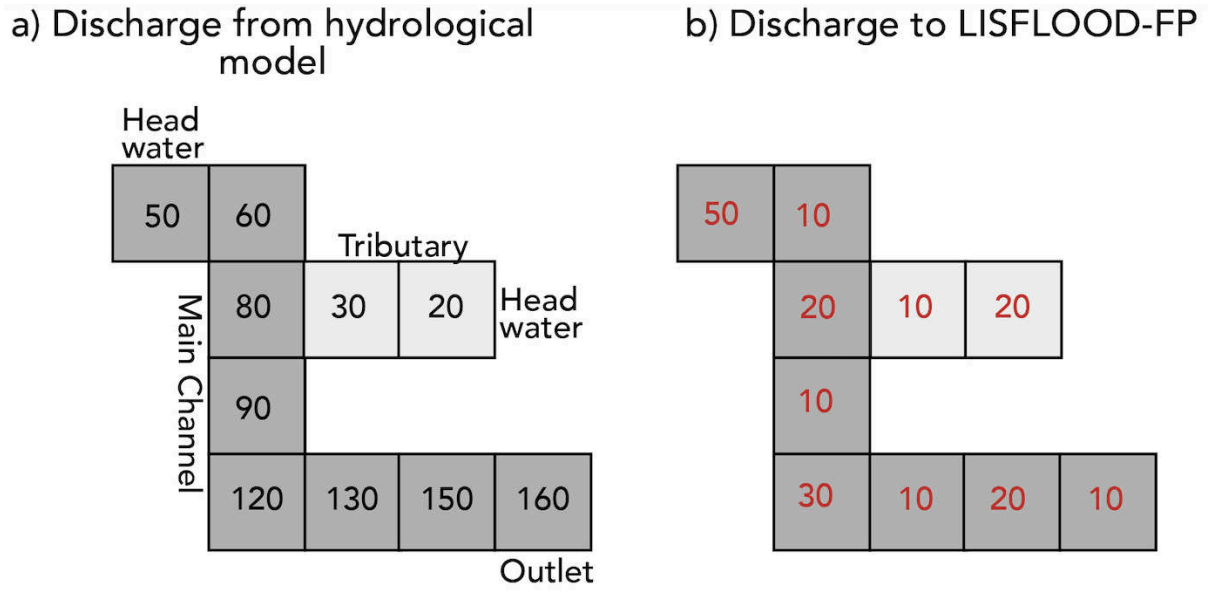

Figure 4.5. Visual explanation on how to fix water mass double-counting

4.2.5 Bed elevation estimation

Estimation of river bed elevations for main channels and tributaries at continental scales is a complex problem as river depths are challenging to obtain via remote sensing (Neal et al., 2012). Despite the existence of different methods to estimate river depths in flood inundation models (Neal et al., 2012; Mersel et al., 2013; Sampson et al., 2015), this study uses a novel method where river depths are adjusted based on the hydrological characteristics of the inflow boundary conditions. Thus, systematic biases usually found in rainfall-runoff models (Zhou et al., 2012) are corrected using the also unknown bathymetry (i.e. we fit a channel conveyance to the river discharge data). First, LISFLOOD-FP was forced using boundary conditions estimated previously in Section 4.2.4 to run a continuous simulation for the entire period (1990-2016) in 1D mode (i.e. only considering main channels and tributaries and excluding the floodplains) to obtain an ensemble of daily water surface elevations.

Initial river bed elevations for use in the 1D only model run were estimated from the ~90 m MERIT DEM by averaging values within a 10 x 10 window along the channel centreline and subsequently smoothing these in order to maintain downstream flow connectivity using LFPtools (Sosa et al., 2020). This initial guess at the bed elevation is obviously incorrect as SRTM only 'sees' the water surface or bank heights, so we use the 1D model run to update the bed elevations to a more realistic value. To achieve this, the mean channel water depths over the entire 26 year simulation period obtained from the 1D only simulations using the initial bed elevations were calculated. The mean channel depth was then subtracted from the smoothed elevations, thus producing a new and more appropriate bed elevation. This technique allows us to apply simulation-based systematic bias adjustment to the input data which is needed due to the potential for considerable absolute discharge errors sometimes found in rainfall-runoff models (Gudmundsson et al., 2012).

Figure 4.6 shows the procedure over the lower part of the main channel of the Elbe basin (~400 km river length). The graph shows the 9861 members corresponding to the daily water surface elevations during the period 1990-2016 (grey lines) in addition to the ensemble mean (red line). The initial "dummy" river bed elevation is shown in blue, and the final calculated bed elevation is shown in orange. The final bed elevation acts as an effective synthetic bathymetry tailored for the input river discharge such that inundation initiation and frequencies are correctly represented. This approach is

also generic and is appropriate for any combination of inundation model and forcing data.

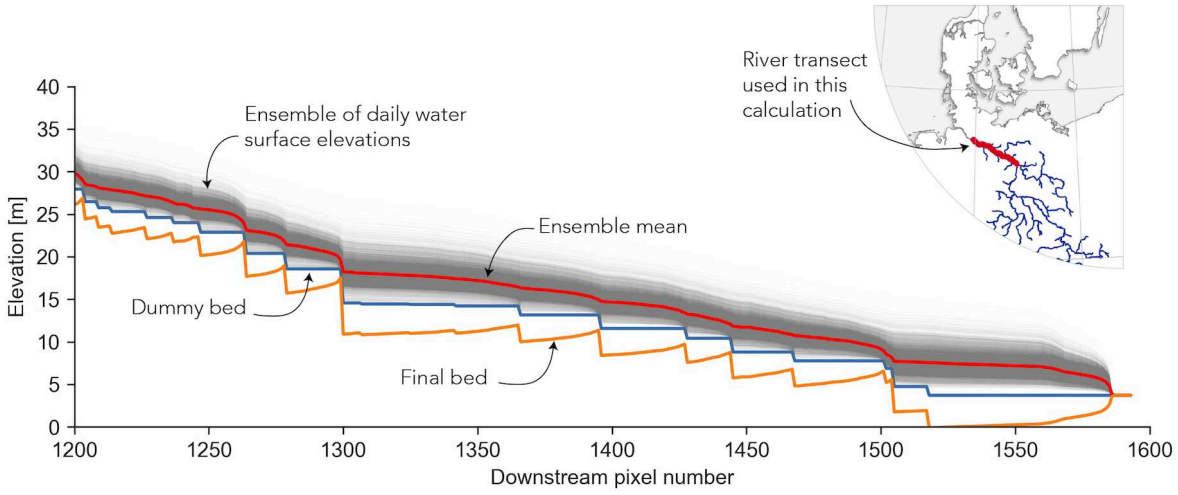

Figure 4.6. Bed elevation estimation for section (~400 km length) in the main channel of the Elbe River in Germany. In total 9,861 members corresponding to the daily water surface elevations during the period 1990-2016 are plotted in grey, the ensemble mean is plotted in red and the final bed in orange.

4.2.6 Including flood protection standards in the model

Flood defences were considered in the European Flood Hindcast by integrating flood protection standards within the modelling framework. Channel bank heights from the river network in LISFLOOD-FP define the height at which water overtops the channels and flooding begins. Thus, very high banks (higher than the adjacent floodplain) will not produce flooding, and conversely, banks at the same height (or lower) than the floodplain will generate extensive inundation (Bates et al., 2013). Later, if bank heights can be adjusted to represent a flood protection standard value, for example, the 100-yr return period water level, the river network will be able to account for protection at that level, implicitly. Flood protection standards can be related to bank heights in two steps:

1. Finding the discharge associated with a specific flood protection standard in terms of return period.
2. Relating the discharge found in Step 1 to a water level.

Step 1 can be solved using flood frequency analysis (FFA) or fitting a statistical distribution to the annual discharge maxima, while Step 2 can simply relate a discharge

value to its corresponding water level via a rating curve. Both methods have been extensively used in previous studies (Thorarinsdottir et al., 2018; Kiang et al., 2018). The statistical distribution selected was the Generalised Extreme Value distribution with parameters estimated via Maximum Likelihood Estimation (MLE), while the rating curve was fitted using a non-linear function $y = a(x + b)^c$, where a, b, c are constants and x is a discharge value. When the water level related to a specific return period is found for a particular river cell, it is subsequently added to the bed elevation calculated before in Section 4.2.5 to obtain bank elevations associated with a certain level of flood protection. This procedure is explained in the following paragraph.

Discharge and water levels at every river cell for every time step are needed beforehand, to this end, a simulation in 1D mode was used to obtain these variables using the final bed (see Figure 4.6). The goodness of fit in both the statistical distribution and the rating curve fitting was calculated to prevent rare water level values affecting the derived relationships. In particular, the Kolmogorov-Smirnov (KS) test and the adjusted R2 value were used for assessing the statistical distribution and the rating curve, respectively. KS uses the maximal absolute difference D as its statistic. In this study, we use 1-D and thus let both tests produce a score value ranging from 0 to 1, where the best possible value is 1. In this context, a score value larger than 0.85 was set as a threshold to accept the calculated fitted curve. The curves were subsequently used to calculate water levels related to a certain level of flood protection given in the FLOPROS database for every basin and reach in Figure 4.2. For those neglected river cells (where the goodness of fit was lower than 0.85) the nearest water level was used.

Figure 4.7 shows the procedure described above for a river cell located in the lower part of the main channel of the Elbe basin. The calculated curves obtained goodness of fit values 0.85 and 0.99 for the statistical distribution and the rating curve, respectively. The curves easily relate return periods with discharge, for example, the 100-yr return period in this river cell is a discharge of ~5,552.94 m3/s. That discharge value is considered next to obtain the water level associated with it, namely 13.13 m. This water level is then added to the bed elevation value calculated before in Section 4.2.5 (5.9 m) to obtain 19.03 m as the protected bank elevation.

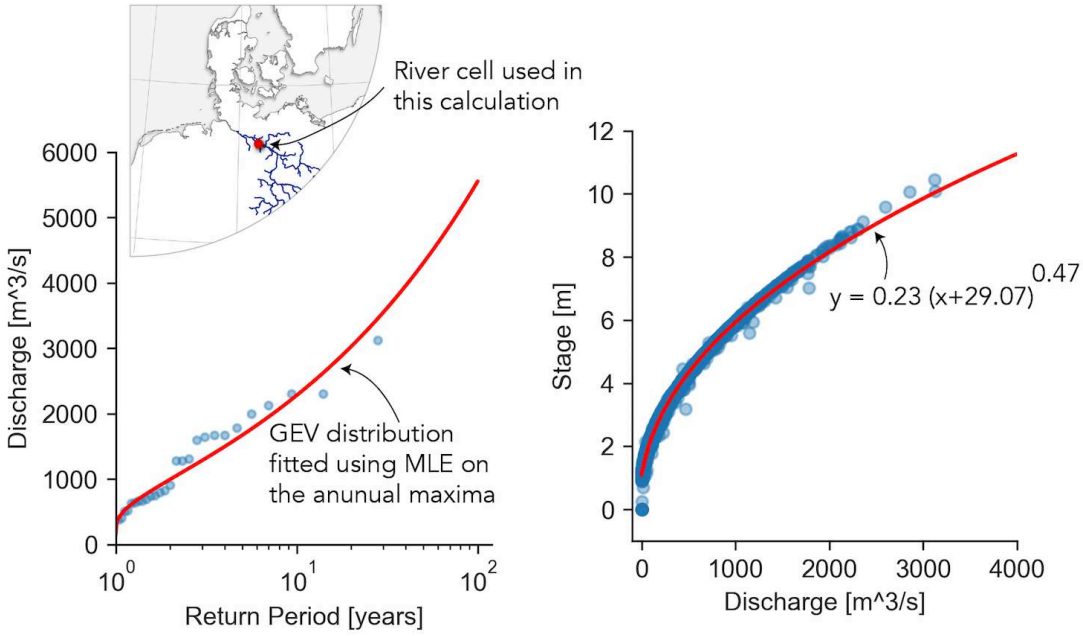

Figure 4.7. Bank height estimation based on flood protection standard level.

4.2.7 Downscaling daily outputs from 1 km to 90 m

The European Flood Hindcast uses a downscaling algorithm (similar to Schumann et al., 2014) to downscale 1 km flood maps to 90 m. In particular, the algorithm takes water surface elevation (WSE) at its original output resolution of 1 km and combines it with the corresponding 90 m DEM. In order to obtain water depths beyond the simulated inundation extent, the algorithm subtracts the WSE value of every wet cell from a larger 90 m DEM kernel. For example, the WSE value is subtracted from a 3 km x 3 km size 90 m DEM. From this arithmetic operation, a grid at 90 m resolution is created with positive values representing the water depth whilst negative values are replaced by no data or dry cells. The final step applies a decay function from the centreline of the river and tributaries following an exponential function of the form $D = C^b$ where D is the final 90 m water depth, C is the proximity distance from the centreline (the farther to the centreline, higher the distance value) and b is a free parameter. Centre lines from main rivers and tributaries were obtained via MERIT Hydro (Yamazaki et al., 2019). The downscaling algorithm is publicly available at https://github.com/jsosa/downscaling

4.2.8 Flood event identification

Flood identification in the European Flood Hindcast is not a straightforward task for several reasons: i) more than one event can occur during the same year; ii) several variables can be used to identify events (i.e. discharge, inundated area, volume); iii) flood event durations in the European Flood Hindcast tend to differ from observed flood durations primarily as the hindcast uses a fixed evaporation rate (5 mm/day) to remove water from river basins that do not drain back to the channel under gravity and also because the model does not account for human interventions in the flooding system. Nonetheless, some simple assumptions can be used to design an automatic algorithm to identify events in the European Flood Hindcast. The algorithm was inspired by (Brocca et al., 2011). In particular, the flood identification algorithm analyses the daily inundated area (m^2) signal to determine possible events. The signal is directly obtained as an output from the LISFLOOD-FP model for each basin. The algorithm discards values under a threshold (T) defined by $T = AP$, where T is the threshold value, A is the basin area in m^2 and P is a fraction between 0 and 1. Thus, with $P = 0.01$, possible events are the ones with an inundated area larger than 1% of the basin area. The algorithm uses a timespan moving window of 7 days to look for the starting date of the event. Finally, the end date of an event is assumed to happen when the peak magnitude is reduced by 30%.

4.3 Results and validation

4.3.1 Evaluation against official flood outlines in the UK

The availability of official flood outlines from historical events in Europe is very limited. Only England and Wales, via the Environment Agency (EA), keep track and release continuous updates of a database containing flood outlines. The database is called "Recorded Flood Outlines" and can be freely accessed from: https://www.data.gov.uk. However, for other countries, free access to historic flood outlines is still restricted or challenging to obtain. Hence, the European Flood Hindcast was validated on specific events in different basins across England and for two basins in mainland Europe.

The "Recorded Flood Outlines" database contains more than 1,500 georeferenced records of historic flooding from rivers, sea and groundwater since 1946. This data set was compiled using digitised aerial photographs and satellite imagery, so the quality of the flood outlines depends entirely on the error associated with those instruments, which can be non-trivial (see e.g. Horritt et al., 2001). It is worth mentioning that the absence of coverage for an area in the data set does not mean that the area did not flood during the event, only that the Environment Agency does not currently have records in this area.

For the comparison, only the "river flood" label from the database was considered. The skill of the European Flood Hindcast was quantified by comparing modelled outlines against the official ones. Official outlines were compared with modelled flood outlines using three scores: Hit rate (H), False alarm ratio (F) and Critical Success Index (C). H tests the proportion of wet benchmark data that was replicated by the model, and ranges from 0 (none of the wet benchmark data are wet in the model data) to 1 (all of the wet benchmark data are wet in the model data). F indicates the proportion of wet modelled pixels that are not wet in the benchmark data, and ranges from 0 (no false alarms) to 1 (all false alarms). C accounts for both overprediction and underprediction, and ranges from 0 (no match between modelled and benchmark data) to 1 (perfect match between modelled and benchmark data). Further details of these scores can be found in Wing et al., (2017).

In previous studies, acceptable performance in terms of Critical Success Index for large scale models has been suggested to be values ranging from 0.5 to 0.7 (Bernhofen et al., 2018; Wing et al., 2017; Dottori et al., 2016; Sampson et al., 2015; Alfieri et al., 2014). Results are considered good with CSI >0.7 and poor with CSI <0.5. A CSI score of < 0.5 effectively means that less than 50% of floodplain cells are correctly predicted as wet or dry. It is worth noting that the range of acceptable, good and poor performance has been shifting upwardly during recent years as improvements in models and new modelling frameworks have been produced. Also, many early studies benchmarked their outputs with models running purely at high-resolutions (30 to 90 m) contrary to this study (simulation at 1 km followed by downscaling to 90 m). Thus, it is important to note that the downscaling technique will add some degree of error to the benchmarking scores. Finally, CSI is sensitive to the size of the floodplain in that higher CSI scores are easier to obtain on larger floodplains where the ratio of flooded area edge length is greater.

The comparison used a ~1 km buffer around the modelled flood extent following the technique used in Wing et al., (2017). Additionally, official flood outlines from the EA were distributed in Vector Shapefile format, so for the comparison with the model those maps were rasterized to ~90 m resolution. Figure 4.8 shows the official flood outline extents for seven basins in England during different events. In the panels, the blue colour indicates the outline of the downscaled simulated flood inundation map of the basin from the European hindcast, the green colour shows the official flood outline, and the red colour indicates the agreement between both, i.e. where the model matches the observed flood outline. The location of the rivers mentioned is shown in Figure 4.8a.

Figure 4.8b shows the Trent river basin during the November 2000 event; the model scores were H=0.89, F=0.40 and C=0.56 and are favourable compared to other studies (e.g. Bernhofen et al., 2018), albeit the model gives some overprediction near the city of Nottingham. Figure 4.8c shows a reasonably large area of the Ouse river basin during the flood event of January 1995, the performance of the model in this basin still compares favourably to other studies (e.g. Bernhofen et al., 2018) with scores H=0.86, F=0.46 and C=0.50, thus the H score indicates that the model is able to capture 86% of the flood extent, albeit the lower score of C is mainly due to the model overprediction in the lower part of the basin where a complex flood protection system exists that may not be captured in the FLOPROS data set. The Environment Agency provides few details in regard to this benchmark flood extent, and for this reason it is difficult to indicate the level of error in the observed data. The Severn, Nene, Medway and Thames river basins are compared in Figures 4.8d-g, respectively. The model can capture more than 90% of the benchmark data in these four rivers. The lowest score is for the Thames river which has a C score of 36%, mainly due to the high level of overprediction in the model. The Thames has a complex flood defence system (see yellow lines in Figure 4.8g) which unfortunately the approach used in Section 4.2.6 is not able to capture as the FLOPROS database is not robust enough in such situations. Benchmarking scores for all cases are summarised in Table 4.2.

There are several explanations for differences between the European Flood Hindcast and flood official maps, including: i) errors in the terrain elevation data; ii) errors in the river bathymetry or the method used to account for flood defences; iii) errors in the observed flood outlines; iv) errors in the input river discharge; and v) the need to calibrate hydrodynamic model friction parameters in some settings. Of these, the

dominant error sources are most likely to be the incorrect representation of flood defences and errors in the EFAS river discharge data. The latter can still result in misprediction of inundated areas despite the implicit bias correction used to determine channel conveyance capacity and hence inundation frequency.

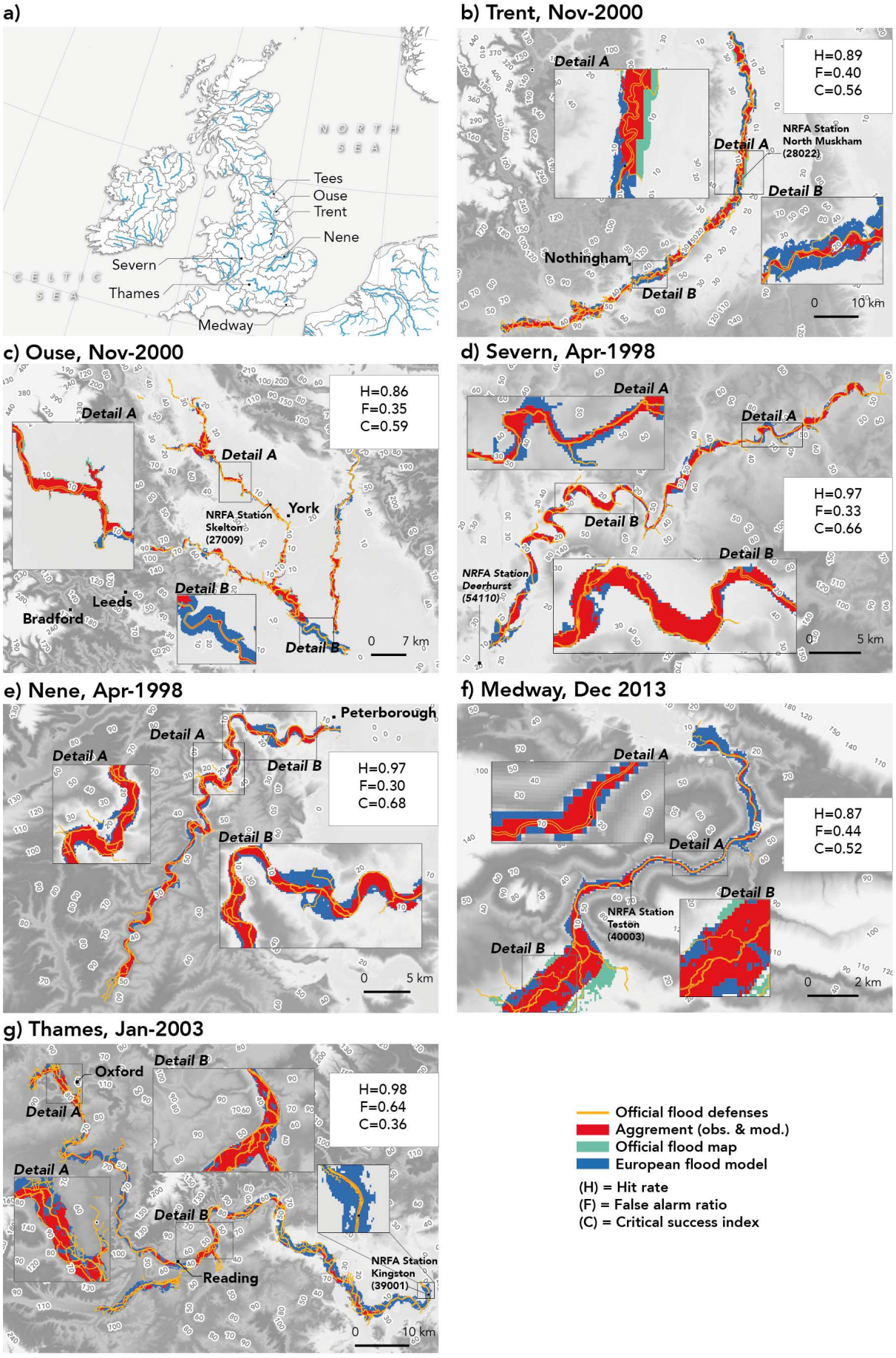
a)
NORTH SEA
CELTIC SEA
Tees
Ouse
Trent
Nene
Severn
Thames
Medway
b) Trent, Nov-2000
Detail A
Detail A
Detail B
Detail B
Nothingham
NRFA Station
North Muskham
(28022)
H=0.89
F=0.40
C=0.56
0
10 km
c) Ouse, Nov-2000
Detail A
Detail A
Detail B
Detail B
York
NRFA Station
Skelton
(27009)
Leeds
Bradford
H=0.86
F=0.35
C=0.59
0
7 km
d) Severn, Apr-1998
Detail A
Detail A
Detail B
Detail B
NRFA Station
Deerhurst
(54110)
H=0.97
F=0.33
C=0.66
0
5 km
e) Nene, Apr-1998
Peterborough
Detail A
Detail A
Detail B
Detail B
H=0.97
F=0.30
C=0.68
0
5 km
f) Medway, Dec 2013
Detail A
Detail A
Detail B
Detail B
NRFA Station
Teston
(40003)
H=0.87
F=0.44
C=0.52
0
2 km
g) Thames, Jan-2003
Oxford
Detail B
Detail A
Detail A
Detail B
Reading
NRFA Station
Kingston
(39001)
H=0.98
F=0.64
C=0.36
0
10 km
Official flood defenses
Aggrement (obs. & mod.)
Official flood map
European flood model
(H) = Hit rate
(F) = False alarm ratio
(C) = Critical success index

Figure 4.8. Official flood outlines comparison with the European Flood Hindcast across different river basins in England. The Recorded Flood Outlines take into account the presence of defences, structures, and other infrastructure where they existed at the time of flooding. It includes flood extents that may have been affected by overtopping, breaches or blockages. Also, it is worth mentioning that the absence of coverage for an area does not mean that the area did not flood during the event, only that the Environment Agency does not currently have records in this area.

4.3.2 EFAS streamflow evaluation against observed river flow

The skill of the EFAS river discharge was evaluated using observed river discharge data from the UK National River Flow Archive (NRFA). Performing this evaluation is crucial as the quality of the input river discharge plays a pivotal role in determining the skill of the flood inundation model (Grimaldi et al., 2019). Figure 4.9 shows hydrographs for the river basins discussed earlier. The hydrograph data was available for all the basins except the Nene river where no records were available for the day of the event. The location and ID number of the gauge stations are displayed in every basin in Figure 4.8. The Kling-Gupta Efficiency (KGE) and the Nash-Sutcliffe Efficiency (NSE) were used to evaluate the performance of the model under two scenarios i) 1-year daily discharge and ii) 15-day daily discharge (with the peak discharge in the middle of the hydrograph).

Table 4.2 summarises KGE and NSE scores for the 1-year and 15-day cases. The scores suggest acceptable performance (0.61>NSE 1-year>0.78 and 0.56>KGE 1-year>0.81) for at least for one-year of observed data before the event in each of the evaluation basins. Hence, these scores indicate the suitability of the EFAS river discharge as input data in the European Flood Hindcast. The situation is different for the 15-day scores or during extreme events as these widely vary and performance decreases substantially (-1.22>NSE Event>0.54 and 0.21>KGE Event>0.77).

Unfortunately, gauge stations are not available in all locations within the domains simulated where the flood inundation model is not performing well and thus the disagreement in flood inundation footprints is sometimes difficult to attribute to errors in the input discharge data. For example, the most significant differences in the Ouse river occur near the river mouth (Detail B in Figure 4.8c), however no observed discharge data is available at this location, so it is difficult to understand whether or not the input data is causing the overprediction observed. In contrast, Detail A in Figure

4.8c, visually shows high performance attributed mainly to the satisfactory agreement of the EFAS river discharge during the event with NSE Event=0.42 and KGE Event=0.74 (see Figure 4.9a).

Similar to the Ouse test case, the European flood inundation model obtained a high performance for the Severn River C=0.66 (see Figure 4.8d) during the event of April 1998, and this high score can be associated to the good performance of the EFAS river discharge data during the event (KGE Event=0.77, NSE Event=0.54) (see Figure 4.9c). The strategic location of the gauge station in the Severn River (at the outlet of the river reach) indeed helps to explain the favourable performance of both the EFAS model and the European Flood Hindcast at this site.

Looking at the event peaks in the Trent and Medway rivers (Figure 6b and Figure 6f), it is evident that the EFAS river discharge data is not able to reach the observed discharge peak (KGE Event<0.25 and NSE Event<0.15). These low scores likely explain the weak performance of the European Flood Hindcast near these locations (Detail A in Figure 4.8b and Detail A in Figure 4.8f), however, no observed river discharge data is available in some areas where large differences occur (Detail B in Figure 4.8b and Detail B in Figure 4.8f) to determine if the flood inundation mismatch can be attributed to the discharge input data.

As mentioned before, the River Thames is a heavily modified catchment with a complex flood defence system (yellow lines in Figure 4.8g). Despite this, the 1-year hydrograph simulated by EFAS (Figure 4.9e) shows good performance (KGE 1-year=0.78 and NSE 1-year=0.81), although some important features are still difficult to capture in the EFAS system. The event of January 2003 in the Thames shows a negative skill score (NSE 1-year=-1.22) at the outlet of the reach (Detail C in Figure 4.8g). This low score is likely to explain the large disagreement found in the flood inundation footprint comparison (Detail C in Figure 4.8g).

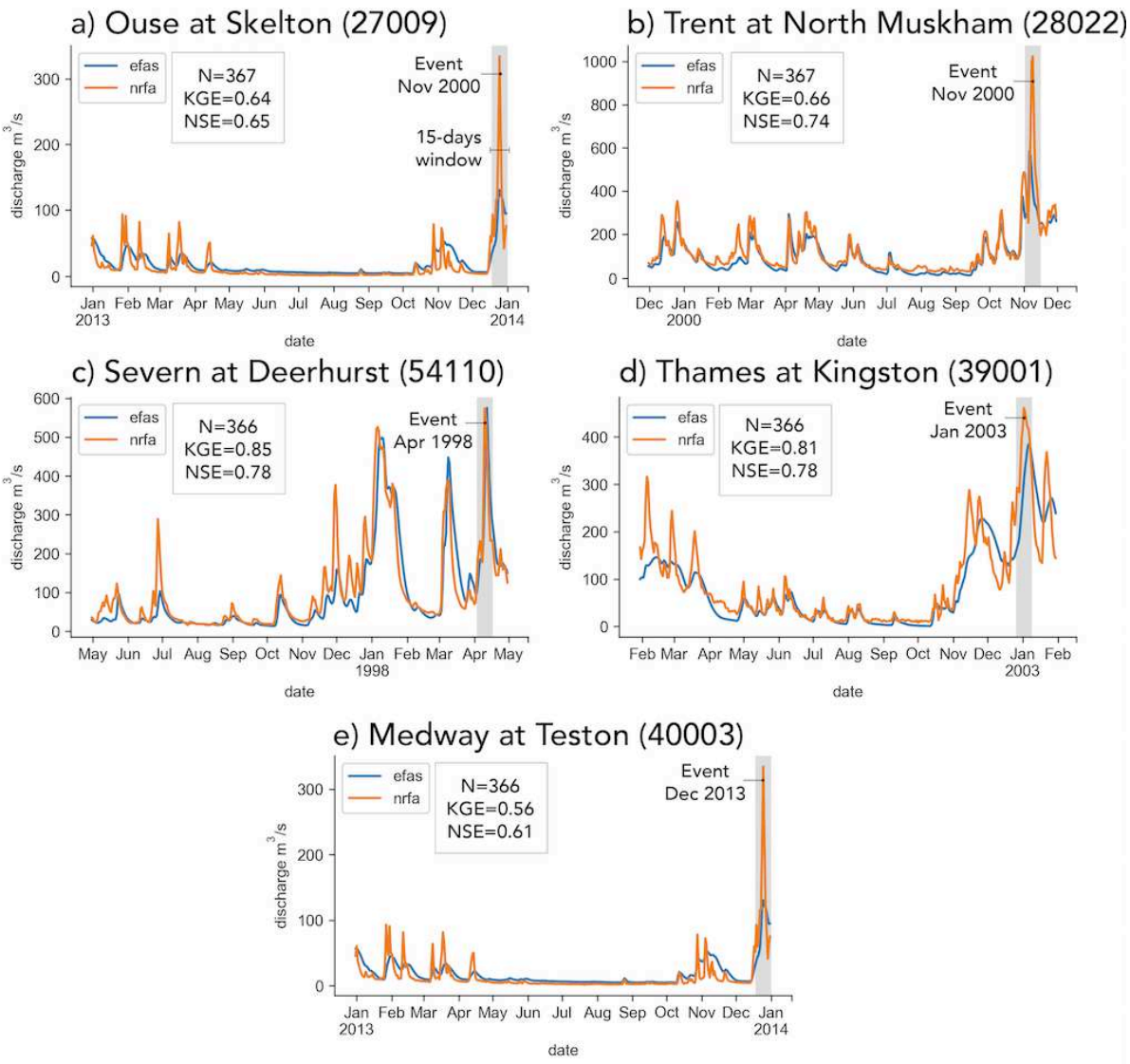

Figure 4.9. Observed river discharge from the National River Flow Archive (NRFA) compared against the EFAS streamflow data.

River basin	H	F	C	NSE: 1-year	KGE: 1-year	NSE: Event	KGE: Event
Trent	0.89	0.40	0.56	0.74	0.66	-0.02	0.21
Ouse	0.86	0.35	0.59	0.65	0.64	0.42	0.74
Severn	0.97	0.33	0.66	0.78	0.85	0.54	0.77
Nene	0.97	0.30	0.68	-	-	-	-
Medway	0.87	0.44	0.52	0.61	0.56	0.15	0.25
Thames	0.98	0.64	0.36	0.78	0.81	-1.22	0.57

Table 4.2. Benchmarking scores of the European Flood Hindcast in the English basins. (H) Hit rate, (F) False alarm ratio, (C) Critical success index, (NSE) Nash-Sutcliffe Efficiency and (KGE) Kling-Gupta Efficiency. KGE/NSE *1-year* indicates the score for a one-year hydrograph and KGE/NSE *Event* indicates the score for a 15-days hydrograph. The 15-days hydrograph is a window which encloses the event with the maximum discharge in the middle of the hydrograph.

4.3.3 Evaluating water depths in the Carlisle 2005 urban flood event

On the 6-7th January 2005, up to 175 mm of rain fell over areas of the Eden river basin (Day, 2005) in North West England which led to severe flooding on the morning of the 8th January of the city of Carlisle. In this section, the performance of the model in terms of flood extent and water depth is benchmarked using observed data from this event.

Figure 4.10 shows water surface elevation (WSE) measurements in addition to the official flood outline during the event of January 2005 for the city of Carlisle, UK for comparison purposes with the corresponding downscaled model output. In terms of flood extent, the model was compared against the official flood outline (black line in Figure 4.10a) from the EA obtaining acceptable skill scores H=1, F=0.45, and C=0.55.

Figure 4.10b shows a benchmark against 175 locations where WSE values were measured post event, with a precision of <0.01 m, average noise error of ~0.1 m and maximum absolute errors at individual measurement points up to 0.5 m (Fewtrell et al., 2011), the European Flood Hindcast achieved an RMSE=0.67 m and MAE=0.55. Note that these values compared well with previous studies (Neal et al., 2009). Neal et al., (2009) modelled this event on a higher resolution grid (25 m), and after calibration the study found that both floodplain (FPn) and channel (CHn) coefficients play an important role in determining flooding at this site and need to be adjusted for optimum model performance. The Neal et al. (2009) study showed that the best performance

was obtained using FPn=0.06 and CHn=0.055, achieving an RMSE=0.32 m and MAE=0.06 for a model based on a 25 m resolution DEM. Nonetheless, for the coefficients used in the European Flood Hindcast (FPn=0.06 and CHn=0.035) Neal et al., (2009) obtained an RMSE=0.85 m and MAE=0.7 which compares well with the scores obtained by the European flood model.

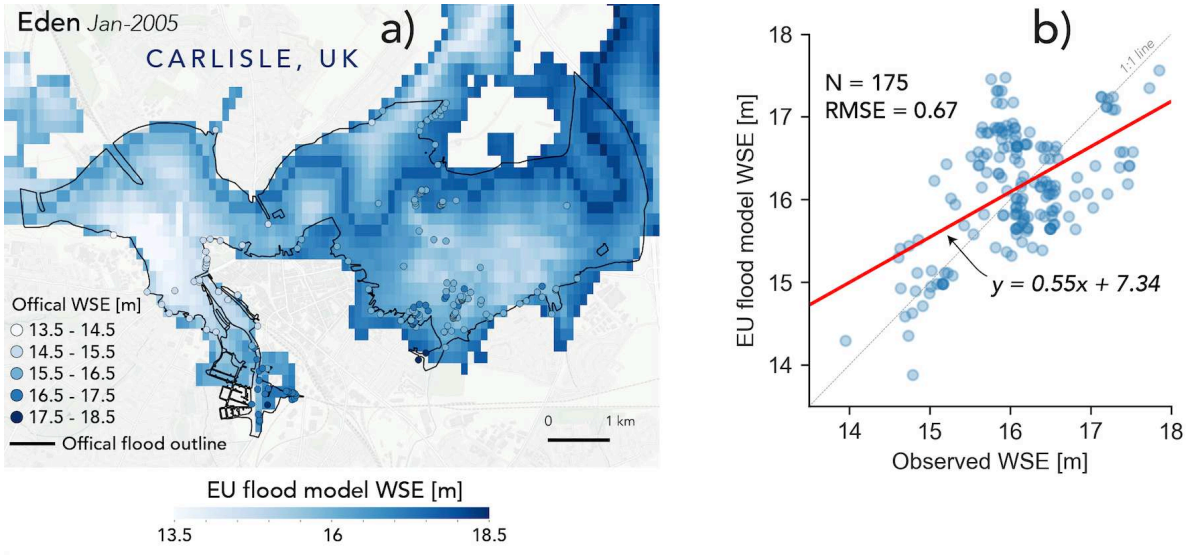

Figure 4.10. Flood depths and outline validation for Carlisle.

4.3.4 Validation against European flood data

In August 2002, a severe flood event hit Germany, Austria, the Czech Republic and Slovakia along the rivers Elbe, Danube and a number of their tributaries. In Germany, in particular, 21 people were killed, and substantial infrastructure was destroyed. The return period of the flood was estimated at 150 years in the city of Dresden and 25 years along the Lower Elbe near the city of Hamburg. The most affected German federal state was Saxony with total economic damage of 8.7 billion Euros, followed by Saxony-Anhalt (1.2 billion EUR) and Bavaria (198 million EUR) (Thieken et al., 2005)

Figure 4.12 shows the comparison of water depths during the event of 25th August 2002 across Europe. Official flood extents were obtained without any source indicating the compilation procedure so it is again difficult to estimate the likely of error of the benchmark. Nonetheless, the model obtained acceptable skill scores H=0.81, F=0.42 and C=0.51 in the Elbe basin in Germany (see Figure 4.11). The figure shows

the location of two principal cities affected during the event: Magdeburg and Dresden (Region A and Region B in Figure 4.12).
Other countries affected during this event were Austria, Croatia, Czech Republic, Germany, Hungary, Poland, Romania and Slovakia. However, no official flood outline extents were available to evaluate the performance of the model over these territories.

As previously noted, the availability of official flood outlines for historical events in mainland Europe are very limited. This study had access to two flood outlines sets of historical events i) the event of October 2000 only for the upper part of the Po basin and ii) the event of June 2013 in the Elbe basin nearby four areas: Prague, Lauenburg, Arneburg and Dessau. Outlines of these events were compared against outputs from the European Flood Hindcast and its comparison scores are presented in Figure 4.13-4.14. A summary of benchmarking scores for mainland Europe is presented in Table 4.3.

River basin	H	F	C
Po	0.85	0.49	0.47
Elbe 2000	0.81	0.42	0.51
Elbe 2013 (Prague)	0.81	0.11	0.73
Elbe 2013 (Lauenburg)	0.90	0.08	0.84
Elbe 2013 (Arneburg)	0.86	0.08	0.80
Elbe 2013 (Dessau)	0.81	0.11	0.73

Table 4.3. Benchmarking scores of the European Flood Hindcast in Europe. (H) Hit rate, (F) False alarm ratio, (C) Critical success index

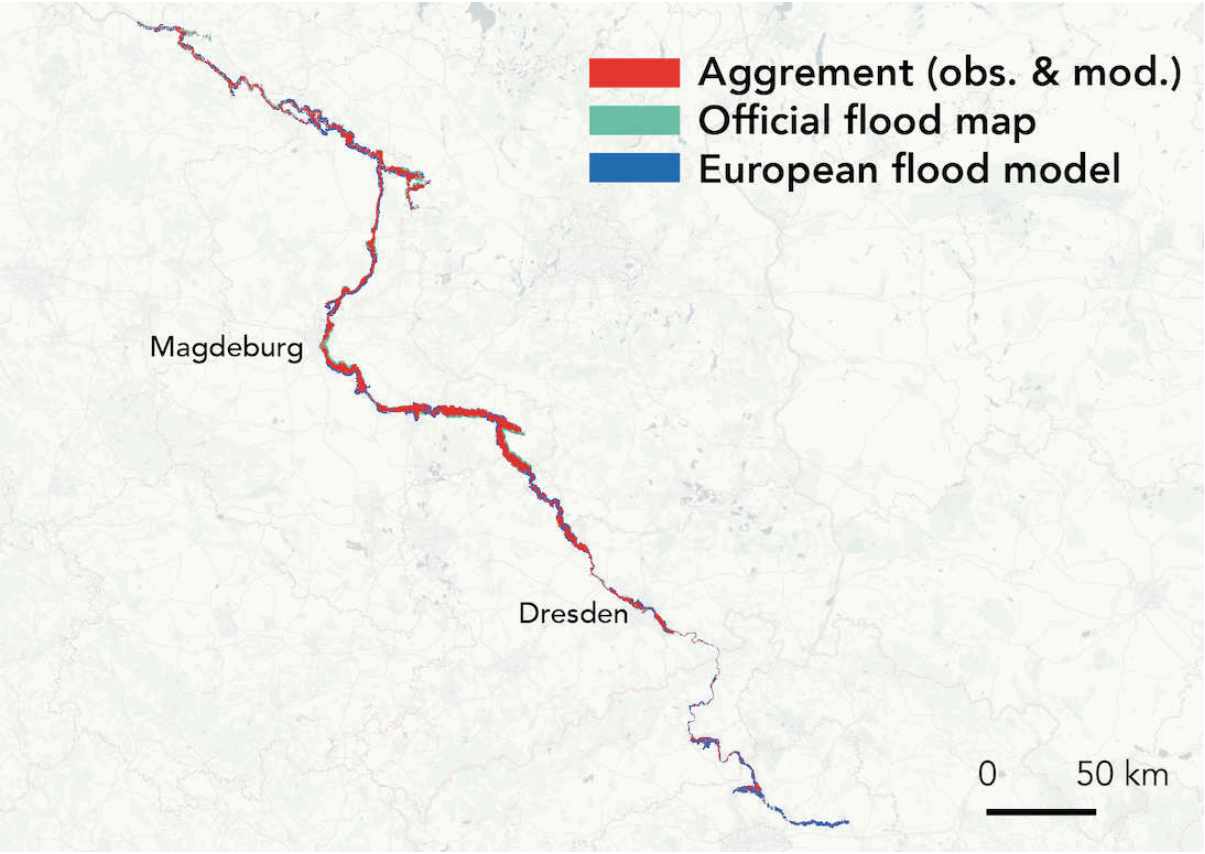

Figure 4.11. European flood model compared against official flood map for the event of August 2002 in the Elbe basin. Comparison scores Hit rate=0.81, False alarm ratio=0.42 and Critical success index=0.51.

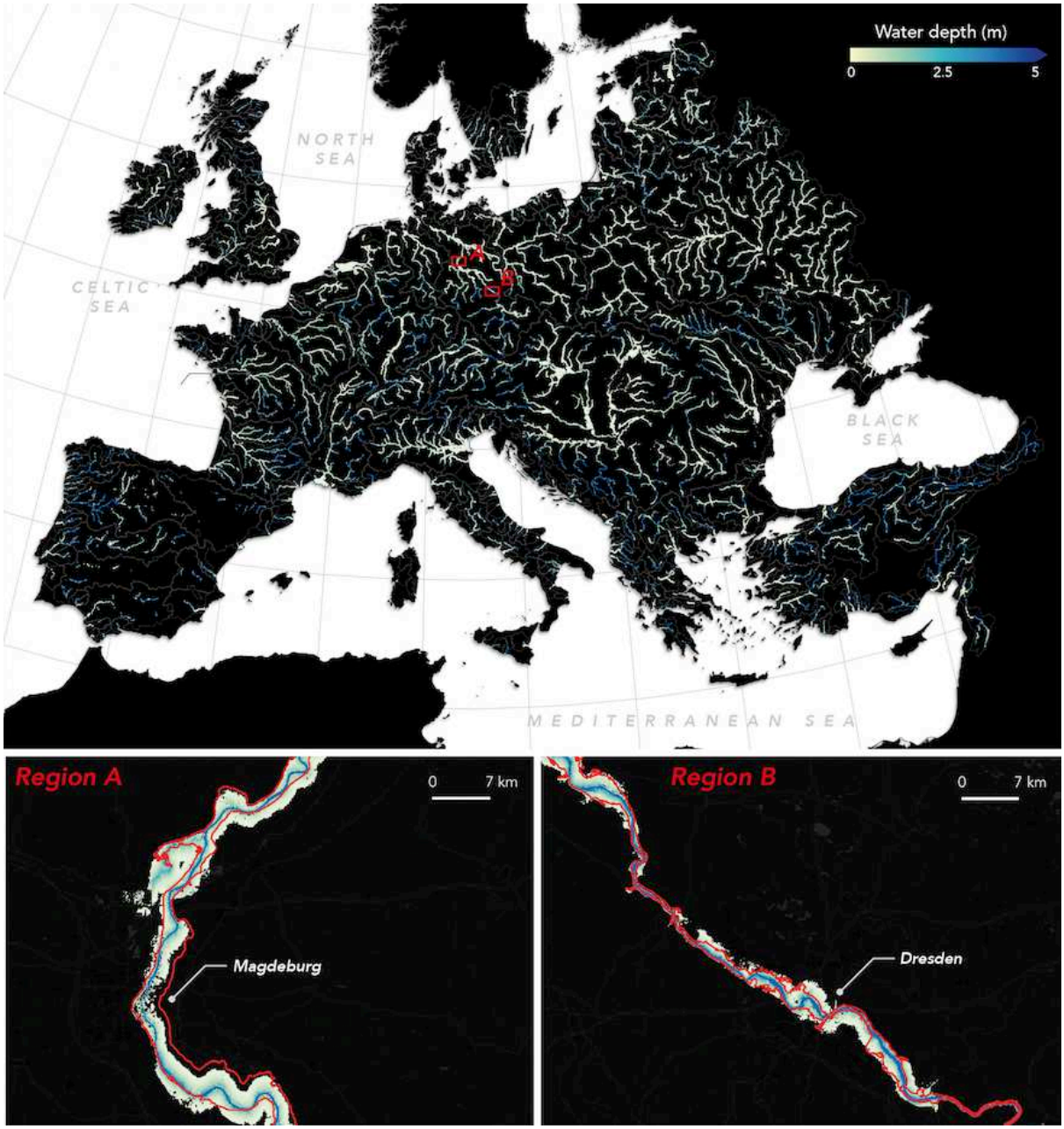

Figure 4.12. Simulated water depths for the 25th August 2002. Two important German cities affected during the event were Magdeburg and Dresden, regions A and B in the figure, respectively. In red is shown the official flood extent during the event.

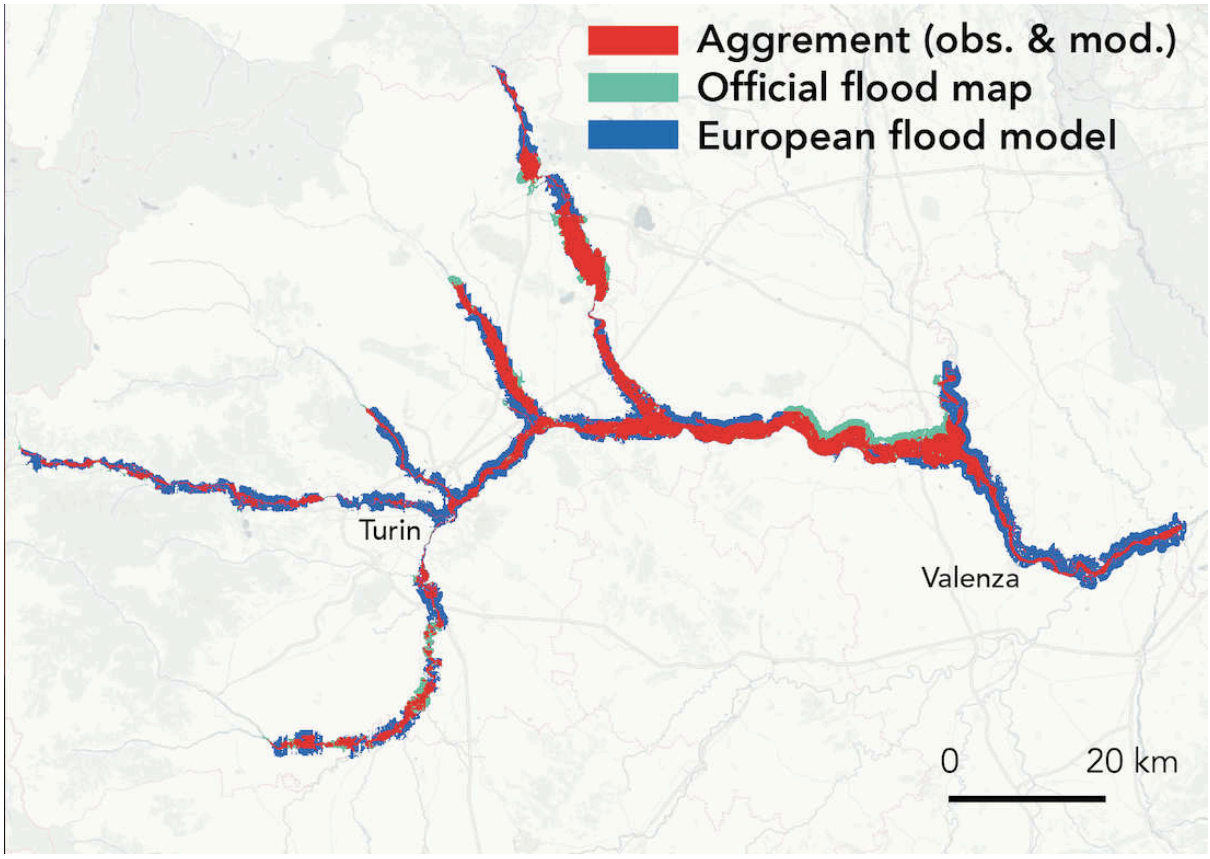

Figure 4.13. European flood model compared against official flood map for the event of October 2000 in the Po basin. Comparison scores Hit rate=0.85, False alarm ratio=0.49 and Critical success index=0.47

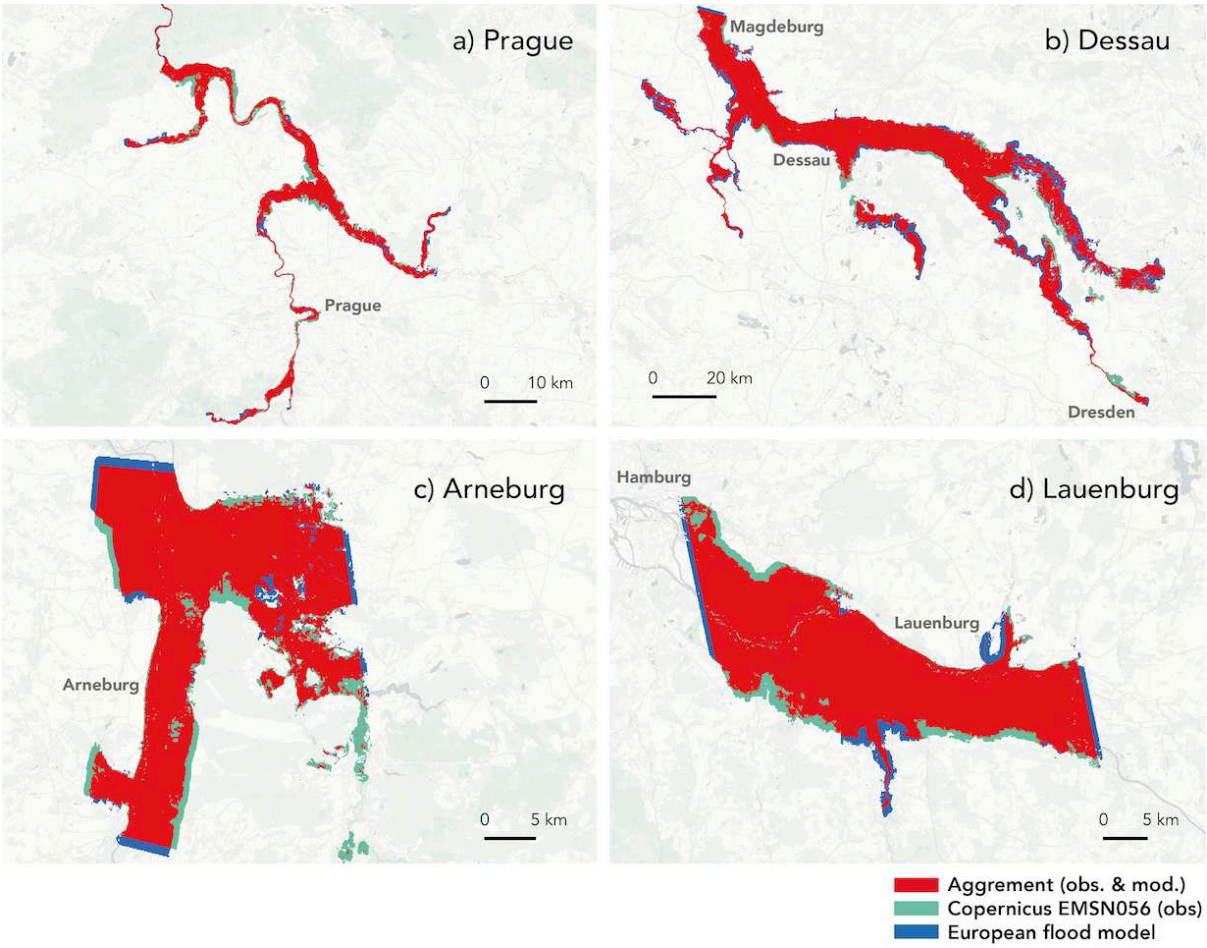

Figure 4.14. European flood model compared against a flood map from the Copernicus Emergency Management Service (EMSN046) for the event of June 2013 in the Elbe basin. Comparison scores **a)** Hit rate=0.81, False alarm ratio=0.11 and Critical success index=0.73 **b)** Hit rate=0.91, False alarm ratio=0.19 and Critical success index=0.75 **c)** Hit rate=0.86, False alarm ratio=0.08 and Critical success index=0.80 **d)** Hit rate=0.90, False alarm ratio=0.08 and Critical success index=0.84

4.3.5 European-wide benchmarking

The lack of flood footprints to benchmark the European Flood Hindcast is very poor, and continental-scale benchmarking is needed to assess the performance of the model. In the absence of flood footprints, discharge time series from gauge stations are used to benchmark. Discharge time series data were obtained from the Global Runoff Data Centre (GRDC). Only stations with a catchment area larger than 2500 km^2 were used (431 in total) as the European Food Hindcast simulates hydraulics on catchment of this size due to limitations to the input boundary conditions (i.e., EFAS).

To obtain discharge time series from the European Flood Hindcast, a buffer of 0.025 degrees (~2.775 km at the equator) around each GRDC stations was created to extract the model discharge time series. In cases where more than one location from model was available, the model location with the highest score was selected and recorded. The benchmarking was carried out using the Kling-Gupta Efficiency (KGE) to summarise the performance of the model. A value of KGE=1 indicates perfect agreement between the model and the observation. A bad model performance is obtained for lower values (i.e., KGE ~ 0). Figure 4.15 shows KGE scores for a wide range of locations across Europe and presents performance scores between the European Flood Hindcast and observed discharge. Unfortunately, observed discharge data in Ukraine, Spain, Greece and Italy were not available for benchmarking. The scores revealed that the model performance is acceptable in river basins in countries like Germany, the Netherlands, Switzerland, Czech Republic, Austria, Lithuania and Southwest France with KGE values raging from 0.15 to 0.75. Lower performance was observed along the Danube River, in Romania, Portugal and some places in Latvia. The bad performance in these areas were primarily caused by errors in the input boundary conditions (EFAS), as well as the need to better-calibrate hydrodynamic model friction parameters.

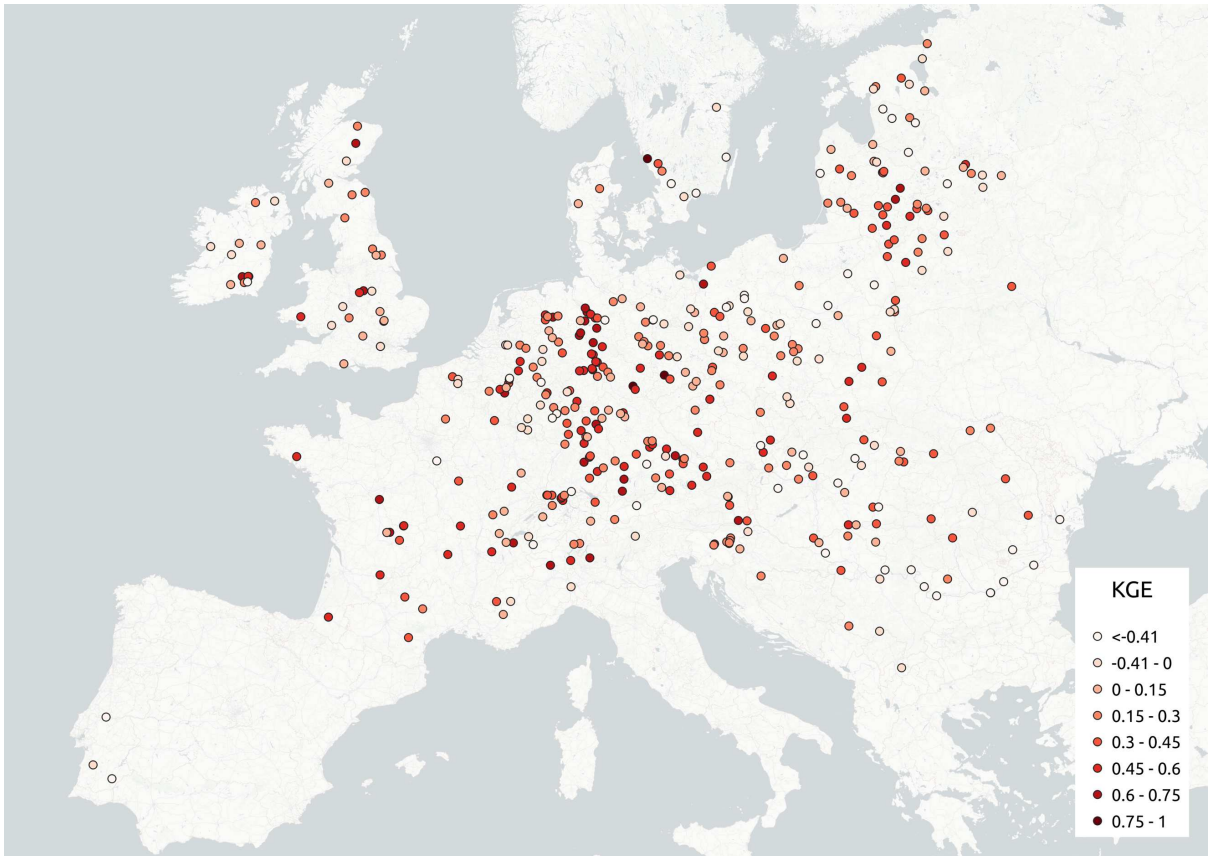

Figure 4.15. European Flood Hindcast benchmark using discharge data from the Global Runoff Data Centre (GRDC)

4.3.6 Identifying important European floods between 1990 and 2016

Recent studies have investigated floods in Europe extensively (Barredo 2009; Alfieri et al., 2015; Berghuijs et al., 2019; Bloschl et al., 2017, 2019). These studies have used streamflow from gauging stations to investigate the nature of floods in Europe in the context of climate change. Flood losses have been also investigated recently using a detailed database of past flood disasters with information on dates, locations, and loses in Europe (Paprotny et al., 2018a, 2018b). In this section, part of the events from the HANZE data set are compared with the European Flood Hindcast archive. This comparison was carried out for the 16 largest river basins in Europe for the 1990-2016 period. An automatic flood detection algorithm was developed to extract dates of major floods from the European Flood Hindcast. Finally, the analysis examined the total number of events per basin, yearly events, and how these results compare to floods reported in the HANZE database.

The HANZE database was constructed using high-resolution maps of present land use and population, and a large compilation of historical statistics. It contains 1564 records (1870–2016) of flash, river, coastal, and compound floods. To use this data set for comparison to the European Flood Hindcast the database was pre-processed as follows. First, the data set was filtered to include only flood events only between 1990 until 2016. Also, only river floods caused by rainfall in addition to flood events with estimated flood loses larger than 100 million EUR were selected. Finally, the location of events in the HANZE data set is defined by the NUTS Level 3 European administrative region. Hence, these regions were aggregated to intersect each basin in European Flood Hindcast (see Figure 4.2).

Flood identification in the European Flood Hindcast is not a straightforward task for several reasons: more than one event can occur during the same year, there are several variables that can be used to identify events (i.e., discharge, inundated area, volume), flood event durations in the European Flood Hindcast tend to differ from observed flood durations as the hindcast used a fixed evaporation rate of 5 mm/day to remove water from river basins that does not drain back to the channel under gravity and also

does not account for the human activity involved in this process. Nonetheless, some simple assumptions can be used to design an automatic algorithm to identify events in the European Flood Hindcast. The algorithm was inspired by (Brocca et al., 2011). In particular, the flood identification algorithm analyses the daily inundated area (m^2) signal to determine possible events. The signal is directly obtained as an output from the LISFLOOD-FP model for each basin. The algorithm discards values under a threshold (T) defined by $T = AP$, where T is the threshold value, A is the basin area in m^2 and P is a fraction between 0 and 1. Thus, with P=0.01 possible events are the ones with an inundated area larger than 1% of the basin area. The algorithm uses a timespan moving window of 7 days to look for the starting date of the event. Finally, the ending date of the events is assumed to happen when the peak magnitude is reduced by 30%.

The comparison between the HANZE and the European Flood Hindcast was carried out for the 16 largest basins in Europe. To capture important events, P was set to between 0.01 and 0.03 in basins to define the inundated area threshold T. It is important to mention that an event in the European Flood Hindcast could end several days after the observed date as the model only uses a constant evaporation rate to remove floodplain water that does not drain back to the channel under gravity. Hence, in order to capture important events, only those with a flood duration larger than 30 days were considered. The analysis examined the total number of events per basin for the period 1990-2016, the yearly evolution for the same period, and how these results compare to reported floods of the HANZE database (see Figure 4.16).

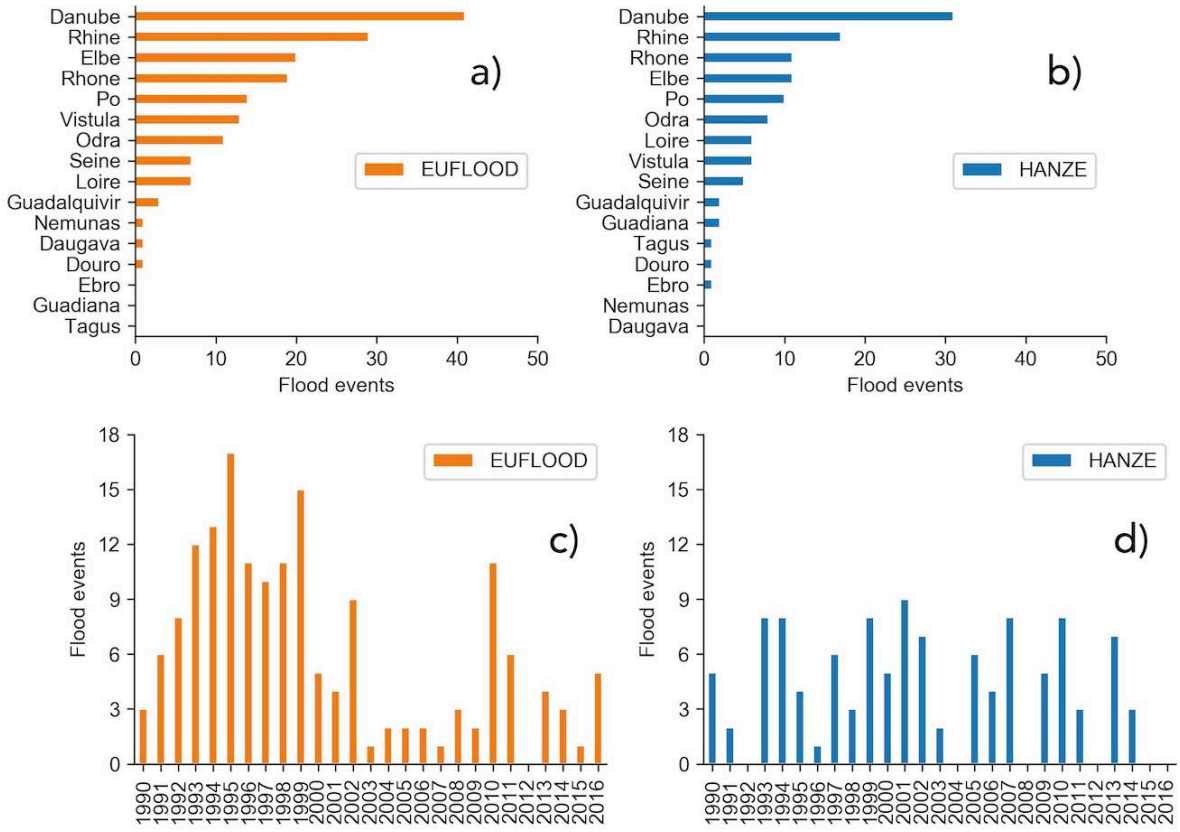

Figure 4.16. European flood events caused by rainfall for the TOP16 largest river basins from the European Flood Hindcast and HANZE data sets between 1990-2016. a-b) flood events per basin. c-d) yearly evolution

Figure 4.16-a-b shows the total number of events per basins in both data sets. In total HANZE reported 112 events with flood loses larger than 100 million EUR between 1990-2016, whilst in the European Flood Hindcast 167 important flood events were identified in the same period. The basin which has suffered the most flood events the Danube, with more than 35 flood events in the last two decades according to both data set. The Danube is followed by the Rhine, Elbe and Rhone river basins. During the same period six basins experienced low flood activity: the Tagus, Douro, Ebro, Daugava and Guadiana river basins have experienced only between zero and two flood events according to both data sets. Figure 4.16-c-d shows the number of flood events per year in both data sets. Important events from the last decade such the Central European floods in 2002 and 2010 are distinguished in both data sets. The high flood activity during 1993, 1994 and 1999 from the HANZE data is also present as high flood activity in the European Flood Hindcast. The low flood activity during for the years

2003, 2004, 2008 and 2012 according to HANZE compare well to the European Flood Hindcast.

Regarding the reason why both data sets do not report exactly the same number of flood events are numerous. For example, if the location of a flood in a given river basin occurs in a non-urban area, its flood loses may be under the 100 million EUR threshold used in the HANZE database. Not all reported floods in the European Flood Hindcast lead to a disaster event as there are other factors which play an important role in floods such as: soil saturation (soil moisture content) or the complexity of the flood defence infrastructure. Therefore, when the soil is saturated and intense rainfall is expected this situation is likely to lead to a flood event. As mentioned before, the impact of complex flood defence infrastructure could be underestimated by the approach used in Section 4.2.7. Nevertheless, the analysis provides at least some confidence that the flood inundation hindcast produces the approximately correct number and spatial distribution of flood events and that analysis of these patterns can yield insights into the nature of flood hazard within Europe.

4.4 Discussion

This study presents the development of a European Flood Hindcast at ~90 m resolution for the period 1990-2016 employing a hydrologic-hydrodynamic model coupling. The simulation framework considered main rivers and tributaries larger than 2,500 km2 for 298 river basins across Europe. While previous studies explored the nature of European floods with the use of river discharge time series or the use of remote sensing techniques applied to satellite imagery, this study used a continuous 2D flood simulation for this purpose. The database produced in this study allows the characterisation of flood events (in terms of occurrence, extent and inundation depth) over time at a reasonable resolution for continental scale flood risk management.

The data set generated in this study was used to identify flood events over time occurring in the largest 16 river basins in Europe. Result suggest that at European scale the 1990s were hit harder by floods than the 2000s and the first half of the 2010's decade. Results also revealed that the least active river basins within the study period (1990-2016) are the Ebro, Guadiana and Tagus and Douro rivers with one to zero events in the last three decades. Similarly, the most active river basins were the Danube, Rhine, Elbe and Rhone. These results compare favourably with previous findings

(Blöschl et al., 2019) where a climatic signal of observed river discharge was associated with increasing floods in northwestern Europe (the Rhine, Elbe and Rhone) and a decreasing in floods in southwestern Europe (the Ebro, Guadiana and Tagus and the Douro).

Since the modelling framework developed in this study can use any form of discharge data (from models or gauges) and the model is already built (bed, bank elevations calculated already), other applications can be considered. For example, the rainfall-runoff model can be prepared to run experiments on climate change. In that scenario, a new set of river discharge data could be generated and easily included to evaluate river hydrodynamic response for that scenario. Another potential application of the model setup is flood inundation forecasting. The EFAS model is a system that runs daily, producing predictions of river discharge a few days ahead. Moreover, the methodology applied here can be easily transferred to other continental or large scale studies worldwide since the modelling framework uses freely available global data with only the river discharge component being dependent on the study area.

Despite the model performance being generally satisfactory for different types of terrain and locations as shown in the test areas in Figure 4.8 (UK), Figure 4.11(Germany), Figure 4.13 (Italy) and Figure 4.14 (Czech Republic and Germany), the model used in this study might need revision in: (i) highly managed rivers and (ii) wetlands (i.e. washes, salt marshes, fens and moors). These two types of situations are difficult even for local scale and highly detailed flood models. In rivers with a high level of water control infrastructure there is no current European-scale database which captures details of the pumps, channels, gates and dikes work together to protect urban areas of from flooding. These features are therefore typically missing from large area models. In wetlands, complexity arises because these areas have shallow terrain elevation gradients and therefore even small amounts of water exceeding the river conveyance capacity can cause widespread flooding. In this case, small errors in the defence or channel size assumptions can have a big input impact on the predicted flood extents. Furthermore, wetlands tend to be formed by braided rivers or rivers that bifurcate from the main channel. This study used the HydroSHEDS hydrography to identify the location of rivers across Europe; this successfully mapped most main channels and tributaries, however the hydrography does not consider bifurcated channels generally present in wetlands areas. At the moment, none of the global scale hydrography databases (HydroSHEDS, MERIT Hydro) can represent bifurcated channels. Both highly

managed rivers and wetlands are still therefore likely to be best modelled at a local scale.

Flood footprints generated in this study were validated using observed flood inundation extents from previous events in the UK, Germany and Italy. Other European countries have a very limited to non-existent records of flood extents or flood depths and this constraints a broader validation of the data set. Unlike the UK where the framework was set up with LIDAR DEM, the continental Europe model used the MERIT DEM. Thus, the ability to predict flood patterns could be improved over continental Europe by better terrain data as LIDAR DEMs are known to significantly increase the accuracy in simulation of flood hydrodynamics (Schumann and Bates, 2018). Although some countries own LIDAR DEM that could have been used in this study, a rigorous procedure is required to fusion different sources of DEM data to be used as terrain elevations and this represents a significant study in its own right.

The forcing data (EFAS) used in the European Flood Hindcast plays an essential role in the modelling chain. EFAS obtained a Kling-Gupta efficiency higher than 0.5 for 75% of all stations during calibration and 57% of all stations during validation (Salamon et al., 2019). Higher skill scores in EFAS were found in large parts of Central Europe, while lower skill scores occurred mostly in the Iberian Peninsula as a result of the strong influence of reservoirs. Nonetheless, EFAS has a fair skill in general, but a few places may show large disagreement with observations. Running the test scenarios from Section 4.3.1 using observed data instead of a hydrological model to evaluate the quality of EFAS might lead to interesting findings, however, restrictions on the location of gauge stations, the number of available measurements and the ability to extend the inundation hindcast to European scale are considerable advantages to using the EFAS output.

The current hydrodynamic simulation framework does not account for reservoirs. Similarly, subsurface links between river basins are not accounted for either in the hydrodynamic model or the hydrological model. The downscaling algorithm adopted in this study acts as a complementary procedure but makes the assumption that subgrid scale hydrodynamic processes are relatively unimportant. Its implementation and performance are computationally cheaper than running a basin scale simulation at high resolution (90 m) as the downscaling only has to be executed once after the simulation has calculated the maximum inundation extent. For this reason, simulating at lower resolution with subsequent downscaling implementation will never produce

better results than running a pure 90 m resolution simulation. However, downscaling is a useful and computationally efficient technique for obtaining detailed flood outlines for multi-decadal simulations of inundation at continental scales.

The European Flood Hindcast used fixed Manning's coefficients for floodplain and channel set to 0.06 and 0.035, respectively. Thus, no calibration was performed to improve the skill of the model, which could lead to some degree of discrepancies in some areas. This situation can be enhanced by running a set of simulations within a sensitivity analysis framework to find the best floodplain and channel coefficients which reduce the error against observations, similar to Neal et al., (2009). Alternatively, the coefficient estimates can be acquired using a land cover classification as a proxy (e.g. van der Sande et al., 2003). Despite this, the results present acceptable skill scores for different terrain types: Figure 4.8 (UK), Figure 4.11 (Germany), Figure 4.13 (Italy) and Figure 4.14 (Czech Republic and Germany).

Another final limitation of the study is that the current modelling framework did not consider the variation of flood protection standards over time. For example, the event of August 2002 in Germany played an important role in improving the flood resilience of that country. After the event, the German government reinforced its flood defence infrastructure. These types of actions against floods are repeated in most developed countries, however, the lack of data concerning defence changes over time impedes its implementation in the model. Nonetheless, the assumption that the current flood protection levels have been installed since the 1990s seems to be broadly sensible.

4.5 Conclusion

We present a method for the development of flood inundation hindcasts at continental scales. Using this approach, a European flood hindcast was simulated for the period 1990-2016 at 1km native resolution, with outputs subsequently downscaled to ~90 m. In total, 298 river basins were considered within a computational framework built upon globally available data sources of terrain elevation, river width, flood protection standards, river discharge. Therefore, the methodology introduced here can be easily transferred to other continental or large-scale studies worldwide.

The European Flood Hindcast framework was used to produce a data set containing a catalogue of flood events which was analysed for the 16 largest basins in Europe.

This indicated that the most affected decade was the 1990's, with the Danube, Rhine, Rhone and Elbe being the most impacted basins. Conversely, the least impacted basins in the same period were the Douro, Ebro, Guadiana and Tagus. These results compare favourably with previous findings (Blöschl et al., 2019) where a climatic signal of observed river discharge was associated with increasing floods in northwestern Europe (the Rhine, Elbe and Rhone) and a decreasing in floods in southwestern Europe (the Ebro, Guadiana and Tagus and the Douro).

Both the methodology and data set in this study can be considered as new contributions to water resources. First, the computational framework improves from previous studies of the same kind in a few aspects: i) it introduces an efficient method to couple hydrological and hydrodynamic models in large scale and high resolution problems; ii) it presents a method to estimate river bathymetry by adjusting the channel conveyance to account for the systematic biases typically found in modelled river discharge; and iii) it describes a methodology to account for flood defences in flood inundation modelling by using as a proxy a database of flood protection standards and adjusting the capacity of the channel to match these. In addition, the data set generated provides useful information to characterise floods in Europe in terms of occurrence, extent and depth that is complementary to previous work. The study can also potentially assist continental scale Flood Risk Management (FRM). The database generated in this study can be used to identify flood hotspots at a continental level useful for insurers, multinational corporations, NGOs and national governments. These organisations can adequately prioritize these areas in rapid disaster response, urban planning or climate change adaptation.

4.6 Postscript

This chapter presents solutions to some open research gaps in continental-scale flood modelling. The chapter introduces an efficient method to couple hydrological and

hydrodynamic models in large scale and high-resolution studies (see Section 4.2.4). River bathymetry is estimated with a method that links inflow river discharge to the channel conveyance to account for systematic biases typically found in simulated discharge (see Section 4.2.5). The chapter also describes a new methodology to account for flood defences in flood inundation models (see Section 4.2.6). These methods were used to build a European flood hindcast that reconstruct flood inundation maps across Europe for a period of 26 years (1990-2016).

The location of rivers and tributaries presented in the European flood was obtained by means of two widely used global hydrography data sets namely, HydroSHEDS and MERIT Hydro. These data sets were derived from terrain elevations sourced from space-borne satellites. In Europe, the use of global hydrography data sets is acceptable as many European countries do not own national hydrographic data to extract the location of rivers from. However, some countries own this information and can be used to derived better estimates of the location of rivers. The next chapter presents a methodology to derive a new hydrography with similar characteristics of global hydrographic data sets but using high quality data sources.

CHAPTER 5

On the extraction of a precise river hydrography in the contiguous US

The previous chapter presented the development of a Pan-European flood hindcast. The framework mostly used global freely available data sets for data consistency. Global hydrography data sets (i.e., HydroSHEDS and MERIT Hydro) were used to identify river centrelines for rivers with upstream catchment area larger than 2500 km^2. Although these centrelines produced good results, we argue that the location of rivers can be improved by using high-quality national data sets of terrain elevation and some source of curated river centrelines. This chapter presents a methodology to obtain a hydrography for continental scale studies based on two components i) a high-fidelity source of terrain elevations and ii) a curated data set of river centrelines. The computational framework is presented for the US however, the same framework can be used in other places where similar data can be obtained.

This chapter consist of a paper in preparation. All simulations, analysis, writing and figures were completed by the lead author with advice from Jeffrey Neal and Paul Bates. All co-authors helped to shape the final manuscript.

Peer-reviewed article associated:
Sosa, J., Hawker, L., Sampson, C., Smith, A., Neal, J., Bates, P. (2020). On the extraction of a precise river hydrography in the contiguous US. In preparation

5.1 Introduction

The geolocation of rivers is one of the key factors used to drive local to global scale studies involving river hydrodynamics (Yamazaki et al., 2011; Neal et al., 2012; Raymond et al., 2013; Zarfl et al., 2015; Sampson et al., 2015). The geolocation can be predicted from a river network usually derived from a flow drainage map calculated from a Digital Elevation Model (DEM). A flow drainage or flow accumulation map is created by counting the number of upstream cells within the drainage basin from the outlet of a particular river basin. To this end, the downslope drainage direction in every cell in the DEM must be calculated first, the later type of map is known as flow direction map. Both the flow accumulation and the flow direction maps are known as hydrographic variables (Tarboton, 1997; 1991). Several studies already have obtained hydrographic information at global scale. For example, HYDRO1K (USGS, 2001) was one of the first data sets with global coverage identifying rivers worldwide at 30 arc-seconds (~900 m at the equator) grid resolution. It was derived from GTOPO30 (USGS, 1997), a global digital elevation model at 30 arc-seconds spatial resolution. With the launch of the Shuttle Radar Terrain Mission (SRTM) (Farr and Kobrick, 2000; Farr et al., 2007) in February 2000, a new database containing hydrographic data at global scale was produced; HydroSHEDS (Lehner et al., 2008). Unlike HYDRO1K this new hydrography derived from the SRTM was more detailed as it was able to capture more river features such as meanders as a result of its higher resolution (3 arc-seconds or ~90 m at the equator), features that previously could not be represented. Nonetheless, due to non-negligible intrinsic errors in the SRTM such as speckle and stripe noise in addition to tree height bias (Rodriguez et al., 2006; Yamazaki et al., 2017) and the coarse resolution of ancillary layers, the geolocation accuracy of rivers in HydroSHEDS is limited (Yamazaki et al., 2019). MERIT DEM (Yamazaki et al., 2017), a 3 arc-seconds multi-source and bias corrected DEM with global coverage and its complement product MERIT Hydro (Yamazaki et al., 2019) are the most recent developments in terms DEM and hydrographic information at global scale, respectively.

Other data sets have implicitly derived river networks globally bypassing the use DEMs and instead using satellite imagery. The Global River Width from Landsat (GRWL) (Allen and Pavelsky, 2018) is one example of this approach. The study obtained river widths estimates from the entire Landsat inventory storing these values within centre lines of the river masks. The centre lines were limited by the availability,

quality and resolution of the Landsat observations. Meaning that places with no observed rivers or low fidelity to extract rivers were not captured. A summary showing main characteristics of these sets is presented next in Table 5.1. These efforts have allowed us to locate main rivers and channels within catchment areas larger than 50 km^2 in regions where this was not possible before.

Data source	Comments	Reference
HYDRO1K	~900 m resolution at the equator, coverage between 90°N – 90°S	USGS, 2001
HydroSHEDS	~90 m resolution at the equator, coverage between 60°N – 60°S	Lehner et al., 2008
MERIT Hydro	~90 m resolution at the equator, coverage between 90°N – 60°S	Yamazaki et al., 2019
GRWL	coverage limited to rivers "seen" by Landsat	Allen and Pavelsky, 2018

Table 5.1. Summary of current hydrographic data sets available at global scale.

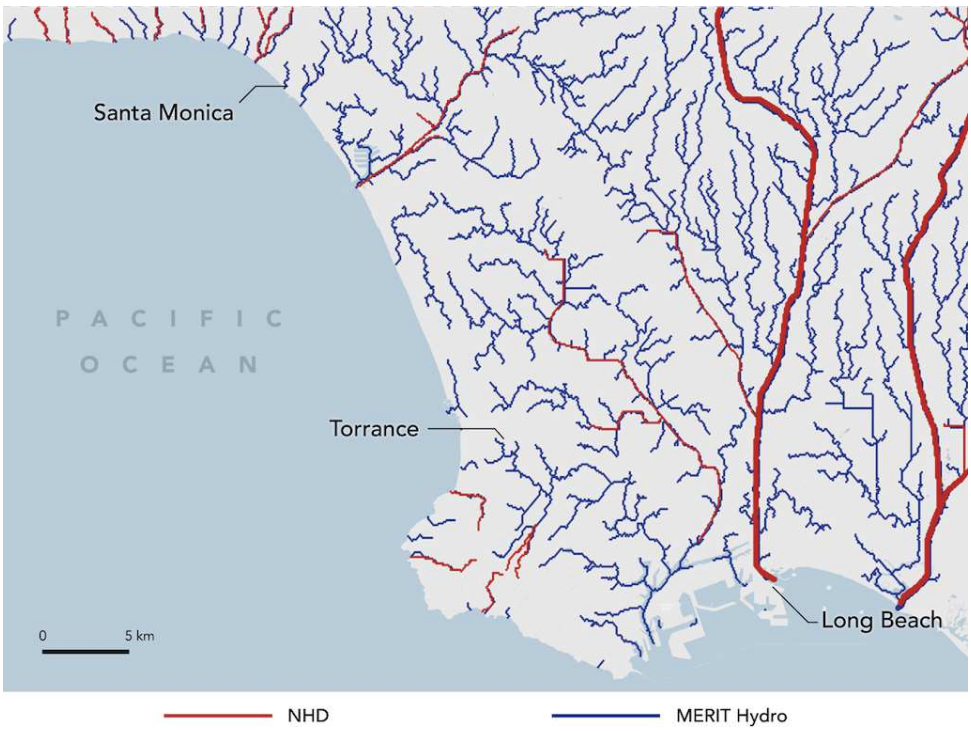

Figure 5.1. Comparison between NHDPlus and MERIT Hydro in Los Angeles, CA.

At country level, some nations have developed their own river network data sets, this has been possible thanks to the availability of high-quality data sources to extract this information from. In the US for example, the National Hydrographic Dataset (NHD) (Simley et al., 2009) is the most comprehensive data set that provides this type of information. This data set was created by a joint collaboration between the US Geological Survey (USGS), the US Environmental Protection Agency (EPA), and the Natural Resources Conservation Service (NRCS) and it was derived from 7.5-minute series topographic maps at a scale of 1:24,000. Complementary to NHD is National Hydrography Dataset Plus (NHDPlus) (McKay et al., 2012), an ancillary data set that provides "added-value attributes" to the river network allowing each link in the network to have extra information such as flow direction, flow accumulation area, flow volume and flow velocity. Both the NHD and NHDPlus are continuously updated to meet the water resource needs of the nation.

NHDPlus is a widely recognised product that accurately maps rivers across US. However, there are some disadvantages to using the NHDPlus for flood simulations. First, this data product currently lacks the representation of river links in some areas. For example, Figure 5.1 shows a comparison between NHDPlus (version 2.1) and MERIT Hydro in Los Angeles County. The NHDPlus misses links in the river network that might not necessarily be identified as rivers but are important depressions in the terrain. These extra links are important in urban flood models, both where pluvial flooding is common, or in fluvial flooding where missing river network links can lead to significant overestimates of flood extent (Wing et al., 2018). MERIT Hydro, a global scale river network, identifies those missing links but its accuracy is limited by the global MERIT DEM. Another disadvantage of NHDPlus is that the layers are distributed in vector format, which presents difficulties for studies using rectangular grids to estimate output variables such as hydraulic models. Rectangular based grid models require estimates of flow accumulation at the granular level, with a value for every pixel, which is the format of the MERIT Hydro and Hydrosheds datasets.

In this study we introduce UShydro a new hydrography for the contiguous US created by means of the National Hydrography Dataset Plus (NHDPlus) and the National Elevation Dataset (NED) at 90 m spatial resolution. The new data set offers a river network that combines the best of NHDPlus but includes additional river links and is in a raster-based format suitable for computational studies based on rectangular grids. Thus, by directly integrating NED as source data set, the new hydrography ensures

good linkage between terrain elevation and the river network in the US. The data set provides a flow accumulation map in the form of global studies so that studies already using HydroSHEDS and MERIT Hydro can be updated with the new data set in a seamless way. The dataset was benchmarked against recent global hydrographic studies such as HydroSHEDS and MERIT Hydro and the original NHDPlus data set. Finally, the computational framework used to calculate the new hydrography is fast and it can be easily replicable in other areas of interest.

5.2 Data and methods

5.2.1 Data

UShydro was built upon the National Elevation Dataset (NED) (Gesch et al., 2009) a seamless raster product primarily derived from USGS DEMs at 10 and 30 meters spatial resolution. The NED is provided at a variety of resolutions ranging from 1/9 (~3.4 m) to 1 arc-seconds (~30 m). This study used the ~30m DEM as it fully covers the continuous US in addition to part of the Canada and Mexico territory. Including terrain information in Canada and Mexico is relevant as the US has some transboundary river basins such as the Columbia, Rio Grande and Colorado Rivers. Previous studies have shown that merely a DEM unaccompanied with any ancillary layer is not sufficient to derive accurate river networks maps (Lehner et al., 2008; Yamazaki et al., 2019). This study used as ancillary layers the National Hydrography Dataset Plus (NHDPlus) (McKay et al., 2012) a high-resolution river network, and the global hydrography MERIT Hydro (Yamazaki et al., 2019). A summary of data sets used in this study is shown next in Table 5.2.

Data source	Comments	Source
NED	1 arc-seconds (~30 m) resolution	Gesch et al., 2009 https://viewer.nationalmap.gov/basic/
NHDPlus v2.1	Contains ~2.7 million line-type features	McKay et al., 2012 https://viewer.nationalmap.gov/basic/
MERIT Hydro	3 arc-seconds (~90 m) resolution	Yamazaki et al., 2019 http://hydro.iis.u-tokyo.ac.jp/~yamadai/MERIT_Hydro/

Table 5.2. Data sources used in this study to generate a new hydrography in the contiguous US.

UShydro was built at 90 m spatial resolution allowing interchangeability with global hydrographic studies such HydroSHEDS and MERIT Hydro, however higher resolution can be achievable using the same computational framework presented in the next sections. In order to produce a hydrography at 90 m resolution, the NED data set was upscaled to 3 arc-seconds (~90 m) using bilinear interpolation and subsequently tiled into 53 tiles with 5°x5° extent each to cover the contiguous US territory (see Figure 5.2). Tiling was necessary to make some calculations more manageable in computer memory. NHDPlus is a vector-based database containing ~2.7 million features of rivers and streams. The NHDPlus database was downloaded from the United States Geological Survey (USGS) servers in a stand-alone file in Geodatabase format. From the database, only the feature "NHDFlowline_Network" was used. Later, the attribute "DivDASqKm" which states for "Divergence-routed drainage area" was extracted and rasterised at 3 arc-seconds resolution (~90 m) resolution and tiled into 53 tiles of 5°x5° extent matching the tiles created for the NED data set. From the MERIT Hydro database, the "Upstream drainage area" variable was used with no additional preprocessing as this data was tiled already. The "Divergence-routed drainage area", "Upstream drainage area" and flow accumulation area are interchangeable concepts which corresponds to the drainage area upstream a particular river cell in the basin. For example, headwater cells in a basin will have a value of 0 km^2 whilst the basin outlet will have a value corresponding to its drainage basin area (e.g., Colorado River 618,000 km^2).

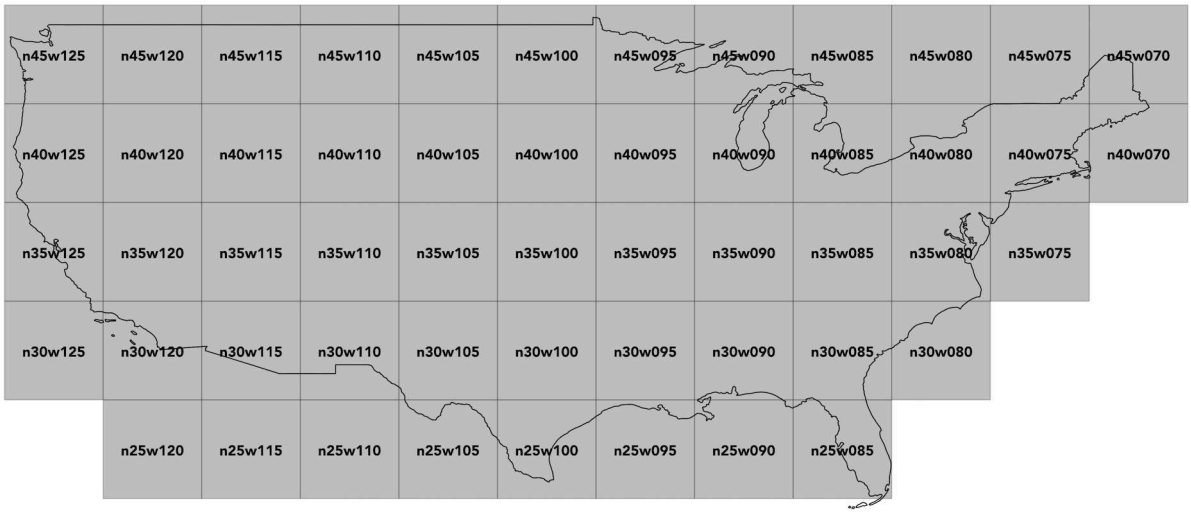

Figure 5.2. Spatial coverage of USHydro for the contiguous US divided into 53 - 5°x5° tiles.

Trans-national river basins (e.g. Columbia, Rio Grande and Colorado) share territory with Canada and Mexico and are not fully represented in NHDPlus, however they are important to produce a correct river network. To tackle this issue, main channels and rivers from NHDPlus were fused with MERIT Hydro (Yamazaki et al., 2019) to complete the missing information. To this end, rivers larger than 1,000 km^2 in MERIT Hydro were manually connected at the border of Mexico and Canada with NHDPlus creating a fused drainage network. For rivers lower than this threshold, elevation depressions from NED were used to infer the network.

5.2.2 DEM conditioning: Stream-burning

DEM conditioning is the procedure of modifying the elevations in the DEM in order to allow full downstream drainage (Yamazaki et al., 2019). First, the DEM should be modified by lowering elevations in areas where rivers are forcing downstream drainage in a process known as "stream-burning" (Lindsay, 2016b). Additionally, spurious depressions such as sinks and flat areas that create depressions where no lower neighbouring cell must be treated also as they break down the natural downstream flow routing.

In this study, the DEM conditioning begins with the "stream-burning" process (Saunders, 1999; Lindsay, 2016b). To this end, main rivers and channels centre lines are incorporated in the DEM by "burning" a new value for the centre line elevation in order to constrain interim streamline cells to maintain downstream routing. This study used river vector centrelines from the two sources processed before NHDPlus (in the contiguous US) and MERIT Hydro (in Canada and Mexico). The drainage basin area given by these datasets (see e.g. Figure 3b the NHDPlus data set near Detroit) was used to modify the DEM elevation in order to keep local monotonic descent in the network. The relationship between drainage area and DEM elevation was given by Equation 5.1:

$$E = \frac{10}{\frac{\log(N)}{\log(1.5e^{-2})} - C} \qquad (5.1)$$

where, E is the new value to be burned in the DEM, N is the drainage area and C is a constant value calculated via trial and error with $C = -99$. This form of the equation was used as it can handle drainage areas with values larger than 1 million km^2 (largest accumulation value in the US is ~2.9 million Km^2 in the Mississippi River) and avoid truncation of the number. Thus, by transforming the flow accumulation area into a value between -100 and 0 with decimals changing seamlessly but correctly for double-precision computations. Figure 5.3c shows the final conditioned DEM after applying Equation 5.1 for a small area near Detroit, MI.

5.2.3 DEM conditioning: Depressions

The NHDPlus data set contains a vast number of streams (~2.7 million line-type features) in the continuous US, however, it has disconnections in some areas which cause the natural downstream flow routing to break down. Thus, although rivers were burned into the DEM, they still may cause problems in the estimation of an accurate river network due to the lack connectivity. Another source of river network disconnection is due to spurious sinks or depressions where no lower neighbour cell can be identified thereby impeding natural downstream flow. Previous studies have tackled these issues in one of two ways (after Rieger, 1998): i) depression-filling approaches where the elevations of grid cell interiors are raised to the closes depression ii) depression-breaching approaches where grid cell elevations are lowered to create a single-cell wide breach channel connecting the bottom of a closed depression to some downslope point.

In this study, two depression-filling approaches and one depression-breaching method were tested. First, the "FillDepressions" algorithm available in WhiteboxTools (Lindsay, 2018) was used to fill depressions in every tile. The tiles were clipped with a buffer of 0.01° (~1 km) to avoid problems at the edges of the tile. Later, the "Priority-Flood" algorithm described in Barnes et al. (2014) and the "BreachDepressionsLeastCoast" algorithm (Linday and Dhun, 2015) were also evaluated in the same manner. In each case, the final flow accumulation area was benchmarked against observed values following the procedure described in Section 5.3.1. After analysis the "Priority-Flood" approach obtained the lowest flow accumulation error and it was the method selected to produce the final data set in this study. Figure 5.3c shows the final conditioned DEM for a small area near the city of Detroit, MI.

Inland or endorheic basins are natural geological landforms that retains water but have no hydrological connection to the marine environment (Nichols et al., 2007). The outlet location of this type of basins have been identified in the NHDPlus data set under the "Sinks" feature and facilitated its integration in UShydro. So that by directly burning the rivers from NHDPlus, endorheic basins were implicitly considered with no additional steps. The priority-flood depression algorithm was calibrated via a threshold value to not remove these features after passing the algorithm.

5.2.4 Flow directions and flats

Once the conditioned DEM is prepared, the next step consists of determining which direction water will flow in a given cell. Thus, a flow direction map containing direction information at every pixel must be generated. Several methods already exist for this purpose, for example, the D8 method (O'Callaghan and Mark, 1984) calculates flow directions by identifying the neighbouring pixel which gives the steepest slope within a 3x3 window. Another method is Rho8 (Fairfield and Leymarie, 1991) which improves the conventional D8 method by representing in a better way flow direction in high slope areas. D8 and Rho8 are "convergent flow" methods where only one cell can be assigned for descending flow however "divergent methods" also exist where the descending flow can be diverted into different neighbouring cells within the 3x3 window. This is case with the algorithm of Quinn (1991) where one or more neighbouring cells contain information about the descending flow. Other divergent methods from the literature are the ones proposed in Freeman (1991), Holmgreen (1994), Tarboton (1997) and Seibert and McGlynn (2007).

This study used the D8 approach in the calculation of flow direction as this convergent method is computationally inexpensive compared to divergent methods. A divergent method will demand more computational resources as, to date, there is not an efficient (i.e. in the context of continental scale studies) algorithm to calculate flow accumulation from a divergent flow direction map. As a consequence, the new river network generated in this study does not represent braided rivers and deltas which commonly exhibit divergent flow. Figure 5.3d shows flow directions for a small area near Detroit, MI using the D8 approach.

Flats or depressions with no local elevation gradient are intrinsic to lakes in the NED data set. Flats can also occur as a consequence of the stream-burning process described

in Section 5.2.2, but regardless their origin this is an issue that needs to be solved. Technically the problem arises as no flow direction can be assigned since the D8 algorithm is not able to find a downslope cell. UShydro used an efficient algorithm to solve flats by assigning drainage directions in flats (Barnes et al., 2014) the method superimposes a gradient away from higher terrain with a gradient towards lower terrain to solve this issue.

5.2.5 Flow accumulation

Once flow directions are calculated and flats have been treated in every tile, upstream flow accumulation can be estimated for each pixel. At continental scale this task is rather challenging as rivers are generally contained within different tiles and the algorithm should be able to count the number of cells upstream. Thus, the flow accumulation algorithm must take into account this point and identify rivers from different tiles. Despite this, several computer codes exist that can calculate flow accumulation (e.g., TauDEM Tarboton, 2005; WhiteboxTools Lindsay, 2018; TopoToolbox Schwanghart et al., 2010) but their efficiency over continental scale areas is limited due to lack of efficient memory allocation or parallel computing implementations. This study therefore used a parallel flow accumulation algorithm with efficient memory management implemented in RichDEM (Barnes, 2017; Barnes, 2018).

All steps mentioned so far were grouped together in an automatic computational framework to facilitate debugging, testing and allow replication of the framework in other areas. The entire framework took ~6 hours to obtain flow accumulation successfully for the entire US territory on an Intel(R) Xeon(R) CPU E5-2650 v3 @ 2.30GHz, 64 GB RAM. Figure 5.3a shows flow accumulation areas for rivers larger than 250 km2 and Figure 5.3e presents an inset of the accumulation for the city of Detroit, MI.

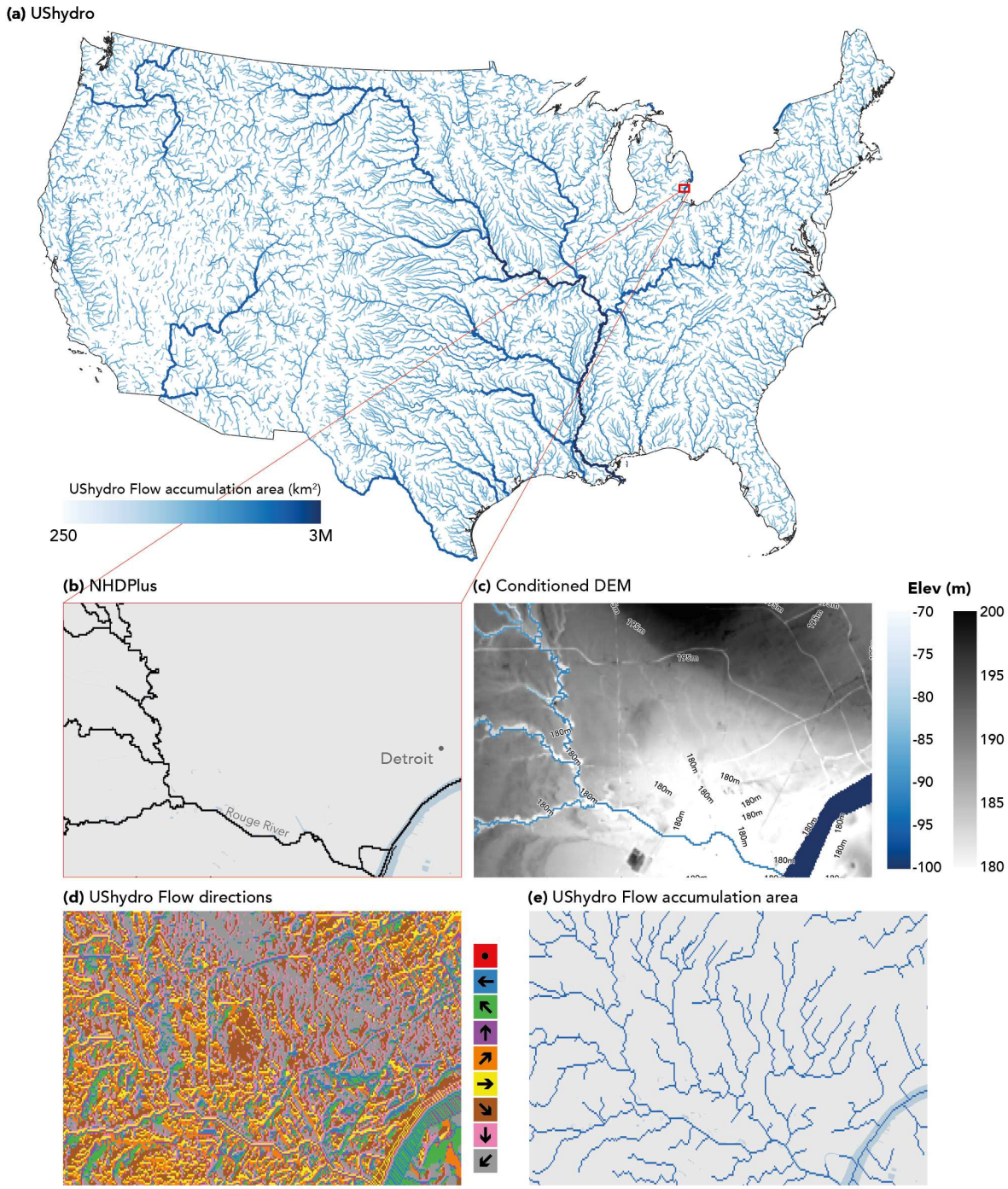

Figure 5.3. The UShydro data set a) Flow accumulation areas larger than 250 km^2 b) NHDPlus river network near Detroit c) Conditioned DEM d) D8 Flow directions e) Zoom-in view of UShydro in the city of Detroit.

5.3 Results

5.3.1 Flow accumulation area evaluation

In this section, the flow accumulation area from NHDPlus was compared with UShydro and two global hydrographic data sets HydroSHEDS and MERIT Hydro. The flow accumulation test helped to inspect the connectivity of the river network from the head waters to the river outlet. NHDPlus was considered as the ground truth data set as it has been continuously revised and updated and it has a large community of personnel reporting issues in the data, despite that is not exempt from errors. The comparison used 90 m rasterised maps from NHDPlus and 90 m raster maps from the target data sets (i.e. UShydro, HydroSHEDS and MERIT Hydro). At this resolution evaluating every river cell demands a considerable computing effort, for this reason two scenarios were chosen i) an evaluation of all river cells with a flow accumulation area larger than 1,000 km^2 and ii) a sample of ~200 thousand rivers cells for rivers larger than 1 km^2. Then, the flow accumulation error was evaluated as follows. First, once a river cell in NHDPlus is detected, a radius of 2 km in the target data set is fixed to find the closest flow accumulation area with the minimum error, this approach was also used by Yamazaki et al., (2019). Finally, the flow accumulation area error was estimated according to Equation 5.2:

$$Error = \frac{measured - observed}{observed} * 100\% \qquad (5.2)$$

where $measured$ is the flow accumulation area in any of the hydrographic data sets (i.e. UShydro, HydrosSHEDS and MERIT Hydro) and $observed$ is the flow accumulation area of the ground truth data set (i.e. NHDPlus).

Figure 5.4 shows results of the comparison for a) UShydro b) HydroSHEDS and c) MERIT Hydro. Maps located in the left side show the percentage error for the rivers larger than 1,000 km^2 upscaled to 1 km resolution and aggregated using the "maximum" for visualization purposes. Scatters plots on the right side show the percentage error for a sample of ~200 thousand cells for rivers across different sizes (i.e. >1 km^2). Results suggest that UShydro improves the representation of endorheic basins compared to global data sets where the UShydro error is <5%. These basins are mostly located the Great Basin area in Nevada and part of Oregon, Utah and California. In

particular basins such as the Humboldt, the new hydrography presents large improvements over global hydrographic studies (5% compared to 35% on average). In the state of California, UShydro indicates better agreement with NHDPlus for the two major rivers in the area the Sacramento and the San Joaquin rivers with errors lower than 5%, whilst global hydrographic studies ~50%. Similar patterns are repeated in other states. Complexity and size of the Mississippi River basin makes it challenging to accurately obtain flow accumulation errors lower than ~25% on average in UShydro, the reason is because the river formed by many tributaries producing a cumulative error. MERIT Hydro shows better agreement at the lower part of the basin near Louisiana (error ~10%), however, its performance decreases in the upper part of the basin near Nebraska and South Dakota.

A 90 m flow accumulation raster map contains vast amount of information and it was computationally challenging to fit it into memory. For this reason, a sample of 200 thousand river cells in for each data set were compared to evaluate the performance of the hydrographic studies across a different range of river sizes. Scatter plots at the right margin in Figure 5.4 show the how the flow accumulation error varies across different sizes when compare to NHDPus. The bins in the scatter plots range from -100% to +100% with a step of 2% in the x-axis, whilst from $10e^0$ to $10e^7$ linearly spaced into 151 values in the y-axis. The colour bar on the right side shows the number of river cells contained within each bin. The comparison suggest that all the target data sets present discrepancies across difference sizes with values ranging between -100% and 100%. Nonetheless, most of cells have an error that varies between -5% to 5% (see Table 5.3). UShydro presents an improvement over global hydrographic studies as results suggest that 72.78% of sample data lies within -5% and 5% error compared to 62.41% and 57.72% for MERIT Hydro and HydroSHEDS, respectively. The cause of error for the remaining data that do not fit within this range can be attributed to several factors, for example, connectivity issues either in the benchmarking data or in the target data set. Further analysis in specific areas might be important to assess the main cause of these errors.

	UShydro	**MERIT Hydro**	**HydroSHEDS**
-5% > Error < 5%	72.78%	62.41%	57.72%

-2% > Error < 2%	59.60%	49.41%	44.28%

Table 5.3. Flow accumulation benchmark for different hydrographic studies and NHDPlus for a sample of 200 thousand cells.

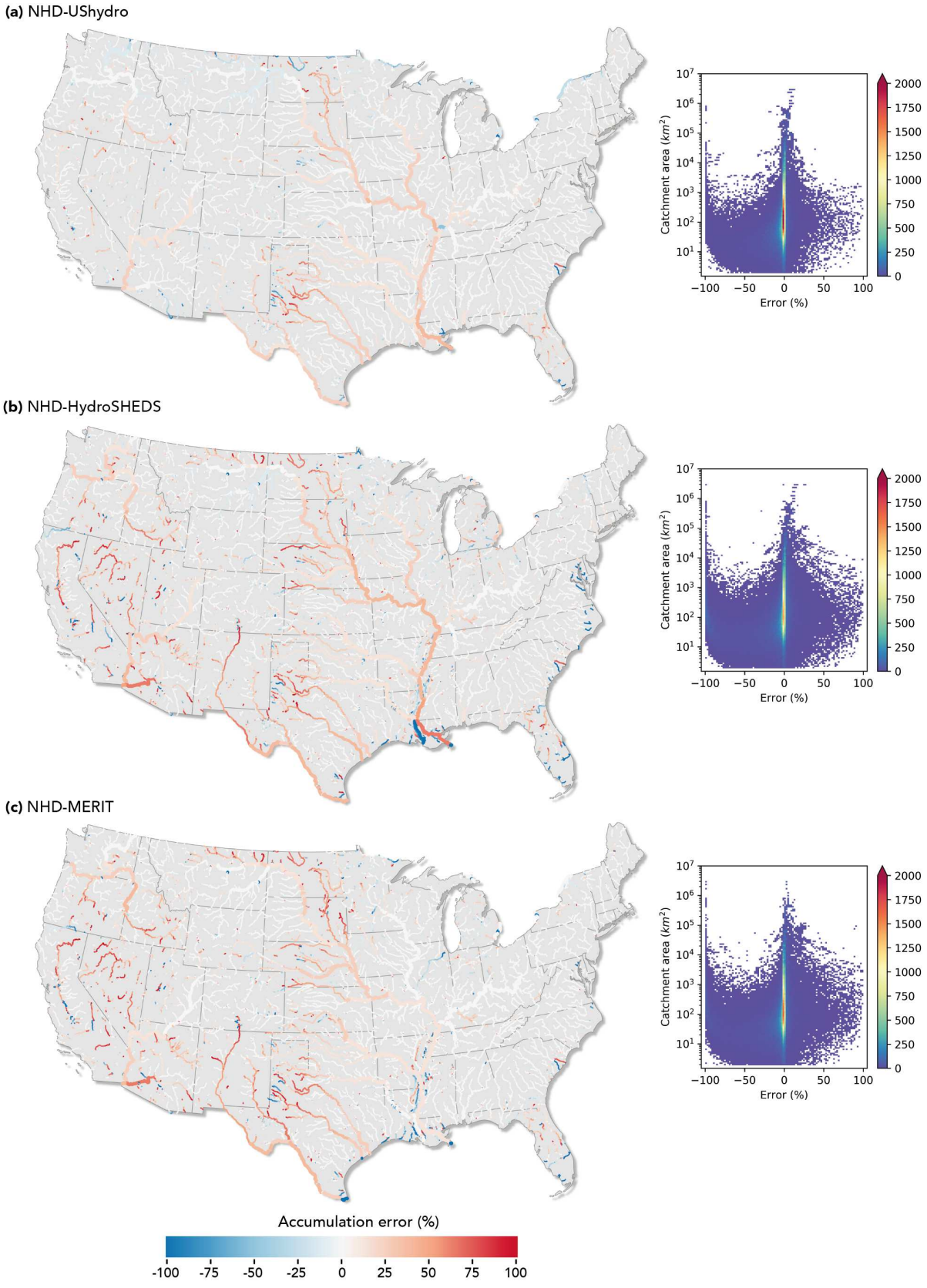

Figure 5.4. Flow accumulation comparison between NHDPlus and a) UShydro b) HydroSHEDS and c) MERIT Hydro. Maps on left margin show the percentage error for river cells larger than 1,000 km^2 upscaled to 1 km spatial resolution and aggregated using the "maximum" for visualization purposes.

Scatters plots on the right margin show the percentage error for a sample of ~200 thousand cells for rivers across a different range sizes for river cells larger than 1 km² in flow accumulation area.

5.3.2 Stream geolocation evaluation

In addition to the flow accumulation error, the geolocation of the rivers and streams was also evaluated. To this end, NHDPlus was used again due to high fidelity of the data set. One of the considerations for this evaluation is that the error indicator must be in accordance with the scale of the river, for example, a 1,000 m distance error is significantly important for a river with a catchment area <5 km², and considerably low for a larger river or a catchment area >10,000 km² (Yamazaki et al., 2019). One way to take into this issue is by calculating the error relative the catchment area as follows. First, once a river cell in the NHDPlus is identified, a fixed radius of 2 km is used to identify the cell with the minimum flow accumulation error and its distance (D) to the NHDPlus cell. Then, D was divided by the NHDPlus river cell flow accumulation associated (A). Later, to range the error between -100% and 100% the least squares method was used where the maximum possible error occurs when $max(D)/min(A)$ whilst the minimum error when $min(D)/max(A)$.

Geolocation accuracy errors are presented in Figure 5.5 for two scenarios i) all river cells larger than 1,000 km² and a 200 thousand sample for river cells larger than 1 km². Results suggest that the target data sets present very small differences for larger rivers (i.e. catchment area >1000 km²) errors are in most cases <5%. The benchmark indicates that 95.14% of the data sample has a geolocation error <5% in UShydro, a marginal improvement over the global data sets with 94.40% and 93.16% for MERIT Hydro and HydroSHEDS, respectively (see Table 5.4). Scatter plots in Figure 5.5 show the geolocation errors distributed along different river cell sizes from the data sample. The target data sets present very small differences between the datasets for rivers larger than 100 km², nonetheless the error increases largely for small rivers (<100 km²) (see Figure 5.5-bcd).

	UShydro	MERIT Hydro	HydroSHEDS
Error <5%	95.14%	94.40%	93.16%
Error <2%	82.87%	79.53%	77.01%

Table 5.4. Geolocation error benchmark for different hydrographic studies and NHDPlus for a sample of 200 thousand cells.

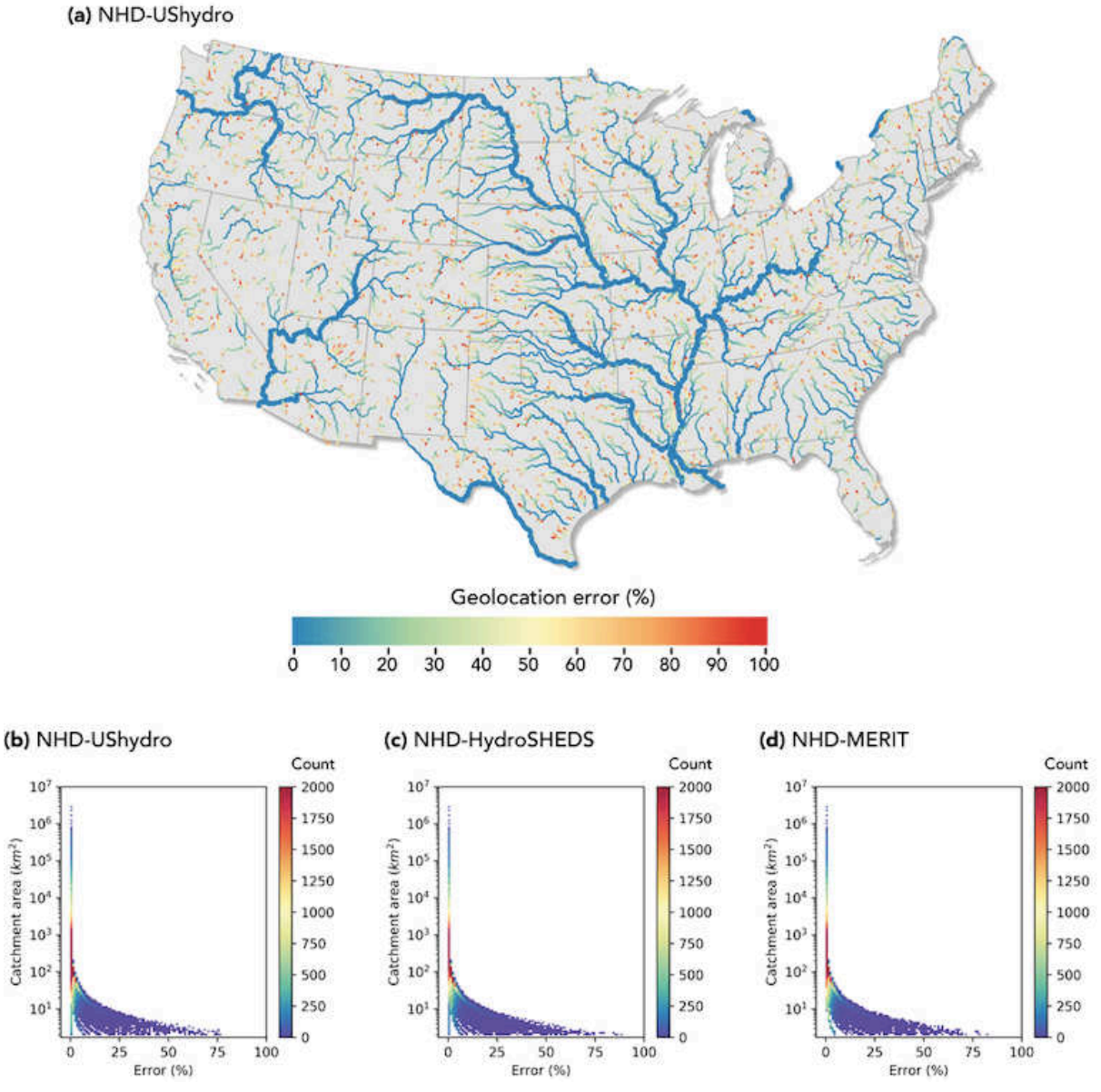

Figure 5.5. Stream geolocation comparison between UShydro, HydroSHEDS and MERIT Hydro against NHDPlus a) Shows UShydro error againt NHDPlus for rivers larger than 1,000 km² (catchment area) upscaled to 1 km² spatial resolution and aggregated using the "maximum" for visualization purposes. Error for a data sample of 200 thousand cells along different sizes in b) UShydro c) HydroSHEDS and c) MERIT hydro.

5.3.3 NHDPlus uncovered areas

The information contained in NHDPlus is very precise as the data set is under active development, however, it misses stream information in some areas. In this section, the total number of rivers and streams from NHDPlus are compared with UShydro to estimate the percentage of information missing by NHDPlus at county level. In doing so, both data sets were clipped following boundaries of the US counties. Then, a threshold to the flow accumulation or drainage area of 0.1 km^2 was applied to extract a raster-based river network. Next, the total amount of pixels in UShydro were subtracted from the total number found in NHDPlus to obtain the number of missing cells. This calculation was carried using the resulting UShydro data set (~90m resolution) and the rasterised version of NHDPlus (~90m resolution) calculated previously in Section 5.2.1. The missing cells difference was divided by the total number of cells found within county (at ~90m resolution) to obtain the percentage of territory within the country uncovered by NHDPlus (Figure 5.6). Results found that in all cases NHDPlus misses stream and rivers information in particular the ones with drainage areas lower than 5km^2. In some counties, the missing information can be up to 25% of the territory.

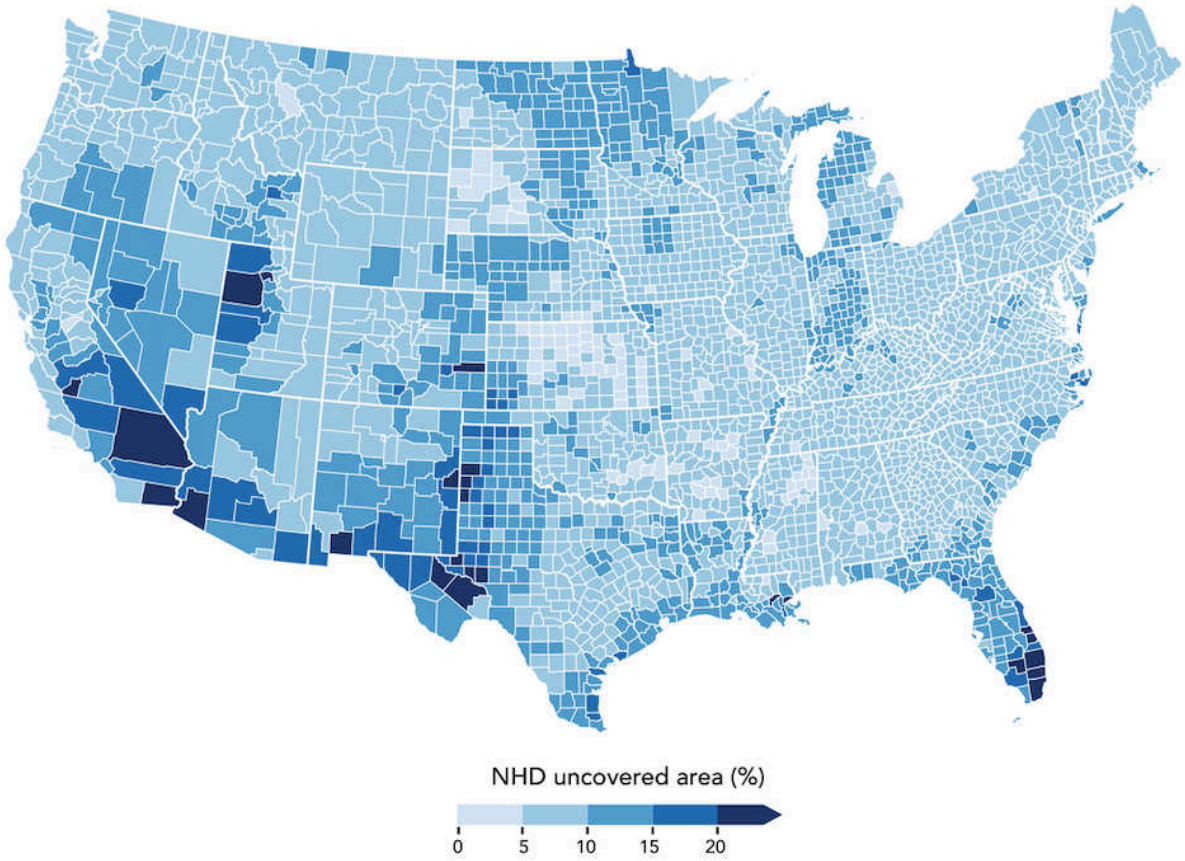

Figure 5.6. Percentage of territory uncovered by NHDPlus compared to UShydro for rivers and streams with catchment area larger than 0.1 km^2.

Missing streams are further investigated for the Top10 most populated counties. Table 5.5 shows the percentage of uncovered territory by NHDPlus for different catchment size classes for the most populated counties in the US. Percentage were calculated by subtracting the number of cells found within a catchment size class (e.g. rivers with catchment size between 0.1 and 5 km^2) by the number of cells found in NHDPlus for the same class. The difference was divided total amount of cells within the county territory. Results found that for Los Angeles, CA, where by 10,105,518 people live (official estimate July 2018), NHDPlus miss stream and rivers for 13% of its territory mostly very small streams (i.e. 0 – 5 km^2). Similar results were found other well populated counties.

County	0-5 (km^2)	5-10	10-100	100-1k	1k-10k	10k-100k	>100k	TOTAL (%)
Los Angeles	12.9	0.1	0.0	0.0	0.0	0.0	0.0	13.0
Cook	11.5	-0.1	-0.1	-0.1	0.0	0.0	0.0	11.3
Harris	14.0	-0.1	-0.2	0.0	0.0	0.0	0.0	13.7
Maricopa	19.7	-0.4	0.0	0.0	0.0	0.0	0.0	19.2
San Diego	9.6	-0.3	-0.1	0.0	0.0	0.0	0.0	9.2
Orange	10.3	-0.1	-0.1	0.0	0.0	0.0	0.0	10.1
Miami-Dade	20.7	0.9	0.2	0.2	0.0	0.0	0.0	22.0
Dallas	11.4	-0.6	-0.2	-0.1	0.0	0.0	0.0	10.5
Kings	12.2	1.1	0.5	0.0	0.0	0.0	0.0	13.8
Riverside	16.1	-0.3	0.0	0.0	0.0	0.0	0.0	15.8

Table 5.5. Percentage of uncovered territory by NHDPlus for different river catchment sizes for the Top10 most populated counties in the US.

Although the size of rivers not captured by NHDPlus is small, and some hydrological studies might ignore these streams, other studies will consider information of streams at this level to be important. For example, pluvial flood modelling, where intense amount of rainfall produce inundation in urban areas, generally require smaller rivers to be included for any modelling to be effective.

5.3.4 UShydro insights

The relationship between the number of stream links and the size of the largest river in US counties is investigated next. To this end, the flow accumulation layer from UShydro was used and clipped according to each county in the US. Then, each link in the stream network was identified and the quantile 0.95 calculated to the get an estimate of the size of the largest river in the county. Figure 5.7 shows the relationship between the number of links and the largest river size in the county. Data shows that most large rivers (catchment size >150,000 km^2) are present in the Midwest and Southeast regions. In these regions, the density of rivers (i.e. the number of reaches) varies from 2 until 25 thousand. Another important region is the north-western region where most rivers can be characterised as midsize (<150,000 km^2) and densely packed (>10,000 reaches). Unlike the east, the southwest and western regions present streams of small size generally ending up in endorheic basins in the Great Basin area.

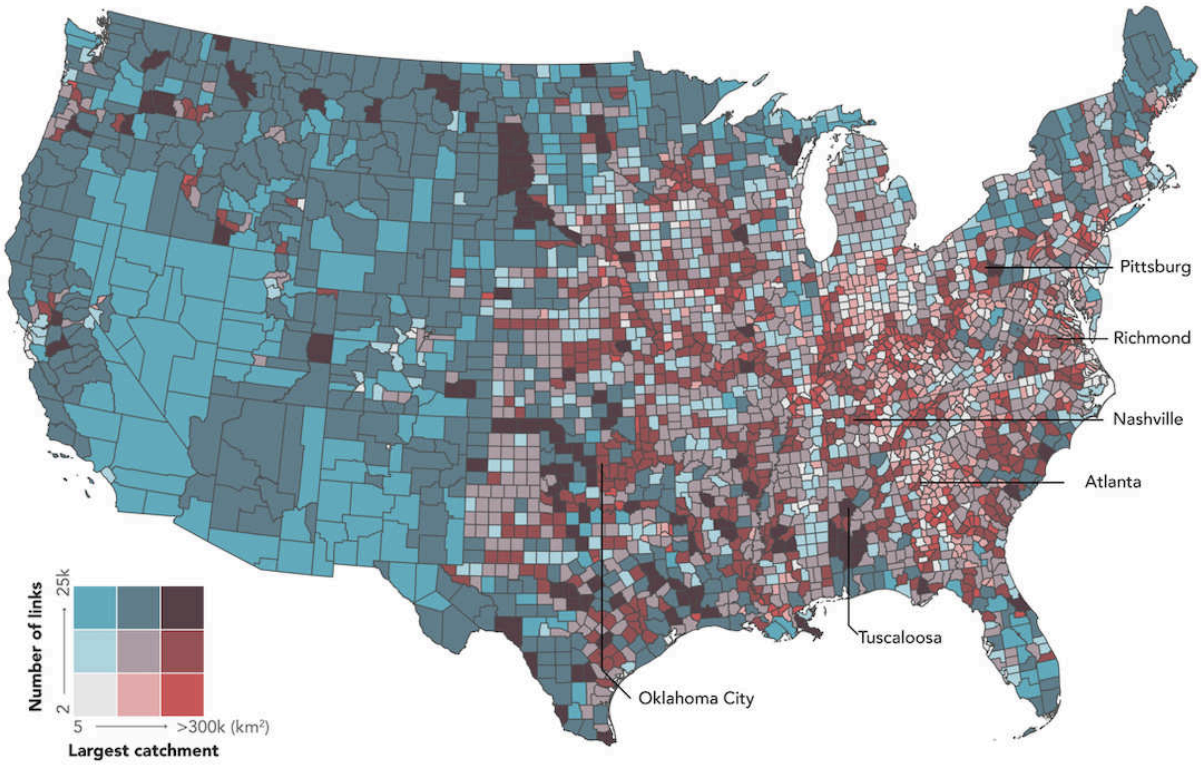

Figure 5.7. Relationship between river links and the size of the largest river at county level using UShydro.

5.4 Discussion

The geolocation of rivers has been mapped by different studies based on spaceborne DEMs and ancillary water body layers, and the analysis of Landsat imagery e.g. GRWL. These approached allowed georeferenced river and stream maps to be obtained in a consistent manner across the entire terrestrial land surface. However, in data rich areas where high quality terrain elevation and ground-truth layers of water bodies are accessible, higher quality hydrography layers that improves connectivity and geolocation accuracy can be constructed. This study presents UShydro a new hydrography for the contiguous US using National Elevation Dataset (NED), a high-resolution terrain data, and the extended version of the National Hydrography Dataset (NHDPlus), an ancillary vector layer of river and channel centre lines. This new hydrographic data set presents advantages over NHDPlus as it extends its coverage in areas with limited mapping.

The NHDPlus database contains ~2.7 million georeferenced rivers and channels within the contiguous US, despite that, its use is limited due the absence of some minor river links in the network and connectivity issues (see Figure 5.1). It was found that the proportion of missing links can reach up to 25% for territory county (see Figure 5.6) varying from 9.2% to 19.2% for the Top 10 most populated counties. Both constraints prevent the use of NHDPlus data in hydrological studies where river size and connectivity are relevant for example, flood hazard mapping (Sampson et al., 2015; Wing et al., 2017). Thus, UShydro was created to fill the absence of minor rivers in NHDPlus while maintaining connectivity between main rivers, streams and water bodies. The new hydrography was evaluated and from a sample of 200 thousand cells the flow accumulation error was between -5% and 5% for 72.78% of the sample whilst global studies obtained values lower than 62.41% (see Table 5.4). The improvement over global hydrographic studies were more evident in the Great Basin area largely characterised by endorheic basins (see Figure 5.4). Small differences were found in the evaluation of geolocation accuracy where a UShydro reported errors with values lower %5 in 95.14% of a data sample whilst global studies lower than 94.40% (See Table 5.5).

Like other DEM-based hydrographic studies such as HydroSHEDS and MERIT Hydro, UShydro has limitations regarding its ability to represent bifurcated channels particularly present in braided rivers and delta areas. This limitation is intrinsic for flow directions derived from the D8 algorithm. Thus, complex river structures, such the case of the Old River Control Structure which diverts part of the Mississippi river into the Atchafalaya River, will not be represented in the hydrography. This lack of ability contributed as source of error during the evaluation of UShydro in the evaluation of the data set in Sections 5.3.1 and 5.3.2.

5.5 Conclusions

A new hydrography for the contiguous US was generated by means of the National Elevation Dataset (NED) and the National Hydrography Dataset Plus (NHDPlus). The new data set extents the current coverage of the NHDPlus in areas with low coverage usually derived from disconnected reaches at the head waters.

Global river network data sets such as HydroSHEDS and MERIT Hydro have produced hydrographic information that could fill the NHDPlus gaps however, they

have been based on global DEMs and not on a country specific DEM. GRWL implicitly produced a river network nonetheless, its coverage is limited by the Landsat imagery quality so only important rivers are represented. The data set produced in this study used a country specific DEM in combination with and existent river network to map reaches not captured by NHDPlus. The linkage between both databases allowed a hydrography that offers a HydroSHEDS-like product (i.e. a raster-based product) but with better geolocation accuracy and improved connectivity. The later particularly notable for endorheic river basins in the Great Basin area.

The new hydrography has a resolution of ~90m (at the equator) and is distributed in GeoTIFF format using 53 tiles of 5°x5° which mosaic the entire contiguous US. The variables distributed are flow direction and flow accumulation maps. We envisage that the new hydrography will improve river hydrodynamic predictions involving hydrographic variables in the contiguous US despite limitations discussed in Section 5.4.

5.6 Postscript

This chapter presented a methodology to generate a hydrography based on high-quality data source of terrain elevation and the location of curated river centrelines, the later typically with partial coverage. The case study is in the US where the National Elevation Dataset (NED) and the National Hydrography Dataset Plus (NHDPlus) were used to generate a new hydrography for the contiguous US. The resulting hydrography presented better accuracy than global hydrography data sets especially in endorheic basins.

The next chapter summarise main findings in this thesis and general conclusions.

CHAPTER 6

Conclusions

6.1. Main findings

Flood modelling is still a field in active development where flood footprint accuracy (i.e. inundated area, flood extent) is a key factor in disaster risk management (Schuman et al., 2018). Over the last decade, producing accurate flood maps over national to global scale domains has become an important element in flood modelling (Schumann and Bates, 2018). The primary research aim of this thesis has been to improve our understanding of techniques for continental-scale flood modelling. In this view, this thesis achieved three objectives: **i)** it has developed an open-source software package to streamline the pre-processing of input data for continental scale flood studies; **ii)** it has used this toolbox to develop a 26-year European Flood Hindcast using simulated river discharge; and **iii)** it has created a framework to generate a new hydrography from a high-quality national data source. Brief details of these objectives are provided next.

Frist, the development of the open-source software package *LFPtools* to automatically pre-process input data for hydraulic models using regular grids in a computationally efficient manner is presented in Chapter 3. This software package encompasses tools to deal with DEM resampling, bank elevation estimation, bed elevation estimation, river width subtraction and interpolation, elevation smoothing algorithms, continent basin splitting, and more. The development towards a general-purpose set of tools to prepare flood inundation models at any scale does not exist, so that this was one of the motivations to create such package. The tools were evaluated in the Severn basin in the UK. Outputs of the test case were compared with the official flood extent footprint of a real event and satisfactory model performance

was obtained: Hit rate = 0.79, False alarm ratio = 0.24 and Critical success index = 0.63.

LFPtools integrates seamlessly with modelling chains for the estimation of floods at any scale. In Chapter 4, *LFPtools* was used to create the first European Flood Hindcast based on 26 years of simulated river discharge across 298 basins, the set of tools immensely facilitated the preparation of input data for the 298 basins. Without automatic tools preparing data for such a number of basins would have been extremely laborious. The modelling framework that enabled the hindcast introduced new methods in three areas: i) river bed estimation tailored for inflow river discharge; ii) flood defences integration in flood models; and iii) continental scale hydrological-hydraulic coupling.

Lastly, in creating the hindcast it became clear that current hydrography data sets need to be further investigated for continental scale flood models. This thesis therefore developed a framework to generate a new hydrography from a high-quality national DEM, in particular, a hydrography derived from the National Elevation Dataset (NED) and the National Hydrography Dataset Plus (NHDPlus) (Chapter 5). Key results from these chapters are presented next.

i. The fast deployment of flood modelling studies at continental scales can be streamlined by the adoption of software packages that automate the process.

LISFLOOD-FP is a well-recognised hydrodynamic model to simulate floodplain inundation. However, building a flood model can be time-consuming since input data need to be processed from a variety different sources and adapted to a particular user's problem. This thesis introduced in Chapter 3, *LFPtools*, an open-source Python software package to help prepare input data for flood studies. The package encompasses the most frequently used methods for flood inundation modelling data preparation, and also facilitates the addition of new ones if desired. *LFPtools* can be thought of as a platform to streamline the preparation of flood inundation studies in different fields by bringing ease of use to non-expert users and efficiency to expert ones. It is built on top of the state-of-the-art Python libraries to handle large sets of data and it is in active development. It is important to mention that

these tasks could be done in a GIS package, but only with quite extreme difficulty and for small data arrays.

LFPtools can be used within a modelling framework to build a continental-scale flood hindcast or reanalysis, a modelling framework of continental-scale flood extent for an early warning system or even within a framework to predict flood inundation variables (flood extent, water depth, etc) in a climate change context. Thus, we envisage that this innovative set of tools will help to significantly reduce long pre-processing times and boost geoscience studies involving flood hydrodynamics in between. As LFPtools is open-source, users can revise the code, modify or add new methods easily and transparently. The source code is available at: http://github.com/jsosa/lfptools

ii. It is possible to obtain continental scale flood inundation maps for multi-decal periods using a coupled hydrological-hydrodynamic model chain.

Traditionally, the characteristics of floods at continental scales have been investigated using river discharge from gauge stations and satellite imagery via remote sensing techniques. While these techniques provide information about the occurrence frequency and extent of floods, sampling in time and space may be sparse and they cannot provide information about flood inundation depth. Efficient floodplain inundation models can overcome these issues, but generally only over local scale areas and limited time periods. This thesis presented in Chapter 4 an automated modelling framework to produce a multi-decal flood depth time series (or flood hindcast) for Europe. The framework used free globally available sources of river width, flood protection standards, terrain information and hydrography to represent river geometries explicitly. The flood model was forced with simulated daily river discharge coupled to a floodplain inundation model to map flood patterns over 26 years (1990-2016) in 298 European river basins.

Both the methodology and data set in presented in Chapter 4 can be considered as new contributions to continental scale flood modelling. First, the computational framework improves from previous studies of the same kind in a few aspects: i) it introduces an efficient method to couple hydrological and hydrodynamic models in large scale and high resolution problems; ii) it presents a method to estimate river

bathymetry by adjusting the channel conveyance to account for the systematic biases typically found in modelled river discharge; and iii) it describes a methodology to account for flood defences in flood inundation modelling by using as a proxy a database of flood protection standards and adjusting the capacity of the channel to match these.

The data generated in the European Flood Hindcast was evaluated against official maps in several basins in the UK and mainland Europe obtaining Critical Score Index values of 0.52 – 0.84. Later, an automatic flood detection algorithm was developed to extract important flood events in the hindcast data set. Results found that between 1990-2016 Europe experienced around 161 important flood events, with the Danube, Rhine, Elbe, Rhone and Po being the most affected river basins. Conversely, the least active basins in terms of fluvial floods were the Nemunas, Daugava, Douro, Ebro, Guadiana and Tagus during the same period.

iii. The geolocation accuracy of river centrelines improves when high quality terrain elevations and a source of main most important river centrelines are used.

The geolocation and direction of flow of rivers are key factors used to drive accurate continental and local scale flood studies, such as the flood hindcast introduced in Chapter 4. Generally, global hydrography data sets such HydroSHEDS and MERIT Hydro are used for this purpose, however, they may misrepresent some river locations as these data sets are derived from space-borne satellites instead of national data sources. In the US, the National Hydrography Dataset Plus (NHDPlus) provides this information in a continuously revised dataset. However, the data set has missing information that could reach up to 25% of county area. One way to overcome this issue is to use global hydrographic data sets based on spaceborne DEMs. This is beneficial for areas with poor terrain data, however areas with a full coverage of accurate terrain data, such the US, are not advantaged. Chapter 5 therefore presents UShydro, a new hydrography built on the National Elevation Dataset (NED) and the National Hydrography Dataset Plus (NHDPlus) which extends the current coverage of NHDPlus in the contiguous US and provides better estimates of flow accumulation and geolocation accuracy over global hydrographic data sets.

Global river network data sets such as HydroSHEDS and MERIT Hydro have produced hydrographic information that could fill the NHDPlus gaps however, they have been based on global DEMs and not on a country specific DEM. This is a problem as global DEMs contain error bias derived from the nature of the space-borne satellite. These biases result from: i) speckle errors caused by the variability of surface reflectance over flat areas; ii) stripe patterns characterised by a regular height undulation with a wavelength of 500 m to 100 km; iii) absolute error bias produced when there is a shift in the average elevation over large areas (~20 km); and iv) positive biases in the elevation due to misrepresentation of topography beneath forest canopies and buildings.

The data set produced in Chapter 5 used a national DEM in combination with and existing river network to map reaches not captured by NHDPlus. The linkage between both databases allowed a hydrography that offers a HydroSHEDS-like product but with better geolocation accuracy and improved connectivity, where the new hydrography obtained a flow accumulation error between -5% and 5% for 72.78% of a representative sample of the data set (200,000 locations) whilst global studies obtained values lower than 62.41%. The Improvements are particularly notable for endorheic river basins in the Great Basin area. The framework developed to produce these data can be easily transferable to other locations.

6.2. Synthesis

Global to continental scale flood models are being used by insurers, multi-national corporations, NGOs and national governments to tackle problems such as rapid flood disaster response, urban planning and climate change adaptation. Despite recent advances in this field (Winsemius et al., 2013; Alfieri et al., 2014; Wing et al., 2018), researchers have found that there are some topics that still need attention. This thesis presented new developments in the field which advance our understanding in different topics outlined below.

First, workflow automation is key to developing flood inundation models at scale. Building flood inundation models from scratch demands a considerable amount of time and, as data are manipulated based on the user's skills, it could potentially be subject to errors if the task has to be repeated several times. In this thesis a software

package is proposed in Chapter 3 to standardise the building process of flood models. The package is free and open source (http://github.com/jsosa/lfptools) so researches can revise, edit or add more methods to the package. It contains several methods that have been widely adopted by researchers in this field, thus we envisage that the package will be used to create applications involving floods in a more easy, fast and standardised way.

Second, flood have been characterised using in-situ time series of river discharge for many years. Despite the fact that this approach has been widely adopted to determine flood occurrence, flooding is a three-dimensional process where a volume of water is spread over the floodplain. Thus, the relevance of inundation area and inundation depth are important variables to consider for any kind of flood assessment. Thanks to advances in floodplain hydrodynamic modelling and computational power, today it is possible to explore new ways to characterise floods. In this thesis, a Flood Inundation Hindcast was proposed to investigate the nature of floods. Similar to river discharge, a flood hindcast provides flood inundation estimates varying in time. By adding the temporal component, it is possible to investigate the evolution of floods by investigating its occurrence, inundated area and inundation depth. Building such application had not been possible without automated computational framework due the intense data processing that a study of this magnitude needs. Chapter 4 presented a European Flood Hindcast where inundation dynamics for 298 river basins were computed. The hindcast used freely available data sets at global scale to facilitate the replication of the computational framework. In the building the process a few unexplored aspects were investigated. For example, coupling hydrological-hydrodynamic models have been limited to basin scale studies (Grimaldi et al., 2019; Felder et al., 2017), in this thesis in Section 4.2.4 a method was proposed to extend this to continental scales. Another aspect that required attention was the estimation of channel conveyance for a certain river flow. A solution to this aspect was presented in Section 4.2.5 where a synthetic river bed was produced tailored for the input river discharge. Similar to the river bed, flood defences were estimated and implemented implicitly in the computational framework using flood protection standards values as explained in Section 4.2.6. The data catalogue of the European Flood Hindcast contained daily estimates of flood inundation. Later, identification of events was possible using the methodology explained in Section 4.2.8. Analysis suggested that between 1990-2016 the

Danube, Rhine, Rhone and Elbe were the most impacted basins. Conversely, the least impacted basins in the same period were the Douro, Ebro, Guadiana and Tagus. These results compare favourably with previous findings (Blöschl et al., 2013) where a climatic signal of observed river discharge was associated with increasing floods in northwestern Europe (the Rhine, Elbe and Rhone) and a decreasing in floods in southwestern Europe (the Ebro, Guadiana and Tagus and the Douro).

Lastly, continental scale flood modelling has been made possible thanks to global scale data sets of terrain elevation, river width and hydrography. The hydrography provides information about the geolocation of the river centrelines. Thus, incorrect geolocation can lead to inundation in areas where no flooding is expected or, conversely, flooding in unexpected areas. Thus, the geolocation of rivers has become in an important component in flood modelling. Generally, hydrography data sets derived from space-borne satellites have been adopted to identify the location of rivers (e.g., HydroSHEDS, MERIT Hydro), nonetheless some countries own national data sources that can help to obtain river geolocations with higher accuracy than can be achieved with global data sets. In Chapter 5 the accuracy of a hydrography derived from national data sources was explored. The case study concerned the US as it owns freely available national maps to generate the hydrography. The new hydrography used the National Elevation Dataset (NED) and the National Hydrography Dataset Plus (NHDPlus) to generate a new data set. Whilst NHDPlus could have been used to directly replace global hydrography data sets, for example HydroSHEDS, in flood models, it was found that NHDPlus misses up to 25% river coverage in some US counties. Thus, the new hydrography not only extends the NHDPlus coverage but also improves its accuracy over global hydrography data sets. The new data set obtained a flow accumulation error between -5% and 5%, and a river geolocation accuracy (defined as the relation nearest distance/accumulation) between -5% and 5%. Finally, the new data set was integrated in a modelling framework that combines fluvial, pluvial and coastal modelling to estimate flood hazard under current and future climate (Bates et al., 2020). The study became the basis of the flood hazard layers maps of the First Street Foundation (FSF) project 'FloodFactor' (www.floodfactor.com), FSF is an organisation which main aim is to quantify and communicate America's flood risk.

6.3. Recommendations and future research

This section presents some recommendation and future research lines of this thesis. In particular these recommendations are for the case studies introduced in Chapter 4 and 5.

Chapter 4 presented a European Flood Hindcast for 298 basins. The modelling framework simulated 26 years of inland flooding at high resolution (~90 m). However, due to the complexity of the framework the coastal component was omitted. Under the current changing climate, it would have been interesting to explore coastal flooding and consequently compound flooding as well. To this end, a source of sea level rise estimates must be used. For example, Muis et al., 2016 generated a global reanalysis of storm surges and extreme sea levels that could have been integrated in the European Flood Hindcast framework. The framework is flexible and allows users also to include probability distributions of future sea level, however the methods to build such integration only exist at local scale and future runoff will also be required (Quinn et al., 2013).

The framework developed in Chapter 4 used historical river discharge to produce a flood hindcast, however, the framework can use any form of discharge data (from models or gauges) and since the model is already built (bed, bank elevations calculated already), other applications can be considered. For example, a rainfall-runoff model can be prepared to run experiments on climate change. In that scenario, a new set of river discharge data could be generated and easily included to evaluate river hydrodynamic response for that scenario. Another potential application of the model setup is flood inundation forecasting. The EFAS model is a system that runs daily, producing predictions of river discharge a few days ahead. Moreover, the methodology applied here can be easily transferred to other continental or large scale studies worldwide since the modelling framework uses freely available global data with only the river discharge component being dependent on the study area.

Flood protection standards in the European Flood Hindcast were considered as static over time as this is the only information available to date, however, it would therefore be interesting to explore flood protection standards varying over time. In context, the event of August 2002 in Germany played an important role in

improving the flood resilience of that country. After the event, the German government reinforced its flood defence infrastructure. These types of actions against floods are repeated in most developed countries, however, the lack of data concerning defence changes over time impedes its implementation in models.

The European Flood Hindcast used freely globally available DEM as source of terrain elevations across Europe. This seamless DEM is available for all European countries. However, better estimates of inundation are expected with higher quality terrain elevations. Thus, blending global DEM with LIDAR data where it is available will produce better flood predictions.

Chapter 5 presented a new hydrography for the contiguous US based on national scale data sets of terrain elevations (NED) and river centrelines (NHDPlus). The new hydrography, however, lacks the ability to represent bifurcated channels particularly present in braided rivers and deltas. This limitation is intrinsic for flow directions derived from the D8 algorithm. It will be interesting to explore a method to overcome this issue and thus represent in a better way complex river structures such the Old River Control Structure which diverts part of the Mississippi river into the Atchafalaya River, for example. Finally, it would have been interesting to estimate the error that different hydrography data sets make to flood model outputs. This is relevant for flood modellers as they can use this information to minimise the uncertainty introduced in their modelling chains.

The findings of this thesis have shown that flood modelling at continental scale is a challenging problem but nonetheless feasible. Whilst most development to date has been devoted towards the estimation of flood depths for a particular return period, this thesis presented the basis for floodplain estimation for long periods time (in the order of years) based on simulated discharge. This type of simulations will enable scientists in the field to investigate flood characteristics from a very different perspective, especially in the context of the current changing climate.

This page was intentionally left blank.

References

Alfieri, L., Burek, P., Dutra, E., Krzeminski, B., Muraro, D., Thielen, J., & Pappenberger, F. (2013). GloFAS – global ensemble streamflow forecasting and flood early warning. *Hydrology and Earth System Sciences*, *17*(3), 1161–1175. https://doi.org/10.5194/hess-17-1161-2013

Alfieri, L., Burek, P., Feyen, L., & Forzieri, G. (2015). Global warming increases the frequency of river floods in Europe. *Hydrology and Earth System Sciences*, *19*(5), 2247–2260. https://doi.org/10.5194/hess-19-2247-2015

Alfieri, Lorenzo, Salamon, P., Bianchi, A., Neal, J., Bates, P., & Feyen, L. (2014). Advances in pan-European flood hazard mapping. *Hydrological Processes*, *28*(13), 4067–4077. https://doi.org/10.1002/hyp.9947

Alfieri, Lorenzo, Bisselink, B., Dottori, F., Naumann, G., de Roo, A., Salamon, P., et al. (2017). Global projections of river flood risk in a warmer world: RIVER FLOOD RISK IN A WARMER WORLD. *Earth's Future*, *5*(2), 171–182. https://doi.org/10.1002/2016EF000485

Alfieri, Lorenzo, Dottori, F., Betts, R., Salamon, P., & Feyen, L. (2018). Multi-Model Projections of River Flood Risk in Europe under Global Warming. *Climate*, *6*(1), 6. https://doi.org/10.3390/cli6010006

Allen, G. H., & Pavelsky, T. M. (2018). Global extent of rivers and streams. *Science*, *361*(6402), 585–588. https://doi.org/10.1126/science.aat0636

de Almeida, G. A. M., & Bates, P. (2013). Applicability of the local inertial approximation of the shallow water equations to flood modeling. *Water Resources Research*, *49*(8), 4833–4844. https://doi.org/10.1002/wrcr.20366

de Almeida, G. A. M., Bates, P., Freer, J. E., & Souvignet, M. (2012). Improving the stability of a simple formulation of the shallow water equations for 2-D flood modeling. *Water Resources Research*, *48*(5). https://doi.org/10.1029/2011WR011570

Andreadis, K. M., Schumann, G. J.-P., & Pavelsky, T. (2013). A simple global river bankfull width and depth database: Data and Analysis Note. *Water Resources Research*, *49*(10), 7164–7168. https://doi.org/10.1002/wrcr.20440

Archer, L., Neal, J. C., Bates, P. D., & House, J. I. (2018). Comparing TanDEM-X Data With Frequently Used DEMs for Flood Inundation Modeling. *Water Resources Research*, *54*(12). https://doi.org/10.1029/2018WR023688

Ballesteros-Cánovas, J. A., Sanchez-Silva, M., Bodoque, J. M., & Díez-Herrero, A. (2013). An Integrated Approach to Flood Risk Management: A Case Study of Navaluenga (Central Spain). *Water Resources Management*, *27*(8), 3051–3069. https://doi.org/10.1007/s11269-013-0332-1

Barker, L., Hannaford, J., Muchan, K., Turner, S., & Parry, S. (2016). The winter 2015/2016 floods in the UK: a hydrological appraisal. *Weather*, *71*(12), 324–333. https://doi.org/10.1002/wea.2822

Barnes, R. (2017). Parallel non-divergent flow accumulation for trillion cell digital elevation models on desktops or clusters. *Environmental Modelling & Software*, *92*, 202–212. https://doi.org/10.1016/j.envsoft.2017.02.022

Barnes, R. (2018). *RichDEM: High-performance terrain analysis* (preprint). PeerJ Preprints. https://doi.org/10.7287/peerj.preprints.27099v1

Barnes, R., Lehman, C., & Mulla, D. (2014a). An efficient assignment of drainage direction over flat surfaces in raster digital elevation models. *Computers & Geosciences*, *62*, 128–135. https://doi.org/10.1016/j.cageo.2013.01.009

Barnes, R., Lehman, C., & Mulla, D. (2014b). Priority-flood: An optimal depression-filling and watershed-labeling algorithm for digital elevation models. *Computers & Geosciences*, *62*, 117–127. https://doi.org/10.1016/j.cageo.2013.04.024

Barredo, J. I. (2009). Normalised flood losses in Europe: 1970–2006. *Natural Hazards and Earth System Sciences*, *9*(1), 97–104. https://doi.org/10.5194/nhess-9-97-2009

Bartholmes, J., Thielen, J., & Kalas, M. (2008). Forecasting medium-range flood hazard on European scale. *Georisk: Assessment and Management of Risk for Engineered Systems and Geohazards*, *2*(4), 181–186. https://doi.org/10.1080/17499510802369132

Bates, P., Trigg, M., Neal, J., & Dabrowa, A. (2013). *LISFLOOD-FP user manual*. UK: School of Geographical Sciences, University of Bristol.

Bates, P. D., Horritt, M. S., & Fewtrell, T. J. (2010). A simple inertial formulation of the shallow water equations for efficient two-dimensional flood inundation modelling. *Journal of Hydrology*, *387*(1–2), 33–45. https://doi.org/10.1016/j.jhydrol.2010.03.027

Bates, P. D., Neal, J., Sampson, C., Smith, A., & Trigg, M. (2018). Progress Toward Hyperresolution Models of Global Flood Hazard. In *Risk Modeling for Hazards and Disasters* (pp. 211–232). Elsevier. https://doi.org/10.1016/B978-0-12-804071-3.00009-4

Bates, P. D., Quinn, N., Sampson, C. C., Smith, A. M., Wing, O. E. J., Sosa, J., et al. (2020). *Combined modelling of US fluvial, pluvial and coastal flood hazard under current and future climates* (preprint). Hydrology. https://doi.org/10.1002/essoar.10504362.1

Batista e Silva, F., Lavalle, C., & Koomen, E. (2013). A procedure to obtain a refined European land use/cover map. *Journal of Land Use Science*, *8*(3), 255–283. https://doi.org/10.1080/1747423X.2012.667450

van Beek, L. P. H., Wada, Y., & Bierkens, M. F. P. (2011). Global monthly water stress: 1. Water balance and water availability: GLOBAL MONTHLY WATER STRESS, 1. *Water Resources Research*, *47*(7). https://doi.org/10.1029/2010WR009791

Berghuijs, W. R., Allen, S. T., Harrigan, S., & Kirchner, J. W. (2019). Growing spatial scales of synchronous river flooding in Europe. *Geophysical Research Letters*. https://doi.org/10.1029/2018GL081883

Bernhofen, M. V., Whyman, C., Trigg, M. A., Sleigh, P. A., Smith, A. M., Sampson, C. C., et al. (2018). A first collective validation of global fluvial flood models for major floods in Nigeria and Mozambique. *Environmental Research Letters*, *13*(10), 104007. https://doi.org/10.1088/1748-9326/aae014

Bertola, M., Viglione, A., Lun, D., Hall, J., & Blöschl, G. (2020). Flood trends in Europe: are changes in small and big floods different? *Hydrology and Earth System Sciences*, *24*(4), 1805–1822. https://doi.org/10.5194/hess-24-1805-2020

Biancamaria, S., Bates, P. D., Boone, A., & Mognard, N. M. (2009). Large-scale coupled hydrologic and hydraulic modelling of the Ob river in Siberia. *Journal of Hydrology*, *379*(1–2), 136–150. https://doi.org/10.1016/j.jhydrol.2009.09.054

Blöschl, G., Nester, T., Komma, J., Parajka, J., & Perdigão, R. A. P. (2013). The June 2013 flood in the Upper Danube Basin, and comparisons with the 2002, 1954 and 1899 floods. *Hydrology and Earth System Sciences*, *17*(12), 5197–5212. https://doi.org/10.5194/hess-17-5197-2013

Blöschl, Günter, Hall, J., Parajka, J., Perdigão, R. A. P., Merz, B., Arheimer, B., et al. (2017). Changing climate shifts timing of European floods. *Science*, *357*(6351), 588–590. https://doi.org/10.1126/science.aan2506

Blöschl, Günter, Hall, J., Viglione, A., Perdigão, R. A. P., Parajka, J., Merz, B., et al. (2019). Changing climate both increases and decreases European river floods. *Nature*, *573*(7772), 108–111. https://doi.org/10.1038/s41586-019-1495-6

Bonnifait, L., Delrieu, G., Lay, M. L., Boudevillain, B., Masson, A., Belleudy, P., et al. (2009). Distributed hydrologic and hydraulic modelling with radar rainfall input: Reconstruction of the 8–9 September 2002 catastrophic flood event in the Gard region, France. *Advances in Water Resources*, *32*(7), 1077–1089. https://doi.org/10.1016/j.advwatres.2009.03.007

Bradbrook, K. F., Lane, S. N., Waller, S. G., & Bates, P. D. (2004). Two dimensional diffusion wave modelling of flood inundation using a simplified channel representation. *International Journal of River Basin Management*, *2*(3), 211–223. https://doi.org/10.1080/15715124.2004.9635233

Brakenridge, G. R. (2018). Flood Risk Mapping From Orbital Remote Sensing. In Guy J-P. Schumann, P. D. Bates, H. Apel, & G. T. Aronica (Eds.), *Geophysical Monograph Series* (pp. 43–54). Hoboken, NJ, USA: John Wiley & Sons, Inc. https://doi.org/10.1002/9781119217886.ch3

Brocca, L., Melone, F., & Moramarco, T. (2011). Distributed rainfall-runoff modelling for flood frequency estimation and flood forecasting. *Hydrological Processes*, *25*(18), 2801–2813. https://doi.org/10.1002/hyp.8042

Carbajal, C., & Harding, J. (2006). SRTM C-band and ICESat laser altimetry elevation comparisons as a function of tree cover and relief. *Photogramm. Eng. Remote Sens*, *72*(287–298).

Carroll, M. L., Townshed, J. R., Di Miceli, C. M., Noojipady, P., & Sohlberg, R. A. (2009). A new global raster water mask at 250 m resolution. *International Journal of Digital Earth2*, *2*, 291–308.

Castellarin, A., Di Baldassarre, G., & Brath, A. (2011). Floodplain management strategies for flood attenuation in the river Po. *River Research and Applications*, *27*(8), 1037–1047. https://doi.org/10.1002/rra.1405

Cleveland, W. S. (1979). Robust Locally Weighted Regression and Smoothing Scatterplots. *Journal of the American Statistical Association*, *74*(368), 829–836. https://doi.org/10.1080/01621459.1979.10481038

Cohen, S., Wan, T., Islam, M. T., & Syvitski, J. P. M. (2018). Global river slope: A new geospatial dataset and global-scale analysis. *Journal of Hydrology*, *563*, 1057–1067. https://doi.org/10.1016/j.jhydrol.2018.06.066

Coxon G, Freer J, Westerberg I K, Wagener T, Woods R and Smith P J 2015 A novel framework for discharge uncertainty quantification applied to 500 UK gauging stations *Water Resources Research*. 51 5531–46. https://doi.org/10.1002/2014WR016532

Courant, R., Friedrichs, K., & Lewy, H. (1928). □ber die partiellen Differenzengleichungen der mathematischen Physik. *Mathematische Annalen*, *100*(1), 32–74. https://doi.org/10.1007/BF01448839

Crippen, R., et, al, & et, al. (2016). NASADEM global elevation model: Methods and progress, ISPRS International Archives of the Photogrammetry Remote Sensing and Spatial Information Sciences. *XLI-B4*, 125–128. https://doi.org/10.5194/isprs-archives-XLI-B4-125-2016

Degiorgis, M., Gnecco, G., Gorni, S., Roth, G., Sanguineti, M., & Taramasso, A. C. (2012). Classifiers for the detection of flood-prone areas using remote sensed elevation data. *Journal of Hydrology*, *470–471*, 302–315. https://doi.org/10.1016/j.jhydrol.2012.09.006

Deltares. (2020). *SOBEK 3, D-Flow 1D. User manual*. Deltares.

DHI. (2017). *Mike 11 - A modelling system for Rivers and Channels. User Guide*.

Dottori, F., Salamon, P., Bianchi, A., Alfieri, L., Hirpa, F. A., & Feyen, L. (2016). Development and evaluation of a framework for global flood hazard mapping. *Advances in Water Resources*, *94*, 87–102. https://doi.org/10.1016/j.advwatres.2016.05.002

Dottori, F., Kalas, M., Salamon, P., Bianchi, A., Alfieri, L., & Feyen, L. (2017). An operational procedure for rapid flood risk assessment in Europe. *Natural Hazards and Earth System Sciences*, *17*(7), 1111–1126. https://doi.org/10.5194/nhess-17-1111-2017

Dottori, F., Szewczyk, W., Ciscar, J.-C., Zhao, F., Alfieri, L., Hirabayashi, Y., et al. (2018). Increased human and economic losses from river flooding with anthropogenic warming. *Nature Climate Change*, *8*(9), 781–786. https://doi.org/10.1038/s41558-018-0257-z

Downing, J. (2012). Global abundance and size distribution of streams and rivers. *Inland Waters*, *2*(4), 229–236. https://doi.org/10.5268/IW-2.4.502

Dufourmont, H., Gallego, J., Reuter, H., & Strobl, P. (2014). *EU-DEM Statistical Validation*. European Environment Agency.

Emerton, R., Zsoter, E., Arnal, L., Cloke, H. L., Muraro, D., Prudhomme, C., et al. (2018). Developing a global operational seasonal hydro-meteorological forecasting system: GloFAS-Seasonal v1.0. *Geoscientific Model Development*, *11*(8), 3327–3346. https://doi.org/10.5194/gmd-11-3327-2018

Fairfield, J., & Leymarie, P. (1991). Drainage networks from grid digital elevation models. *Water Resources Research*, *27*(5), 709–717. https://doi.org/10.1029/90WR02658

Farr, T. G., & Kobrick, M. (2000). Shuttle radar topography mission produces a wealth of data. *Eos, Transactions American Geophysical Union*, *81*(48), 583. https://doi.org/10.1029/EO081i048p00583

Farr, T. G., Rosen, P. A., Caro, E., Crippen, R., Duren, R., Hensley, S., et al. (2007). The Shuttle Radar Topography Mission. *Reviews of Geophysics*, *45*(2). https://doi.org/10.1029/2005RG000183

Feng, M., Sexton, J. O., Channan, S., & Townshend, J. R. (2016). A global, high-resolution (30-m) inland water body dataset for 2000: first results of a topographic–spectral classification algorithm. *International Journal of Digital Earth*, *9*(2), 113–133. https://doi.org/10.1080/17538947.2015.1026420

Fewtrell, T. J., Neal, J. C., Bates, P. D., & Harrison, P. J. (2011). Geometric and structural river channel complexity and the prediction of urban inundation. *Hydrological Processes*, *25*(20), 3173–3186. https://doi.org/10.1002/hyp.8035

Fluet-Chouinard, E., Lehner, B., Rebelo, L.-M., Papa, F., & Hamilton, S. K. (2015). Development of a global inundation map at high spatial resolution from topographic downscaling of coarse-scale remote sensing data. *Remote Sensing of Environment*, *158*, 348–361. https://doi.org/10.1016/j.rse.2014.10.015

Freeman, T. G. (1991). Calculating catchment area with divergent flow based on a regular grid. *Computers & Geosciences*, *17*(3), 413–422. https://doi.org/10.1016/0098-3004(91)90048-I

Gallant, J., & Read, A. (2009). Enhancing the SRTM data for Australia. *Proc. Geomorphometry*, *31*, 149–154.

Gallaum, H., Dohr, K., Martin, P., Stumpf, A., & Huge, J. (2019). *EU-Hydro - River Net User Guide 1.2*. European Environment Agency.

Gesch, D., Evans, G., Mauck, J., Hutchinson, J., & Carswell, W. J. (2009). *The National Map—Elevation: U.S. Geological Survey Fact Sheet 2009-3053*.

Goutal, N., Lacombe, J. M., Zaoui, F., & El-Kadi-Abderrezzak, K. (2012). MASCARET: a 1-D open-source software for flow hydrodynamic and water quality in open channel networks. *River Flow*, *1*, 1169–1174.

GRDC. (2007). Major River Basins of the World/Global Runoff Data Centre. *D 56002, Federal Institute of Hydrology (BfG)*.

Grimaldi, S., Schumann, G. J. -P., Shokri, A., Walker, J. P., & Pauwels, V. R. N. (2019). Challenges, Opportunities, and Pitfalls for Global Coupled Hydrologic-Hydraulic Modeling of Floods. *Water Resources Research*, *55*(7), 5277–5300. https://doi.org/10.1029/2018WR024289

Grohman, G., Wagener, G., & Strebeck, J. (2006). Filling SRTM voids: The delta surface fill method. *Photogramm. Eng. Remote Sens.*, *72*, 213–216.

Gudmundsson, L., Wagener, T., Tallaksen, L. M., & Engeland, K. (2012). Evaluation of nine large-scale hydrological models with respect to the seasonal runoff climatology in Europe: LAND SURFACE MODELS EVALUATION. *Water Resources Research*, *48*(11). https://doi.org/10.1029/2011WR010911

Gupta, H. V., Kling, H., Yilmaz, K. K., & Martinez, G. F. (2009). Decomposition of the mean squared error and NSE performance criteria: Implications for improving hydrological modelling. *Journal of Hydrology*, *377*(1–2), 80–91. https://doi.org/10.1016/j.jhydrol.2009.08.003

Hall, J., & Blöschl, G. (2018). Spatial patterns and characteristics of flood seasonality in Europe. *Hydrology and Earth System Sciences*, *22*(7), 3883–3901. https://doi.org/10.5194/hess-22-3883-2018

Hawker, L., Rougier, J., Neal, J., Bates, P., Archer, L., & Yamazaki, D. (2018). Implications of Simulating Global Digital Elevation Models for Flood Inundation Studies. *Water Resources Research*, *54*(10), 7910–7928. https://doi.org/10.1029/2018WR023279

Herman, J., & Usher, W. (2017). SALib: An open-source Python library for Sensitivity Analysis. *The Journal of Open Source Software*, *2*(9), 97. https://doi.org/10.21105/joss.00097

Hey, R. D., & Thorne, C. R. (1986). Stable Channels with Mobile Gravel Beds. *Journal of Hydraulic Engineering*, *112*(8), 671–689. https://doi.org/10.1061/(ASCE)0733-9429(1986)112:8(671)

Hirabayashi, Y., Mahendran, R., Koirala, S., Konoshima, L., Yamazaki, D., Watanabe, S., et al. (2013). Global flood risk under climate change. *Nature Climate Change*, *3*(9), 816–821. https://doi.org/10.1038/nclimate1911

Hirpa, F. A., Salamon, P., Beck, H. E., Lorini, V., Alfieri, L., Zsoter, E., & Dadson, S. J. (2018). Calibration of the Global Flood Awareness System (GloFAS) using daily streamflow data. *Journal of Hydrology*, *566*, 595–606. https://doi.org/10.1016/j.jhydrol.2018.09.052

Holmgren, P. (1994). Multiple flow direction algorithms for runoff modelling in grid based elevation models: An empirical evaluation. *Hydrological Processes*, *8*(4), 327–334. https://doi.org/10.1002/hyp.3360080405

Horritt, M. (2003). Waterline mapping in flooded vegetation from airborne SAR imagery. *Remote Sensing of Environment*, *85*(3), 271–281. https://doi.org/10.1016/S0034-4257(03)00006-3

Horritt, M. S., Mason, D. C., & Luckman, A. J. (2001). Flood boundary delineation from Synthetic Aperture Radar imagery using a statistical active contour model. *International Journal of Remote Sensing*, *22*(13), 2489–2507. https://doi.org/10.1080/01431160116902

Hough, S. E., Altidor, J. R., Anglade, D., Given, D., Janvier, M. G., Maharrey, J. Z., et al. (2010). Localized damage caused by topographic amplification during the 2010 M 7.0 Haiti earthquake. *Nature Geoscience*, *3*(11), 778–782. https://doi.org/10.1038/ngeo988

Hunter, N. M., Bates, P. D., Neelz, S., Pender, G., Villanueva, I., Wright, N. G., et al. (2008). Benchmarking 2D hydraulic models for urban flooding. *Proceedings of the Institution of Civil Engineers - Water Management*, *161*(1), 13–30. https://doi.org/10.1680/wama.2008.161.1.13

Hunter, Neil M., Horritt, M. S., Bates, P. D., Wilson, M. D., & Werner, M. G. F. (2005). An adaptive time step solution for raster-based storage cell modelling of floodplain inundation. *Advances in Water Resources*, *28*(9), 975–991. https://doi.org/10.1016/j.advwatres.2005.03.007

Hunter, Neil M., Bates, P. D., Horritt, M. S., & Wilson, M. D. (2007). Simple spatially-distributed models for predicting flood inundation: A review. *Geomorphology*, *90*(3–4), 208–225. https://doi.org/10.1016/j.geomorph.2006.10.021

Huţanu, E., Mihu-Pintilie, A., Urzica, A., Paveluc, L. E., Stoleriu, C. C., & Grozavu, A. (2020). Using 1D HEC-RAS Modeling and LiDAR Data to Improve Flood Hazard Maps Accuracy: A Case Study from Jijia Floodplain (NE Romania). *Water*, *12*(6), 1624. https://doi.org/10.3390/w12061624

Jongman, B., Hochrainer-Stigler, S., Feyen, L., Aerts, J. C. J. H., Mechler, R., Botzen, W. J. W., et al. (2014). Increasing stress on disaster-risk finance due to large floods. *Nature Climate Change*, *4*(4), 264–268. https://doi.org/10.1038/nclimate2124

Juston, J., P.-E. Jansson, and D. Gustafsson (2014), Rating curve uncertainty and change detection in discharge time series: Case study with 44-year historic data from the Nyangores River, Kenya, *Hydrological Processes*, 28, 2509–2523, http://doi.org/10.1002/hyp.9786

Kiang, J. E., Gazoorian, C., McMillan, H., Coxon, G., Le Coz, J., Westerberg, I. K., et al. (2018). A Comparison of Methods for Streamflow Uncertainty Estimation. *Water Resources Research*, *54*(10), 7149–7176. https://doi.org/10.1029/2018WR022708

Knoben, W. J. M., Freer, J. E., & Woods, R. A. (2019). Technical note: Inherent benchmark or not? Comparing Nash–Sutcliffe and Kling–Gupta efficiency scores. *Hydrology and Earth System Sciences*, *23*(10), 4323–4331. https://doi.org/10.5194/hess-23-4323-2019

Koks, E. E., Thissen, M., Alfieri, L., De Moel, H., Feyen, L., Jongman, B., & Aerts, J. C. J. H. (2019). The macroeconomic impacts of future river flooding in Europe. *Environmental Research Letters*, *14*(8), 084042. https://doi.org/10.1088/1748-9326/ab3306

Komi, K., Neal, J., Trigg, M. A., & Diekkrüger, B. (2017). Modelling of flood hazard extent in data sparse areas: a case study of the Oti River basin, West Africa. *Journal of Hydrology: Regional Studies*, *10*, 122–132. https://doi.org/10.1016/j.ejrh.2017.03.001

Kundzewicz, Z. W., Pińskwar, I., & Brakenridge, G. R. (2013). Large floods in Europe, 1985–2009. *Hydrological Sciences Journal*, *58*(1), 1–7. https://doi.org/10.1080/02626667.2012.745082

Lamb, R., Crossley, M., & Waller, S. (2009). A fast two-dimensional floodplain inundation model. *Proceedings of the Institution of Civil Engineers - Water Management*, *162*(6), 363–370. https://doi.org/10.1680/wama.2009.162.6.363

Laudon, H., Berggren, M., Ågren, A., Buffam, I., Bishop, K., Grabs, T., et al. (2011). Patterns and Dynamics of Dissolved Organic Carbon (DOC) in Boreal Streams: The Role of Processes, Connectivity, and Scaling. *Ecosystems*, *14*(6), 880–893. https://doi.org/10.1007/s10021-011-9452-8

Lehner, B., & Döll, P. (2004). Development and validation of a global database of lakes, reservoirs and wetlands. *Journal of Hydrology*, *296*(1–4), 1–22. https://doi.org/10.1016/j.jhydrol.2004.03.028

Lehner, B., & Grill, G. (2013). Global river hydrography and network routing: baseline data and new approaches to study the world's large river systems. *Hydrological Processes*, *27*(15), 2171–2186. https://doi.org/10.1002/hyp.9740

Lehner, B., Verdin, K., & Jarvis, A. (2008). New Global Hydrography Derived From Spaceborne Elevation Data. *Eos, Transactions American Geophysical Union*, *89*(10), 93. https://doi.org/10.1029/2008EO100001

Lehner, B., Liermann, C. R., Revenga, C., Vörösmarty, C., Fekete, B., Crouzet, P., et al. (2011). High-resolution mapping of the world's reservoirs and dams for sustainable river-flow management. *Frontiers in Ecology and the Environment*, *9*(9), 494–502. https://doi.org/10.1890/100125

Leopold, L. B., & Maddock Jr., T. (1953). *The hydraulic geometry of stream channels and some physiographic implications* (Report No. 252) (p. 64). Washington, D.C. Retrieved from http://pubs.er.usgs.gov/publication/pp252

Lindsay, J. (2018). *WhiteboxTools User Manual*. Retrieved from https://jblindsay.github.io/wbt_book/

Lindsay, J.B., & Dhun, K. (2015). Modelling surface drainage patterns in altered landscapes using LiDAR. *International Journal of Geographical Information Science*, *29*(3), 397–411. https://doi.org/10.1080/13658816.2014.975715

Lindsay, John B. (2016). The practice of DEM stream burning revisited: The Practice of DEM Stream Burning Revisited. *Earth Surface Processes and Landforms*, *41*(5), 658–668. https://doi.org/10.1002/esp.3888

Lu, X., Zhuang, Q., Liu, Y., Zhou, Y., & Aghakouchak, A. (2016). A large-scale methane model by incorporating the surface water transport: Development of a Methane Model. *Journal of Geophysical Research: Biogeosciences*, *121*(6), 1657–1674. https://doi.org/10.1002/2016JG003321

Manfreda, S., Di Leo, M., & Sole, A. (2011). Detection of Flood-Prone Areas Using Digital Elevation Models. *Journal of Hydrologic Engineering*, *16*(10), 781–790. https://doi.org/10.1061/(ASCE)HE.1943-5584.0000367

McKay, L., Bondelid, T., Dewald, T., Johnston, J., Moore, R., & Rea, A. (2012). NHDPlus Version 2: User Guide.

Mersel, M. K., Smith, L. C., Andreadis, K. M., & Durand, M. T. (2013). Estimation of river depth from remotely sensed hydraulic relationships: Remotely Sensed Estimation of River Depth. *Water Resources Research*, *49*(6), 3165–3179. https://doi.org/10.1002/wrcr.20176

Miller, J. D., Kjeldsen, T. R., Hannaford, J., & Morris, D. G. (2013). A hydrological assessment of the November 2009 floods in Cumbria, UK. *Hydrology Research*, *44*(1), 180–197. https://doi.org/10.2166/nh.2012.076

Moulinec, C., Denis, C., Pham, C.-T., Rougé, D., Hervouet, J.-M., Razafindrakoto, E., et al. (2011). TELEMAC: An efficient hydrodynamics suite for massively parallel architectures. *Computers & Fluids*, *51*(1), 30–34. https://doi.org/10.1016/j.compfluid.2011.07.003

Muis, S., Verlaan, M., Winsemius, H. C., Aerts, J. C. J. H., & Ward, P. J. (2016). A global reanalysis of storm surges and extreme sea levels. *Nature Communications*, *7*(1), 11969. https://doi.org/10.1038/ncomms11969

NASA/NGA. (2003). SRTMWater Body Data Product Specific Guidance, Version 2.0. available online: http://dds.cr.usgs.gov/srtm/version2_1/SWBD/SWBD_Documentation/.

Nash, J. E., & Sutcliffe, J. V. (1970). River flow forecasting through conceptual models part I — A discussion of principles. *Journal of Hydrology*, *10*(3), 282–290. https://doi.org/10.1016/0022-1694(70)90255-6

Neal, J., Schumann, G., & Bates, P. (2012). A subgrid channel model for simulating river hydraulics and floodplain inundation over large and data sparse areas. *Water Resources Research*, *48*(11). https://doi.org/10.1029/2012WR012514

Neal, J., Dunne, T., Sampson, C., Smith, A., & Bates, P. (2018). Optimisation of the two-dimensional hydraulic model LISFOOD-FP for CPU architecture. *Environmental Modelling & Software*, *107*, 148–157. https://doi.org/10.1016/j.envsoft.2018.05.011

Neal, J. C., Bates, P. D., Fewtrell, T. J., Hunter, N. M., Wilson, M. D., & Horritt, M. S. (2009). Distributed whole city water level measurements from the Carlisle 2005 urban flood event and comparison with hydraulic model simulations. *Journal of Hydrology*, *368*(1–4), 42–55. https://doi.org/10.1016/j.jhydrol.2009.01.026

Nichols, G. (2007). Fluvial Systems in Desiccating Endorheic Basins. In G. Nichols, E. Williams, & C. Paola (Eds.), *Sedimentary Processes, Environments and Basins* (pp. 569–589). Oxford, UK: Blackwell Publishing Ltd. https://doi.org/10.1002/9781444304411.ch23

O'Callaghan, J. F., & Mark, D. M. (1984). The extraction of drainage networks from digital elevation data. *Computer Vision, Graphics, and Image Processing*, *28*(3), 323–344. https://doi.org/10.1016/S0734-189X(84)80011-0

O'Loughlin, F. E., Paiva, R. C. D., Durand, M., Alsdorf, D. E., & Bates, P. D. (2016). A multi-sensor approach towards a global vegetation corrected SRTM DEM product. *Remote Sensing of Environment*, *182*, 49–59. https://doi.org/10.1016/j.rse.2016.04.018

Ordnance Survey. (2019). *OS Terrain 50 User guide and technical specification*. UK: Ordnance Survey. Retrieved from https://www.ordnancesurvey.co.uk/docs/user-guides/os-terrain-50-user-guide.pdf

Papa, F., Prigent, C., Aires, F., Jimenez, C., Rossow, W. B., & Matthews, E. (2010). Interannual variability of surface water extent at the global scale, 1993–2004. *Journal of Geophysical Research*, *115*(D12), D12111. https://doi.org/10.1029/2009JD012674

Pappenberger, F., Beven, K. J., Hunter, N. M., Bates, P. D., Gouweleeuw, B. T., Thielen, J., & de Roo, A. P. J. (2005). Cascading model uncertainty from medium range weather forecasts (10 days) through a rainfall-runoff model to flood inundation predictions within the European Flood Forecasting System (EFFS). *Hydrology and Earth System Sciences*, *9*(4), 381–393. https://doi.org/10.5194/hess-9-381-2005

Pappenberger, F., Dutra, E., Wetterhall, F., & Cloke, H. L. (2012). Deriving global flood hazard maps of fluvial floods through a physical model cascade. *Hydrology and Earth System Sciences*, *16*(11), 4143–4156. https://doi.org/10.5194/hess-16-4143-2012

Pappenberger, Florian, Cloke, H. L., Parker, D. J., Wetterhall, F., Richardson, D. S., & Thielen, J. (2015). The monetary benefit of early flood warnings in Europe. *Environmental Science & Policy*, *51*, 278–291. https://doi.org/10.1016/j.envsci.2015.04.016

Paprotny, D., Morales-Nápoles, O., & Jonkman, S. N. (2017). Efficient pan-European river flood hazard modelling through a combination of statistical and physical models. *Natural Hazards and Earth System Sciences*, *17*(7), 1267–1283. https://doi.org/10.5194/nhess-17-1267-2017

Paprotny, D., Morales-Nápoles, O., & Jonkman, S. N. (2018). HANZE: a pan-European database of exposure to natural hazards and damaging historical floods since 1870. *Earth System Science Data*, *10*(1), 565–581. https://doi.org/10.5194/essd-10-565-2018

Paprotny, D., Sebastian, A., Morales-Nápoles, O., & Jonkman, S. N. (2018). Trends in flood losses in Europe over the past 150 years. *Nature Communications*, *9*(1). https://doi.org/10.1038/s41467-018-04253-1

Pekel, J.-F., Cottam, A., Gorelick, N., & Belward, A. S. (2016). High-resolution mapping of global surface water and its long-term changes. *Nature*, *540*(7633), 418–422. https://doi.org/10.1038/nature20584

Petersen-Øverleir, A., and T. Reitan (2005), Objective segmentation in compound rating curves, *Journal of Hydrology*, 311, 188–201, http://doi.org/10.1016/j.jhydrol.2005.01.016

Pianosi, F., Sarrazin, F., & Wagener, T. (2015). A Matlab toolbox for Global Sensitivity Analysis. *Environmental Modelling & Software*, *70*, 80–85. https://doi.org/10.1016/j.envsoft.2015.04.009

Quinn, N., Bates, P. D., & Siddall, M. (2013). The contribution to future flood risk in the Severn Estuary from extreme sea level rise due to ice sheet mass loss: Future Flood Risk in the Severn Estuary. *Journal of Geophysical Research: Oceans*, *118*(11), 5887–5898. https://doi.org/10.1002/jgrc.20412

Quinn, P., Beven, K., Chevallier, P., & Planchon, O. (1991). The prediction of hillslope flow paths for distributed hydrological modelling using digital terrain models. *Hydrological Processes*, *5*(1), 59–79. https://doi.org/10.1002/hyp.3360050106

Raymond, P. A., Hartmann, J., Lauerwald, R., Sobek, S., McDonald, C., Hoover, M., et al. (2013). Global carbon dioxide emissions from inland waters. *Nature*, *503*(7476), 355–359. https://doi.org/10.1038/nature12760

Rennó, C. D., Nobre, A. D., Cuartas, L. A., Soares, J. V., Hodnett, M. G., Tomasella, J., & Waterloo, M. J. (2008). HAND, a new terrain descriptor using SRTM-DEM: Mapping terra-firme rainforest environments in Amazonia. *Remote Sensing of Environment*, *112*(9), 3469–3481. https://doi.org/10.1016/j.rse.2008.03.018

Rieger, W. (1998). A phenomenon-based approach to upslope contributing area and depressions in DEMs. *Hydrological Processes*, *12*, 857–872.

Rizzoli, P., Martone, M., Gonzalez, C., Wecklich, C., Borla Tridon, D., Bräutigam, B., et al. (2017). Generation and performance assessment of the global TanDEM-X digital elevation model. *ISPRS Journal of Photogrammetry and Remote Sensing*, *132*, 119–139. https://doi.org/10.1016/j.isprsjprs.2017.08.008

Rodríguez, E., Morris, C. S., & Belz, J. E. (2006). A Global Assessment of the SRTM Performance. *Photogrammetric Engineering & Remote Sensing*, *72*(3), 249–260. https://doi.org/10.14358/PERS.72.3.249

Salamon, P., Arnal, L., Asp, S., Baugh, C., Beck, H., Bisselink, B., et al. (2019). *EFAS upgrade for the extended model domain* (Publications Office of the European Union No. EUR 29323 EN). Luxemburg.

Samela, C., Troy, T. J., & Manfreda, S. (2017). Geomorphic classifiers for flood-prone areas delineation for data-scarce environments. *Advances in Water Resources*, *102*, 13–28. https://doi.org/10.1016/j.advwatres.2017.01.007

Sampson, C. C., Smith, A. M., Bates, P. D., Neal, J. C., Alfieri, L., & Freer, J. E. (2015). A high-resolution global flood hazard model. *Water Resources Research*, *51*(9), 7358–7381. https://doi.org/10.1002/2015WR016954

van der Sande, C. J., de Jong, S. M., & de Roo, A. P. J. (2003). A segmentation and classification approach of IKONOS-2 imagery for land cover mapping to assist flood risk and flood damage assessment. *International Journal of Applied Earth Observation and Geoinformation*, *4*(3), 217–229. https://doi.org/10.1016/S0303-2434(03)00003-5

Sanders, B. F., & Schubert, J. E. (2019). PRIMo: Parallel raster inundation model. *Advances in Water Resources*, *126*, 79–95. https://doi.org/10.1016/j.advwatres.2019.02.007

Sanders, B. F., Schubert, J. E., & Detwiler, R. L. (2010). ParBreZo: A parallel, unstructured grid, Godunov-type, shallow-water code for high-resolution flood inundation modeling at the regional scale. *Advances in Water Resources*, *33*(12), 1456–1467. https://doi.org/10.1016/j.advwatres.2010.07.007

Saunders, W. (1999). Preparation of DEMs for use in environmental modeling analysis. *ESRI User Conference*.

Schneider, C., Flörke, M., Eisner, S., & Voss, F. (2011). Large scale modelling of bankfull flow: An example for Europe. *Journal of Hydrology*, *408*(3–4), 235–245. https://doi.org/10.1016/j.jhydrol.2011.08.004

Schumann, G., Brakenridge, G., Kettner, A., Kashif, R., & Niebuhr, E. (2018). Assisting Flood Disaster Response with Earth Observation Data and Products: A Critical Assessment. *Remote Sensing*, *10*(8), 1230. https://doi.org/10.3390/rs10081230

Schumann, G., Bates, P. D., Apel, H., & Aronica, G. T. (2018). Global Flood Hazard Mapping, Modeling, and Forecasting: Challenges and Perspectives. In Guy J-P. Schumann, P. D. Bates, H. Apel, & G. T. Aronica (Eds.), *Geophysical Monograph Series* (pp. 239–244). Hoboken, NJ, USA: John Wiley & Sons, Inc. https://doi.org/10.1002/9781119217886.ch14

Schumann, G. J., Bates, P. D., Apel, H., & Aronica, G. T. (Eds.). (2018). *Global Flood Hazard: Applications in Modeling, Mapping, and Forecasting* (1st ed.). Wiley. https://doi.org/10.1002/9781119217886

Schumann, G. J.-P., Neal, J. C., Voisin, N., Andreadis, K. M., Pappenberger, F., Phanthuwongpakdee, N., et al. (2013). A first large-scale flood inundation forecasting model: Large-Scale Flood Inundation Forecasting. *Water Resources Research*, *49*(10), 6248–6257. https://doi.org/10.1002/wrcr.20521

Schumann, Guy J-P., & Bates, P. D. (2018). The Need for a High-Accuracy, Open-Access Global DEM. *Frontiers in Earth Science*, *6*, 225. https://doi.org/10.3389/feart.2018.00225

Schumann, Guy J.-P., Andreadis, K. M., & Bates, P. D. (2014). Downscaling coarse grid hydrodynamic model simulations over large domains. *Journal of Hydrology*, *508*, 289–298. https://doi.org/10.1016/j.jhydrol.2013.08.051

Schumann, Guy J.-P., Stampoulis, D., Smith, A. M., Sampson, C. C., Andreadis, K. M., Neal, J. C., & Bates, P. D. (2016). Rethinking flood hazard at the global scale. *Geophysical Research Letters*, *43*(19), 10,249-10,256. https://doi.org/10.1002/2016GL070260

Schwanghart, W., & Kuhn, N. J. (2010). TopoToolbox: A set of Matlab functions for topographic analysis. *Environmental Modelling & Software*, *25*(6), 770–781. https://doi.org/10.1016/j.envsoft.2009.12.002

Scussolini, P., Aerts, J. C. J. H., Jongman, B., Bouwer, L. M., Winsemius, H. C., de Moel, H., & Ward, P. J. (2016). FLOPROS: an evolving global database of flood protection standards. *Natural Hazards and Earth System Sciences*, *16*(5), 1049–1061. https://doi.org/10.5194/nhess-16-1049-2016

Seenath, A., Wilson, M., & Miller, K. (2016). Hydrodynamic versus GIS modelling for coastal flood vulnerability assessment: Which is better for guiding coastal management? *Ocean & Coastal Management*, *120*, 99–109. https://doi.org/10.1016/j.ocecoaman.2015.11.019

Seibert, J., & McGlynn, B. L. (2007). A new triangular multiple flow direction algorithm for computing upslope areas from gridded digital elevation models: A NEW TRIANGULAR MULTIPLE-FLOW DIRECTION. *Water Resources Research*, *43*(4). https://doi.org/10.1029/2006WR005128

Shaw, J., Kesserwani, G., Neal, J., Bates, P., & Sharifian, M. K. (2020). *LISFLOOD-FP 8.0: the new discontinuous Galerkin shallow watersolver for multi-core CPUs and GPUs* (preprint). Hydrology. https://doi.org/10.5194/gmd-2020-340

Shen, J. (2020). Influence of Uncertainties in DEM Resolution and Surface Friction to the Building Treatment Methods in Urban Inundation Modelling. *IOP Conference Series: Earth and Environmental Science*, *428*, 012088. https://doi.org/10.1088/1755-1315/428/1/012088

Simley, J. D., & Carswell, W. J. (2009). *The National Map—Hydrography: U.S. Geological Survey Fact Sheet 2009-3054*.

Smith, A., Sampson, C., & Bates, P. (2015). Regional flood frequency analysis at the global scale. *Water Resources Research*, *51*(1), 539–553. https://doi.org/10.1002/2014WR015814

Smith, A., Sampson, C., Neal, J., Bates, P. D., Trigg, M., Freer, J., et al. (2018). Modeling and Mapping of Global Flood Hazard Layers. In Guy J-P. Schumann, P. D. Bates, H. Apel, & G. T. Aronica (Eds.), *Geophysical Monograph Series* (pp. 131–155). Hoboken, NJ, USA: John Wiley & Sons, Inc. https://doi.org/10.1002/9781119217886.ch8

Smith, P. J., Pappenberger, F., Wetterhall, F., Thielen del Pozo, J., Krzeminski, B., Salamon, P., et al. (2016). On the Operational Implementation of the European Flood Awareness

System (EFAS). In *Flood Forecasting* (pp. 313–348). Elsevier. https://doi.org/10.1016/B978-0-12-801884-2.00011-6

Sosa, J. (2018, September 3). Hydroutils. Zenodo. https://doi.org/10.5281/zenodo.1408076

Sosa, J., Sampson, C., Smith, A., Neal, J., & Bates, P. (2020). A toolbox to quickly prepare flood inundation models for LISFLOOD-FP simulations. *Environmental Modelling & Software*, *123*, 104561. https://doi.org/10.1016/j.envsoft.2019.104561

Sutanudjaja, E. H., van Beek, R., Wanders, N., Wada, Y., Bosmans, J. H. C., Drost, N., et al. (2018). PCR-GLOBWB 2: a 5 arcmin global hydrological and water resources model. *Geoscientific Model Development*, *11*(6), 2429–2453. https://doi.org/10.5194/gmd-11-2429-2018

Syme, W. J. (1991). *Dynamically Linked Two-dimensional/One-dimensional Hydrodynamic Modelling Program for Rivers, Estuaries & Coastal Waters* (MEngSc thesis). University of Queensland, Australia.

Tachikawa, T., Hato, M., Kaku, M., & Iwasaki, A. (2011). Characteristics of ASTER GDEM version 2. In *2011 IEEE International Geoscience and Remote Sensing Symposium* (pp. 3657–3660). Vancouver, BC, Canada: IEEE. https://doi.org/10.1109/IGARSS.2011.6050017

Tadono, T., Takaku, J., Tsutsui, K., Oda, F., & Nagai, H. (2015). Status of "ALOS World 3D (AW3D)" global DSM generation (pp. 3822–3825). Proceeding 2015 IEEE International Geoscience and Remote Sensing Symposium (IGARSS). https://doi.org/10.1109/IGARSS.2015.7326657

Takaku, J., Tadono, T., Tsutsui, K., & Ichikawa, M. (2015). Quality status of high resolution global DSM generated from ALOS PRISM. In *2015 IEEE International Geoscience and Remote Sensing Symposium (IGARSS)* (pp. 3854–3857). Milan, Italy: IEEE. https://doi.org/10.1109/IGARSS.2015.7326665

Tarboton, David G. (1997). A new method for the determination of flow directions and upslope areas in grid digital elevation models. *Water Resources Research*, *33*(2), 309–319. https://doi.org/10.1029/96WR03137

Tarboton, David G., Bras, R. L., & Rodriguez-Iturbe, I. (1991). On the extraction of channel networks from digital elevation data. *Hydrological Processes*, *5*(1), 81–100. https://doi.org/10.1002/hyp.3360050107

Tarboton, D.G. (2005). Terrain analysis using digital elevation models (TauDEM). Retrieved from http://hydrology.usu.edu/taudem/

Teng, J., Jakeman, A. J., Vaze, J., Croke, B. F. W., Dutta, D., & Kim, S. (2017). Flood inundation modelling: A review of methods, recent advances and uncertainty analysis. *Environmental Modelling & Software*, *90*, 201–216. https://doi.org/10.1016/j.envsoft.2017.01.006

Thieken, A. H., Müller, M., Kreibich, H., & Merz, B. (2005). Flood damage and influencing factors: New insights from the August 2002 flood in Germany: FLOOD DAMAGE AND INFLUENCING FACTORS. *Water Resources Research*, *41*(12). https://doi.org/10.1029/2005WR004177

Thielen, J., Bartholmes, J., Ramos, M.-H., & de Roo, A. (2009). The European Flood Alert System – Part 1: Concept and development. *Hydrology and Earth System Sciences*, *13*(2), 125–140. https://doi.org/10.5194/hess-13-125-2009

Thorarinsdottir, T. L., Hellton, K. H., Steinbakk, G. H., Schlichting, L., & Engeland, K. (2018). Bayesian Regional Flood Frequency Analysis for Large Catchments. *Water Resources Research*, *54*(9), 6929–6947. https://doi.org/10.1029/2017WR022460

Trigg, M. A., Birch, C. E., Neal, J. C., Bates, P. D., Smith, A., Sampson, C. C., et al. (2016). The credibility challenge for global fluvial flood risk analysis. *Environmental Research Letters*, *11*(9), 094014. https://doi.org/10.1088/1748-9326/11/9/094014

Uhe, P. F., Mitchell, D. M., Bates, P. D., Sampson, C. C., Smith, A. M., & Islam, A. S. (2019). Enhanced flood risk with 1.5 °C global warming in the Ganges–Brahmaputra–Meghna basin. *Environmental Research Letters*, *14*(7), 074031. https://doi.org/10.1088/1748-9326/ab10ee

Ulbrich, U., Brücher, T., Fink, A. H., Leckebusch, G. C., Krüger, A., & Pinto, J. G. (2003). The central European floods of August 2002: Part 1 – Rainfall periods and flood development. *Weather*, *58*(10), 371–377. https://doi.org/10.1256/wea.61.03A

USACE. (2016). *HEC-RAS River Analysis System. User manual version 5.0*. USACE.

USGS. (1997). *GTOPO30 - Global 1 km digital raster data derived from a variety of sources*. Retrieved from https://doi.org/10.5066/F7DF6PQS

USGS. (2001). *HYDRO1k - A global hydrologic database derived from 1996 GTOPO30 data.* Retrieved from https://doi.org/10.5066/F77P8WN0

Van Der Knijff, J. M., Younis, J., & De Roo, A. P. J. (2010). LISFLOOD: a GIS-based distributed model for river basin scale water balance and flood simulation. *International Journal of Geographical Information Science*, *24*(2), 189–212. https://doi.org/10.1080/13658810802549154

de Vente, J., Poesen, J., Verstraeten, G., Govers, G., Vanmaercke, M., Van Rompaey, A., et al. (2013). Predicting soil erosion and sediment yield at regional scales: Where do we stand? *Earth-Science Reviews*, *127*, 16–29. https://doi.org/10.1016/j.earscirev.2013.08.014

Verpoorter, C., Kutser, T., Seekell, D. A., & Tranvik, L. J. (2014). A global inventory of lakes based on high-resolution satellite imagery. *Geophysical Research Letters*, *41*(18), 6396–6402. https://doi.org/10.1002/2014GL060641

Villanueva, I., & Wright, N. G. (2006). Linking Riemann and storage cell models for flood prediction. *Proceedings of the Institution of Civil Engineers - Water Management*, *159*(1), 27–33. https://doi.org/10.1680/wama.2006.159.1.27

Vorogushyn, S., Lindenschmidt, K.-E., Kreibich, H., Apel, H., & Merz, B. (2012). Analysis of a detention basin impact on dike failure probabilities and flood risk for a channel-dike-floodplain system along the river Elbe, Germany. *Journal of Hydrology*, *436–437*, 120–131. https://doi.org/10.1016/j.jhydrol.2012.03.006

Vorogushyn, S., Bates, P. D., de Bruijn, K., Castellarin, A., Kreibich, H., Priest, S., et al. (2018). Evolutionary leap in large-scale flood risk assessment needed. *Wiley Interdisciplinary Reviews: Water*, *5*(2), e1266. https://doi.org/10.1002/wat2.1266

Ward, P. J., Jongman, B., Weiland, F. S., Bouwman, A., van Beek, R., Bierkens, M. F. P., et al. (2013). Assessing flood risk at the global scale: model setup, results, and sensitivity. *Environmental Research Letters*, *8*(4), 044019. https://doi.org/10.1088/1748-9326/8/4/044019

Wessel, B., Huber, M., Wohlfart, C., Marschalk, U., Kosmann, D., & Roth, A. (2018). Accuracy assessment of the global TanDEM-X Digital Elevation Model with GPS data. *ISPRS Journal of Photogrammetry and Remote Sensing*, *139*, 171–182. https://doi.org/10.1016/j.isprsjprs.2018.02.017

Wilson, M., Bates, P., Alsdorf, D., Forsberg, B., Horritt, M., Melack, J., et al. (2007). Modeling large-scale inundation of Amazonian seasonally flooded wetlands. *Geophysical Research Letters*, *34*(15). https://doi.org/10.1029/2007GL030156

Wing, O. E. J., Bates, P. D., Sampson, C. C., Smith, A. M., Johnson, K. A., & Erickson, T. A. (2017). Validation of a 30 m resolution flood hazard model of the conterminous United States: 30 m RESOLUTION FLOOD MODEL OF CONUS. *Water Resources Research*, *53*(9), 7968–7986. https://doi.org/10.1002/2017WR020917

Wing, O. E. J., Bates, P. D., Smith, A. M., Sampson, C. C., Johnson, K. A., Fargione, J., & Morefield, P. (2018). Estimates of present and future flood risk in the conterminous United States. *Environmental Research Letters*, *13*(3), 034023. https://doi.org/10.1088/1748-9326/aaac65

Wing, O. E. J., Bates, P. D., Neal, J. C., Sampson, C. C., Smith, A. M., Quinn, N., et al. (2019). A new automated method for improved flood defense representation in large-scale hydraulic models. *Water Resources Research*, 2019WR025957. https://doi.org/10.1029/2019WR025957

Winsemius, H. C., Van Beek, L. P. H., Jongman, B., Ward, P. J., & Bouwman, A. (2013). A framework for global river flood risk assessments. *Hydrology and Earth System Sciences*, *17*(5), 1871–1892. https://doi.org/10.5194/hess-17-1871-2013

Winsemius, Hessel C., Aerts, J. C. J. H., van Beek, L. P. H., Bierkens, M. F. P., Bouwman, A., Jongman, B., et al. (2016). Global drivers of future river flood risk. *Nature Climate Change*, *6*(4), 381–385. https://doi.org/10.1038/nclimate2893

Wösten, J. H. M., Lilly, A., Nemes, A., & Le Bas, C. (1999). Development and use of a database of hydraulic properties of European soils. *Geoderma*, *90*(3–4), 169–185. https://doi.org/10.1016/S0016-7061(98)00132-3

Wu, H., Adler, R. F., Tian, Y., Huffman, G. J., Li, H., & Wang, J. (2014). Real-time global flood estimation using satellite-based precipitation and a coupled land surface and routing model. *Water Resources Research*, *50*(3), 2693–2717. https://doi.org/10.1002/2013WR014710

Yamazaki, D., Kanae, S., Kim, H., & Oki, T. (2011). A physically based description of floodplain inundation dynamics in a global river routing model. *Water Resources Research*, *47*(4). https://doi.org/10.1029/2010WR009726

Yamazaki, D., Baugh, C. A., Bates, P. D., Kanae, S., Alsdorf, D. E., & Oki, T. (2012). Adjustment of a spaceborne DEM for use in floodplain hydrodynamic modeling. *Journal of Hydrology*, *436–437*, 81–91. https://doi.org/10.1016/j.jhydrol.2012.02.045

Yamazaki, D., Lee, H., Alsdorf, D. E., Dutra, E., Kim, H., Kanae, S., & Oki, T. (2012). Analysis of the water level dynamics simulated by a global river model: A case study in the Amazon River. *Water Resources Research*, *48*(9). https://doi.org/10.1029/2012WR011869

Yamazaki, D., O'Loughlin, F., Trigg, M. A., Miller, Z. F., Pavelsky, T. M., & Bates, P. D. (2014). Development of the Global Width Database for Large Rivers. *Water Resources Research*, *50*(4), 3467–3480. https://doi.org/10.1002/2013WR014664

Yamazaki, D., Sato, T., Kanae, S., Hirabayashi, Y., & Bates, P. D. (2014). Regional flood dynamics in a bifurcating mega delta simulated in a global river model: SIMULATION OF RIVER MEGA DELTA FLOWS. *Geophysical Research Letters*, *41*(9), 3127–3135. https://doi.org/10.1002/2014GL059744

Yamazaki, D., Trigg, M. A., & Ikeshima, D. (2015). Development of a global ~90m water body map using multi-temporal Landsat images. *Remote Sensing of Environment*, *171*, 337–351. https://doi.org/10.1016/j.rse.2015.10.014

Yamazaki, D., Ikeshima, D., Tawatari, R., Yamaguchi, T., O'Loughlin, F., Neal, J. C., et al. (2017). A high-accuracy map of global terrain elevations. *Geophysical Research Letters*, *44*(11), 5844–5853. https://doi.org/10.1002/2017GL072874

Yamazaki, D., Ikeshima, D., Sosa, J., Bates, P. D., Allen, G., & Pavelsky, T. (2019). MERIT Hydro: A high-resolution global hydrography map based on latest topography datasets. *Water Resources Research*, 2019WR024873. https://doi.org/10.1029/2019WR024873

Zarfl, C., Lumsdon, A. E., Berlekamp, J., Tydecks, L., & Tockner, K. (2015). A global boom in hydropower dam construction. *Aquatic Sciences*, *77*(1), 161–170. https://doi.org/10.1007/s00027-014-0377-0

Zhou, X., Zhang, Y., Wang, Y., Zhang, H., Vaze, J., Zhang, L., et al. (2012). Benchmarking global land surface models against the observed mean annual runoff from 150 large basins. *Journal of Hydrology*, *470–471*, 269–279. https://doi.org/10.1016/j.jhydrol.2012.09.002